2012

PROTEIN BASED BIOMIMETIC APPROACHS TO SURFACE HEMOCOMPATIBILITY AND BIOCOMPATIBILITY ENHANCEMENT

Matthew Thomas Dickerson
University of Kentucky, dickerson81@gmail.com

STUDENT AGREEMENT:

I represent that my thesis or dissertation and abstract are my original work. Proper attribution has been given to all outside sources. I understand that I am solely responsible for obtaining any needed copyright permissions. I have obtained and attached hereto needed written permission statements(s) from the owner(s) of each third-party copyrighted matter to be included in my work, allowing electronic distribution (if such use is not permitted by the fair use doctrine).

I hereby grant to The University of Kentucky and its agents the non-exclusive license to archive and make accessible my work in whole or in part in all forms of media, now or hereafter known. I agree that the document mentioned above may be made available immediately for worldwide access unless a preapproved embargo applies.

I retain all other ownership rights to the copyright of my work. I also retain the right to use in future works (such as articles or books) all or part of my work. I understand that I am free to register the copyright to my work.

REVIEW, APPROVAL AND ACCEPTANCE

The document mentioned above has been reviewed and accepted by the student's advisor, on behalf of the advisory committee, and by the Director of Graduate Studies (DGS), on behalf of the program; we verify that this is the final, approved version of the student's dissertation including all changes required by the advisory committee. The undersigned agree to abide by the statements above.

Matthew Thomas Dickerson, Student

Dr. Kimberly W. Anderson, Major Professor

Dr. Stephen Rankin, Director of Graduate Studies

PROTEIN BASED BIOMIMETIC APPROACHS TO SURFACE HEMOCOMPATIBILITY AND BIOCOMPATIBILITY ENHANCEMENT

DISSERTATION

A dissertation submitted in partial fulfillment of
the requirements for the degree of Doctor of Philosophy in the
College of Engineering at the
University of Kentucky

By
Matthew Thomas Dickerson

Lexington, KY

Director: Dr. Kimberly W. Anderson, Professor of Chemical Engineering

Lexington, KY

2012

ABSTRACT OF DISSERTATION

PROTEIN BASED BIOMIMETIC APPROACH TO SURFACE HEMOCOMPATIBILITY AND BIOCOMPATIBILITY ENHANCEMENT

T. pallidum can survive a primary immune response and continue growing in the host for an extended period of time. *T. pallidum* is thought to bind serum fibronectin (FN) through Tp0483 on the surface to obscure antigens. A Tp0483 fragment (rTp0483) was adsorbed onto functionalized self-assembled monolayers (SAMs) with FN. FN capture by adsorbed rTp0483 depended greatly on surface chemistry with COO^- groups being best for FN binding. Hemocompatibility was determined by analysis of plasma protein adsorption, intrinsic pathway activation, and platelet activation. rTp0483+FN bound an equal or lesser amount of fibrinogen (Fg), human serum albumin (HSA), and factor XII (FXII) compared to rTp0483 or FN alone and adsorption of rTp0483 prior to FN greatly decreased platelet activation. Inhibition of protein binding and platelet activation suggested an attenuated hematological response. Biocompatibility of rTp0483 and FN coated surfaces was characterized by macrophage uptake of protein coated polystyrene microspheres (PSMs), macrophage adsorption onto protein coated surfaces, cytotoxic effects of adsorbed rTp0483 and FN, and TNF-α and NO_2^- release in macrophages stimulated with rTp0483 and FN adsorbed and in solution. Addition of FN to rTp0483 on plain and COO^- PSMs reduced phagocytosis compared to rTp0483 alone and on plain PSMs compared to FN alone. On plain PSMs addition of FN to adsorbed rTp0483 decreased TNF-α generation. Adsorption of rTp0483 before FN on large, flat COO^- surfaces decreased macrophage adsorption and TNF-α and NO_2^- generation. High concentrations of rTp0483 were mildly cytotoxic to macrophages. FN binding by Tp0483 on *T. pallidum* likely plays a role in antigenic disguise and rTp0483+FN coatings may potentially inhibit FN and rTp0483 specific interactions with macrophages. Molecularly imprinted polymer coatings were also examined for biomaterial development. Fouling resistant 2-methacryloyloxyethyl phosphorylcholine (MPC) was imprinted with bovine serum albumin (BSA) protein templates to facilitate BSA specific binding. The BSA template was constructed and verified and BSA specific binding quantified using quartz crystal microbalance (QCM) and enzyme linked immunosorbent assay (ELISA). BSA imprinted coatings

were determined to bind significantly more BSA than nonfouling MPC controls demonstrating the feasibility of targeted protein capture.

KEYWORDS: Antigenic Disguise, *Treponema pallidum*, Biomaterial, Hemocompatibility, Molecular Imprinting

Matthew T. Dickerson
Student's Signature

1-4-12
Date

PROTEIN BASED BIOMIMETIC APPROACH TO SURFACE HEMOCOMPATIBILITY AND BIOCOMPATIBILITY ENHANCEMENT

By:

Matthew Thomas Dickerson

Kimberly W. Anderson
Director of Dissertation

Stephen Rankin
Director of Graduate Studies

1-4-12
Date

ACKNOWLEDGEMENTS

First, I would like to thank my research advisers, Dr. Kimberly Anderson, Dr. Leonidas Bachas, and Dr. Marc Knecht. Their great knowledge and steady guidance have been invaluable over the course of my graduate student career. Without them none of this would have been possible. I would also like to thank everyone in the Anderson lab, IGERT program, and throughout the entire Chemical Engineering department for their constant support and friendship. I would like to acknowledge the NSF for funding this research as well as Dr. Caroline Cameron at the University of Victoria, in Victoria, Canada for providing materials related to the production of rTp0483. In addition, I would like to acknowledge Dr. Kazuhiko Ishihara at Tokyo University, Tokyo, Japan for allowing me to study in his lab and Kyoko Fukazawa for teaching me everything I know about polymer synthesis. Moreover, thanks to the NSF and the Japan Society for the Promotion of Science (JSPS) for funding the joint venture. Finally, I would like to acknowledge my parents who have inspired me countless times to never give up and keep pursuing my dreams. Their unwavering faith has always encouraged me when things got tough and allowed me to accomplish my goals.

TABLE OF CONTENTS

LIST OF TABLES

LIST OF FIGURES

Chapter 1: INTRODUCTION

Medical science is an ever-evolving field comprised of diverse areas of research. The development of biomaterials has been an important facet of the field for many years. The term biomaterial refers to synthetic or natural materials that for a period of time augment or replace a portion of the body's function. Man has long searched for ways to replace this lost function as a consequence of injury or disease and in the past century has made significant progress toward this goal. A successful biomaterial is expected to serve its desired function while avoiding unfavorable or harmful interactions with its biological environment. A material that fulfills these prerequisites can be referred to as biocompatible. Many ways of improving material biocompatibility exist, one of which is investigated in this work.

Use of an adsorbed recombinant bacterial protein from *T. pallidum* (rTp0483) along with human serum fibronectin (FN) to form a biocompatible surface coating is explored. Whole *T. pallidum* is able to survive the primary immune response to infection and grow undetected in the host for extended periods of time.[1-3] It was theorized that the immune response to *T. pallidum* is inhibited when the surface protein (Tp0483) binds soluble FN. The phenomenon where a microorganism binds native host materials to conceal its presence is often referred to as antigenic disguise. By adsorbing rTp0483 on a surface along with FN it was hypothesized that the host response could be attenuated in a manner similar to whole *T. pallidum*.

Control of protein surface adsorption using a molecularly imprinted polymer coating was also examined and is presented in Appendix A. Molecular imprinting is a technique used to impart a specific binding affinity for a protein or similar biomolecule into a polymer layer. The molecule of interest is added to a polymer solution either alone or immobilized on a substrate and the polymer is polymerized around the target. After the target is removed the polymer layer retains a high affinity for the original target.[4-6] Use of fouling resistant 2-methacryloyloxyethyl phosphorylcholine (MPC) polymer allows nonspecific protein binding to be limited while specific binding of a selected protein is facilitated.[7-9] By controlling what proteins bind to a surface the host response can be directed leading to improved material biocompatibility.

The primary objective was to investigate the application of surface adsorbed rTp0483 with human serum FN in the preparation of a biocompatible coating. Specific objectives related to this primary objective are listed below.

- Analyze rTp0483 adsorption onto self-assembled monolayers (SAMs)
- Determine orientation, surface distribution, and FN binding affinity of rTp0483 adsorbed onto SAMs
- Investigate binding and desorption kinetics of rTp0483 binding onto SAMs and FN binding onto rTp0483 on SAMs
- Elucidate peptide sequences on rTp0483 and FN responsible for binding

- Investigate hemocompatibility enhancement of rTp0483, FN, and rTp0483+FN coated SAMs by quantifying plasma protein adsorption, intrinsic pathway activation, and platelet activation
- Determine effect of rTp0483, FN, and rTp0483+FN coatings on phagocytosis of polystyrene microspheres and surface adsorption of macrophages
- Compare TNF-α and NO_2^- generation and cytotoxic effects in macrophages when exposed to rTp0483, FN, and rTp0483+FN surface adsorbed and in solution

The objective of the appendix chapter was to determine the feasibility of synthesizing a molecularly imprinted MPC polymer layer for capture of specific proteins for the purpose of controlling the host immune response. Specific objectives related to this primary objective are listed below.

- Synthesize a BSA imprinted MPC polymer coating
- Compare BSA adsorption on BSA imprinted MPC to non-imprinted MPC, MPC imprinted with a template without BSA, and to hydrophobic BMA

Chapter 2 provides relevant background related to the material covered. Biomaterials are discussed along with host immune and hematological responses. The pathophysiology of *T. palldium* is discussed along with how the surface protein Tp0483 is believed to interact with host FN to produce an antigenic disguise.

Chapter 3 reviews several analysis techniques employed including quartz crystal microbalance (QCM), surface plasma resonance (SPR), atomic force microscopy (AFM), and flow cytometry. Relevant kinetic models used to simulate rTp0483 and FN binding and desorption kinetics are also summarized.

Chapter 4 covers the process employed to synthesize recombinant *T. pallidum* protein fragment rTp0483. Protocols employed for protein expression, purification, and validation are described.

Chapter 5 outlines the assembly of functionalized SAMs, which are used in a large number of the studies detailed in this work. In order to verify successful SAM formation experimental data collected is compared to literature and theoretical values.

Chapter 6 explores the binding of rTp0483 to functionalized SAMs and FN binding to adsorbed rTp0483. The binding and desorption kinetics of rTp0483 onto SAMs and FN onto adsorbed rTp0483 are also investigated. In addition, the orientation and surface distribution of rTp0483 monolayers are examined. Finally, antibodies and peptides are employed to probe potential binding sites on rTp0483 and FN.

In Chapter 7 the potential hemocompatibility enhancing effect of adsorbed rTp0483 with FN is evaluated. Adsorption of selected plasma proteins is determined along with intrinsic activity of plasma and activation of platelets in contact with adsorbed protein layers.

Chapter 8 investigates the immunosuppressive effect of adsorbed and free rTp0483 with FN by examining the response of macrophages. Phagocytosis of

protein coated microspheres is analyzed in addition to surface adsorption of macrophages to protein coated surfaces. Potential cytotoxicity of rTp0483 with FN in solution and adsorbed to surfaces is determined as well. Finally, macrophage activation is quantified by measuring the production of TNF-α and NO_2^- in response to rTp0483 with FN in solution and adsorbed to surfaces.

In Chapter 9 overall conclusions based on collected data are made. The relation of FN binding by rTp0483 to *T. pallidum* antigenic disguise and the viability of rTp0483 with FN as a biocompatible surface coating are discussed along with the feasibility of molecular imprinting of proteins as a method to control host response to a biomaterial.

An appendix covers the synthesis of a BSA imprinted MPC polymer coating and the subsequent verification of its effectiveness. BSA binding on BSA imprinted MPC surfaces were compared to unpatterned MPC, patterned MPC without BSA, and BMA onto which proteins adsorb freely.

Chapter 2: BACKGROUND

2.1. Biomaterials

The National Institute of Health (NIH) provides the comprehensive definition of a biomaterial as follows: any substance, other than a drug, or combination of substances, synthetic or natural in origin, which can be used for any period of time, as a whole or as a part of a system which treats, augments, or replaces any tissue, organ, or function of the body.[10] As such, the scope of biomaterial development is vast, encompassing many divergent areas of research. Biomaterials have existed in some form since antiquity; however, in the last century great strides have been made to advance the field.[11] In the 20th century as technology progressed, an array of synthetic polymers, metal alloys, and ceramic formulations were developed to provide the building blocks of modern biomaterial development. As a result of these advances, countless lives were saved or improved through the implementation of biomaterials like stents, joint replacements, and dental prostheses.[11]

2.1.1. Biomaterial Classes

Biomaterials fall into four broad categories composed of metals, ceramics, polymers, and natural materials, which can further be combined in various ways to produce an range of hybrid materials.[11, 12] Metal biomaterials have been most widely employed in the field of orthopedics where mechanical support is required for applications like knee and hip replacement. Important concerns for metallic implants are wear and corrosion resistance as well as the modulus of the

biomaterial.[12, 13] If the modulus is much higher than bone the implant prevents stress transfer to nearby cells which leads to bone resorption and implant loosening and if the modulus is lower than bone it will not be able to bear normal stresses and will fail over time. Commonly used metal materials include various formulations of stainless steel, cobalt chromium alloys, and titanium alloys. Among these, titanium is favored for its good corrosion resistance, appropriate modulus, good biocompatibility, and the ability to form a strong bond with natural bone.[12, 13]

Ceramics are also primarily used in orthopedic applications because ceramic materials are composed of aligned crystalline minerals like natural bone.[12, 14] These ceramic biomaterials offer several advantages including good biocompatibility, high corrosion resistance, and high mechanical strength; however, ceramics are generally more brittle than metals.[12, 14] Some examples of currently employed ceramic biomaterials include inert materials like alumina as well as bioactive materials like hydroxyapatite. Hydroxyapatite ($Ca_{10}(PO_4)_6(OH)_2$) is one of the most widely used ceramic biomaterials; it degrades naturally over time and its main application is the repair of bone defects.[12, 14-16] Apatite is a major component of natural bone composed of calcium and phosphate and when it is contacts hydroxyapatite *in vivo* a strong chemical bond is formed. In addition, hydroxyapatite has been shown to induce bone differentiation and thus speed up bone regeneration.[15, 16]

Polymeric materials comprise the third class of biomaterials. Polymers have a large range of biomaterial applications including vascular grafts, degradable sutures, drug delivery platforms, and tissue regeneration scaffolds.[12, 17, 18] Soft tissues that provide physiological and biochemical function are found throughout

the body; however, there were no biomaterials capable of mimicking these natural functions and thus polymers were developed in order to fulfill this need.[12] The adjustability of polymer composition makes them uniquely qualified to perform this task. By combining different types of monomer units the chemical and physical properties of a polymer can be adjusted to meet a specific need. Polymers can be developed to degrade over a set amount of time or to remain whole indefinitely. A degradable polymer is ideal for a drug delivery system in order to allow the encapsulated therapeutic to escape or for a tissue scaffold in order to allow for cell and tissue migration as well as angiogenesis.[12, 17] On the other hand, a nondegradable polymer is suited for a applications that require an extended residence time such as components of joint implants, heart valves, and vascular grafts.[12]

The fourth class of biomaterial is based on naturally occurring substances. In general, the development of natural biomaterials is based around components of the extracellular matrix (ECM) and is largely focused on the application of collagen, which is the most abundant protein found in the ECM.[12, 19] The ECM refers to the extracellular network of proteins and polysaccharides that lend support to cells located in tissue. The main components of the ECM are polysaccharide-protein complexes known as proteoglycans, which provides resistance against compressive stress, regulate cell migration, and affect protein activity along with a number of proteins including collagen, elastin, FN, and laminin that provide structural and adhesive support for cells.[19] Some key advantages of using natural biomaterials are that they are degraded by normal enzymatic processes and that they share similar

structure with that of the tissue being replaced. As a result, natural biomaterials elicit a more natural healing response including increased cell infiltration, proliferation, and differentiation.[20] These properties make natural biomaterials suitable for tissue regeneration applications. Disadvantages include poor mechanical properties and potential immunogenicity if they are not properly processed.[20] As research in biomaterial development progresses our understanding of underlying biological responses increases and material synthesis techniques evolve. As a consequence, our ability to guide natural biological responses will continue to expand and with it our ability to fight disease and repair injury.

When analyzing the relative merit of potential biomaterials there are two key conditions that must be fulfilled; a biomaterial must successfully execute its desired function and it must be biocompatible. In order to be considered biocompatible a material must be nontoxic, nonthrombogenic, noncarcinogenic, nonantigenic, and nonmutagenic.[21] Material rejection due to these issues resulting in inhibition of function and adverse effects is a constant concern for biomaterials so initial development focused on minimizing biological interactions between the patient and biomaterial. Such materials are often referred to as inert because they do not interact with their physiological environment.[11] The majority of host interactions are initiated by the adsorption of serum proteins onto the biomaterial surface, thus in order to limit these interactions the adsorption of proteins must be prevented.[11] A number of approaches have been developed to accomplish this goal including hydrophilic polymers coatings, phospholipid mimicking polymer coatings, and self-assembled monolayers (SAMs) functionalized with similar hydrophilic head

groups.[22] Each of these techniques relies on the hydrophilic nature of the material to tightly bind a layer of water molecules forming a steric barrier against protein adsorption.[23] These surface modification techniques are promising; however, they are not perfect. Hydrophilic polymer coatings resist protein and cell interactions so in cases where a biologically active surface is desired such coatings are unattractive. Moreover, it has been shown that such coatings are not universally effective in repulsing protein binding and become less effective over time.[24-26] While the development of inert materials continues, more recently, a new approach to biomaterial development has begun to emerge.

2.1.2. Approaches to Surface Biocompatibility Enhancement

Starting in the 1970s major breakthroughs in molecular biology and proteomics revealed various growth factors and enzymes, which have since allowed scientists to artificially regulate biological processes.[11] As scientists began to grasp the complex interactions behind these events biomaterials quickly expanded from simply providing mechanical support and limiting biological interactions to actively promoting or suppressing biological responses in the targeted area. These new biomaterials that actively interact with the body and moderate biological processes are often referred to as bioactive systems.[22]

Natural components of the body are rarely inert. Each part interacts in complex ways with the surrounding environment, thus a completely inert biomaterial is less than ideal. Biomaterials should fulfill any required biological functions in addition to mechanical functions, thus the development of bioactive

materials is the next natural step. For example, a material designed for use as a vascular graft would be expected to effectively transport blood and bear the pressures associated with the process; however, taken a step further, to ensure optimal performance the graft should also repulse nonspecific protein and platelet adhesion while promoting natural endothelial cell layer formation. Common approaches in the development of bioactive systems focus on the integration of adhesion molecules, growth factors, or more general physiochemical interactions into the biomaterial.[27]

Adhesion molecules are proteins and peptides that promote specific biological events including further protein binding and cellular interactions. Typical protein adsorption onto a biomaterial is nonspecific; however, with this type of bioactive system, adsorption is controlled by presenting specific binding sites.[27] By directing the interactions of a material and its environment, it is possible to tune the biological responses to suit a particular application. Continuing the example of a vascular graft, it is possible to selectively promote endothelial cell attachment while preventing platelet binding using this technique. A protein called $\alpha_4\beta_1$ is found on the surface of endothelial cells but not on platelets, so by integrating a corresponding receptor peptide, REDV from the serum protein fibronectin (FN), endothelial cells bound to the graft surface while platelets did not.[27] This approach is sometimes referred to as biomimetics because it attempts to replicate a natural biological response using an artificially constructed system. Biomimetics forms the basis of bacterial antigenic disguise mimicry outlined in the proceeding sections

where a bacterial surface protein is combined with a host serum protein in order to reproduce the ability of whole bacteria to suppress adverse biological responses.

An intriguing alternative to the direct integration of adhesion molecules is the newly emerging field of molecular imprinting. The goal of molecular imprinting is to synthesize a biomaterial capable of selectively binding a predetermined target molecule. This is accomplished by copolymerization of monomers with a cross-linking agent around a template to form a molecularly imprinted polymer (MIP). After the polymer is formed the template is removed and the voids left behind retain high affinity for the target molecule.[4-6] The concept of MIPs is well suited to the construction of tissue regeneration scaffolds. By tuning polymeric scaffolds to recognize key proteins like collagen, FN, or laminin the cellular interactions between the polymeric biomaterial and cells are improved; however, a major obstacle in the development of such MIP systems is nonspecific adsorption of unwanted proteins. Patterning of a non-fouling polymer to promote only the adsorption of a desired target protein offers a solution to this issue. Significant work has focused on the integration of 2-methacryloyloxyethyl phosphorylcholine (MPC) into a number of polymer systems in order to eliminate nonspecific protein adsorption.[7-9] MPC polymer mimics a natural cell membrane by integrating zwitterionic phorphorylcholine functionality onto a polymer backbone.[9] By patterning non-fouling MPC a great deal of control over cell and protein interactions is afforded. In addition, by controlling the dispersal of molecular recognition sites through the scaffold the spatial distribution of proteins and by extension cells can be tailored to correspond to that of natural tissue.[5, 6] Using this approach imprinted,

non-fouling MPC layers were pursued as a means to prepare tunable biomaterial coatings for the control of protein and cell interactions.

The integration of growth factors into bioactive systems is also a commonly employed method to elicit desired biological responses. Growth factors are biologically active chemicals that regulate cellular responses including cell proliferation, differentiation, and protein generation.[27] The integration of growth factors into a bioactive material has major applications in the field of tissue regeneration including the repair of bone defects and soft tissue replacement. Release of growth factors has been employed to increase the rate of bone renewal as well as promote cell migration along with improved angiogenesis.[27, 28] Thus, the inclusion of growth factors can improve the speed of wound healing as well as improve the overall quality of the resultant tissue compared to natural healing.

In addition to specific interactions derived from the inclusion of adhesion molecules and growth factors, more general physiochemical properties such as surface charge have also been exploited in the development of bioactive systems. For example, heparin possesses a strong negative charge, which enables it to act as an effective anti-coagulant but it can also promote or inhibit growth factor binding.[27] Moreover, this property is not limited to heparin but can be observed in a number of other materials granted that the surface is sufficiently sulfonated to produce a similar negative charge density. Through the inclusion of adhesion molecules and growth factors or via nonspecific methods like surface charge it is possible to produce biomaterials that behave in a well-defined manner. Using these

bioactive systems, biomaterials are able to elicit a more natural response thereby increasing to efficacy of the treatment.

2.2. Host Immune Response

The host immune response plays a significant role in material biocompatibility. The immune system is composed of a number of different mechanisms by which the body defends itself against foreign agents. While this system is primarily geared toward fighting infection by pathogenic organisms, certain aspects of the response must be considered with regards to implanted biomaterials. The immune system can be divided into two general categories known as the innate and the adaptive immune responses.[29]

The innate immune system encompasses a number of general immunological responses to foreign materials. These responses do not change based on the target nor does the intensity vary upon re-exposure to the same stimulus.[30] Upon entry into the body, foreign agents including biomaterials are quickly targeted by phagocytic cells like macrophages and dendritic cells.[29] This process is represented in Figure 2.1. These cells are programmed to identify, engulf, and digest foreign materials based on abnormal surface makeup or by recognition of opsonins bound to the surface. An opsonin is a designation given to proteins, which when bound increase the efficiency of phagocytosis.[30] Some common examples include the complement factor C3b and IgG, which is an antibody produced by B cells. This response is typically accompanied by local inflammation and swelling caused by leakage of cells, cytokines, and other proinflammatory substances from the blood

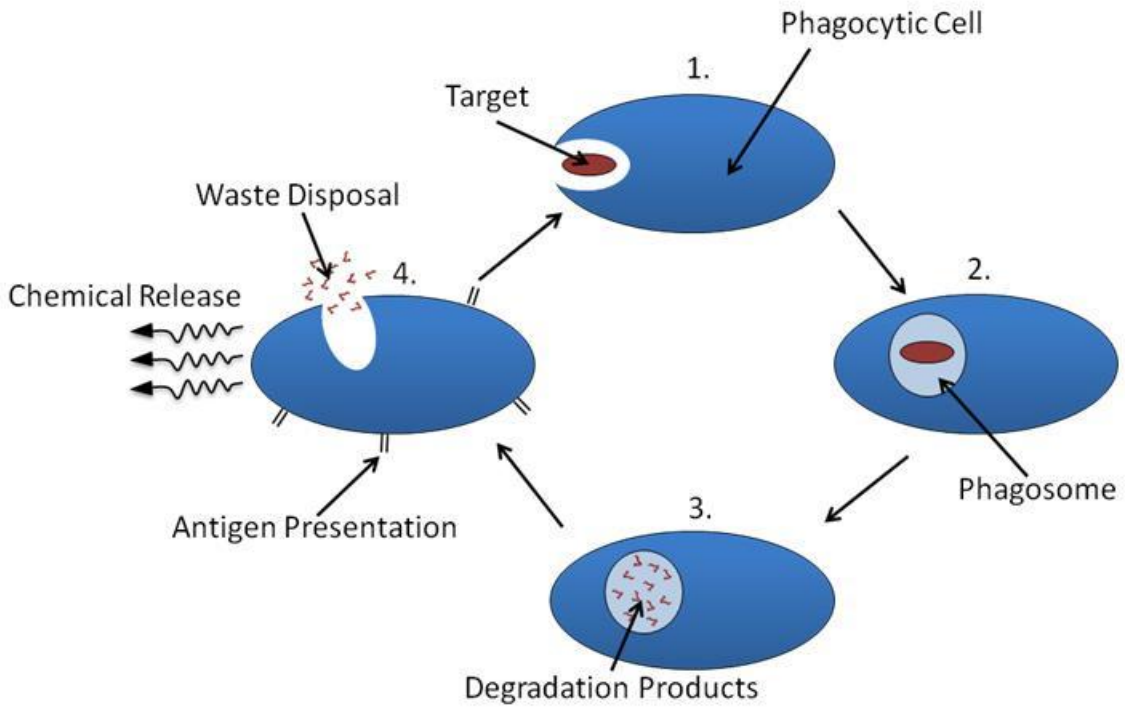

Figure 2.1: Schematic illustrating the process of phagocytosis. (1) The phagocytic cell (macrophage, dendritic cell, etc.) detects antigenic targets and engulfs the foreign agent, (2) once in the cell the target is contained inside a phagosome envelope, (3) the target is enzymatically degraded inside the phagosome, (4) waste products are expelled from the cell, portions of the target may be transported to the surface to present the antigens to other immune cells, and chemicals may be secreted to direct the immune response.

into nearby tissue. Cytokines are highly active chemical messengers that are particularly important because they impact both the innate and adaptive immune response.[29] They are secreted from phagocytic cells and immune cells and have diverse functions including inflammation, immune cell differentiation, and the generation of antimicrobial agents.[29] The presence of this inflammatory response promotes the migration of additional phagocytes to the affected area, allowing the body to better respond to the perceived threat; however, if the event is not quickly

resolved chronic inflammation can cause harm to normal tissues around the site. The migration of such phagocytic cells to the site of a biomaterial a major concern. It is thought that nonspecific adsorption and denaturation of serum proteins on a biomaterial surface as well as leeching of ions from metallic implants may play a role in the recruitment of these cells.[30]

In addition to phagocytic cells, there is a class of proteins found in the body known collectively as complement that acts in a number of ways to combat foreign agents. One serious consequence of the complement response is the lysis of targeted cells; however, more applicable to biomaterial biocompatibility is the coating of the surface with opsonins like complement factor C3b noted above as well as the recruitment of phagocytes.[31] Moreover, complement can lead to inflammation via widening of blood vessels accompanied by capillary leakage, can induce antibacterial activity through the induction of oxidative stresses, and is intimately interconnected with blood clot formation on biomaterial surfaces.[31, 32] It is hypothesized that complement factors may play a role in the adhesion of cells to blood-contacting implants and also instigate frustrated phagocytosis against biomaterials where degradative enzymes and high energy oxygen species are secreted at the surface, which could lead to inflammation and further immune response.[30] One other innate mechanism of note involves natural killer (NK) cells, which are nonspecific immune cells. NK cells are an important defense mechanism against intercellular pathogens because they are able to recognize changes on the surface of abnormal cells and as a response bind to and induce cell death referred to as apoptosis.[29]

The second type of immune response is the adaptive immune response, which unlike innate immunity is highly specific toward designated targets. For example, the blood of an individual recently recovered from measles contains high levels of antibodies against the measles virus; however, the same antibodies are ineffective against the closely related mumps virus.[29] Whereas the innate immune response is rapid and ubiquitous, the adaptive immune response requires time to ramp up and also changes and evolves to face each new perceived threat. The adaptive response can be subdivided into two categories: humoral and cell-mediated immunity. The humoral response is derived from globular, serum proteins known as antibodies and is focused on targeting extracellular agents while the cell-mediated response relies on specialized immune cells and is effective at targeting intercellular agents.[29] Both categories are overseen by specialized lymphocytes, which are a class of immune cells. B cells modulate the humoral response; these lymphocytes become active and differentiate into antibody secreting cells that recognize foreign agents. Such targets are often referred to as antigens and are typically either proteins or polysaccharides associated with a pathogen.[29]

Antibodies are a type of globular protein often referred to as an immunoglobulin. These proteins are composed of two types of polypeptide chains (heavy (50,000-70,000 daltons) and light (23,000 daltons)) that are linked to one another by disulfide bonds. The Fab region is highly variable and is responsible for the specificity of antibodies to their corresponding antigen targets. The Fc region is a constant region and its composition determines the body's response to antibodies

bound to a foreign agent. For example, the constant region of the IgM class of antibodies activates a component of the complement system while the constant region of IgG molecules possesses surface receptors for phagocytic cells.[29] A subset of the activated B cells remains after infection and retain a memory of a particular target, which allows for a stronger and more rapid response to re-infection.

T cells are another class of immune cells that oversees the cell-mediated immune response. Whereas B cells recognize whole antigens, T cells target antigen fragments displayed on the surface of other cells known as antigen presenting cells (APCs). Macrophages and dendritic cells are the primary APCs located throughout the body and as a result the innate and adaptive immune responses are closely related. When these phagocytic cells engulf and digest a foreign agent certain fragments are chosen and moved to the surface of the cell. These cells then migrate to nearby lymph nodes where T cells recognize the presented antigen fragment, activate and replicate to form T cells specific to the target in question. The active T cells seek out and destroy the foreign agent that expresses the specified antigenic target. These cytotoxic T cells are often accompanied by helper T cells, which act as APCs and are typically the driving force behind B cell activation associated with the humoral response. Like B cells, once the threat has been removed a subset of T cells remains with specificity toward the antigenic target in order to quickly respond to subsequent re-infection. This response is relevant to biomaterial biocompatibility; research has demonstrated that certain metals as well as polymers can induce adaptive immune cell based responses often referred to as hypersensitivity.[30] T cells isolated from patients hypersensitive to nickel responded to nickel presented

on the surface of APCs and likewise T cells from patients displaying similar hypersensitivity reacted to stimulation with metal ions.[30] Through a combination of innate and adaptive responses the body is able to mount a formidable defense against attack by pathogenic organisms. Unfortunately, the same mechanisms that defend from harm can also induce unwanted side effects in response to well intentioned biomaterial implants.

2.3. Biomaterial Hemocompatibility

The biological response toward a biomaterial in contact with blood is closely related to the host immune response. When developing a biomaterial it is important to understand how the components of the hematological response interact with the biomaterial as well as with one another in order to limit their effects. Several criteria define a hemocompatible biomaterial: The biomaterial should not induce the formation of blood clots, it should not result in hemolysis or complement activation, it should not produce chronic inflammation, it should not introduce wear particles or toxic substances into the surrounding environment, and it should suffer no inhibition of function.[33] Immediately upon exposure to blood, serum proteins begin to adsorb to the surface of a biomaterial. This milieu is composed of a multitude of components including fibrinogen, which is important to blood clot formation and platelet binding, FN that binds a number of cell types, IgG antibodies, which activate the complement system and bind lymphocytes, albumin that can passivate the surface against adverse reactions, complement factors, which initiate various complement responses, and coagulation factors that regulate clot formation

and resolution.[34] The hematological response to the biomaterial is dependent on the relative amounts of each of these diverse components as well as the manner in which each is adsorbed. As a consequence, protein adsorption is often examined to establish the relative hemocompatibility of a biomaterial.[34-45] An overview of the hematological response is shown in Figure 2.2. There are four primary proteolytic pathways that comprise the hematological response, which are complement activation, intrinsic pathway activation, extrinsic pathway activation, and fibrinolysis. Complement activation associated with blood coagulation works in a manner identical to the innate immune response. Some degradation products such as C3a are potent inflammatory agents while factors C5-C9 facilitate platelet adhesion and aggregation.[33] The extrinsic and intrinsic pathways are interconnected molecular pathways that are central in the formation of a stable fibrin network in a blood clot. Figure 2.3 illustrates the general mechanism for the extrinsic and intrinsic pathways. The extrinsic pathway is initiated by a transmembrane protein, tissue factor (TF), that is displayed on the surface of and liberated from platelets and leukocytes after to exposure to inflammatory stimuli or physical trauma.[46] A reaction between TF and cofactors set in motion a cascade of proteolytic reactions that result in the synthesis of thrombin, which cleaves fibrinogen into fibrin monomers. These monomers polymerize to form a fibrin network that provides physical support for blood clot formation.[33, 34, 43, 46] The intrinsic pathway proceeds in a similar manner to the extrinsic pathway; however, it is initiated by a surface mediated activation of clotting factor XII (FXII). FXII exists in the blood in an inactive form known as a zymogen, but when it adsorbs to a

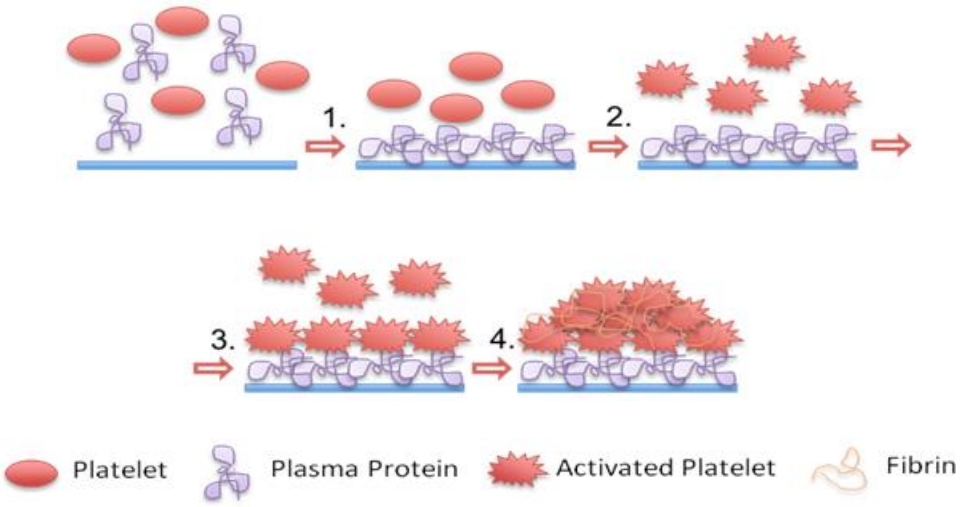

Figure 2.2: Overview of the hematological response. (1) Plasma proteins adsorb and change conformation, (2) proteins trigger thrombin generation and signal platelet activation, (3) activated platelets bind and activate more platelets along with other biological pathways, (4) fibrin network forms and a blood clot forms on the surface.

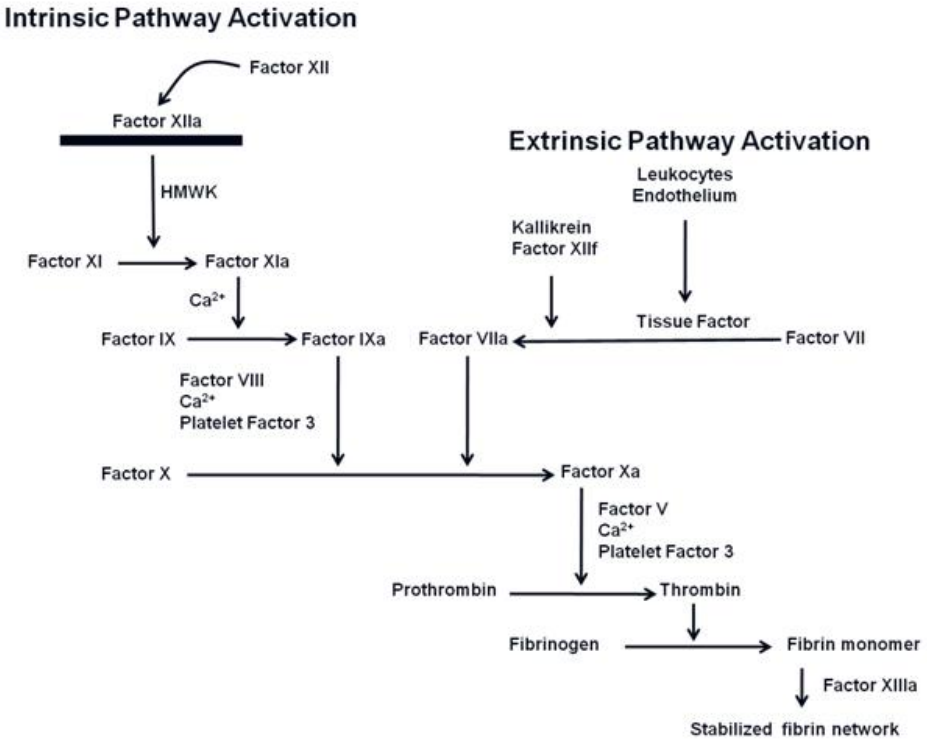

Figure 2.3: Intrinsic and extrinsic clotting pathways. Intrinsic activation initiated by adsorption and autoactivation of FXII. Extrinsic activation initiated by the release of TF and activation of FVII. Both cascades generate a stable crosslinked fibrin network for blood clot stabilization.

negatively charged surface it undergoes a conformation change producing an active product (FXIIa). FXIIa in turn promotes the conversion of inactive prekallikrein to kallikrein, which facilitates FXIIa formation in the presence of high-molecular-weight kininogen (HMWK).[33, 43] Thus, a positive feedback loop is creating amplifying intrinsic activity. The production of FXIIa begins a series of additional activation events resulting in thrombin generation and fibrin polymerization.[33, 34, 43, 46] The fourth important pathway is fibrinolysis, which exists to balance coagulation by the extrinsic and intrinsic pathways. Fibrinolysis is the process by which blood clots are broken down through the enzymatic degradation of the fibrin network by plasmin.[46] Plasmin is created through the conversion of plasminogen by either tissue-type plasminogen activator (t-PA) or urokinase-type plasminogen activator (u-PA). The two activators are produced in response to the coagulation cascade; t-PA is released from endothelial cells exposed to thrombin while u-PA is normally present as prourokinase and is subsequently activated due to the presence of plasmin and intrinsic pathway precursors. At the same time, t-PA and u-PA are regulated by the presence of plasminogen activation inhibitors (PAIs).[46] In addition to these humoral responses cellular interactions play an important role in the hematological response to a biomaterial the most important of which is the involvement of platelets. Platelets are activated by the thrombin generated during coagulation and as a result bind to surface adsorbed fibrinogen proteins. These activated platelets secrete an array of clotting factors that activate additional platelets, increase clotting, and cause inflammation. In addition, changes occur in the structure of activated platelets resulting in a more negatively charged surface,

which facilitates the surface activated events associated with the intrinsic pathway.[33, 39, 43] The activation and subsequent aggregation of platelets at the surface of a biomaterial is an important indicator of a hematological response and is commonly analyzed along with the previously mentioned humoral responses to determine the hemocompatibility of a biomaterial.[35, 37-43, 45, 47, 48] By attenuating protein adsorption, intrinsic pathway activation, and/or platelet activation is may be possible to increase surface hemocompatibility.

2.4. *Treponema pallidum* and Antigenic Disguise

Syphilis is a chronic, multi-stage, sexually transmitted disease caused by the spirochete bacterium *Treponema pallidum.* The invasiveness of *T. pallidum* combined with its ability to thrive in the face of the host immune response are well documented.[1-3] The structure and composition of the outer membrane of *T. pallidum* differs greatly from typical gram negative bacteria; the outer membrane of *T. pallidum* is a fragile and fluid layer that lacks lipopolysaccharide (LPS), a common feature of most gram negative bacteria, as well as surface proteins.[49, 50] LPS is a potent inflammatory agent that is a major contributor in the immune response to pathogenic organisms.[49, 50] *T. pallidum's* unique outer membrane is thought to play a central role in the ability of the bacteria to evade the immune response and establish a chronic infection.[50-58] The surface of *T. pallidum* possesses less than 1% of the number of proteins commonly found on the surface of *E. coli*.[59, 60] Past research has suggested that there are a number of outer membrane proteins (OMPs) on the surface of *T. pallidum* based on interactions with whole bacteria but these

studies did not present definitive evidence. Some of these candidates are a laminin-binding protein labeled Tp0751, a FN- and laminin binding protein labeled Tp0136, and a protein labeled TprK, which was shown to induce the production of opsonic antibodies.[51, 61, 62] Recently, the first definitive evidence of a *T. pallidum* surface protein was confirmed. The protein is a barrel assembly machinery protein A (BamA), Tp0326, and is associated with outer membrane maintenance.[50] Because of the paucity of antigenic targets *T. pallidum* has earned the name the "stealth pathogen".[1, 56] Despite this well earned reputation, the bacteria elicits a robust immune response during the primary stage of infection, after which it enters a latent phase characterized by periodic reoccurrence of disease symptoms. The initial immune response is likely due to recognition of one or more antigenic outer membrane proteins OMPs on the bacteria, but it remains unclear why a subset of the bacteria are able to persist within the host and produce a secondary infection at a later time.[51, 54-58] TprK was shown to undergo sequence variation, which may contribute to immunoevasiveness and it has also been shown that antibody generation against Tp0326 is not sufficient to eliminate *T. pallidum*.[58, 61, 62] For Tp0326, antibodies produced in a rabbit host were able to bind to the protein but antibodies produced in a human were directed at an inaccessible portion of the protein, which rendered them ineffective.[50] These results suggest that *T. pallidum* may adapt and change over time in answer to the host immune response.

FN is a dimeric glycoprotein with a molecular weight of approximately 440 kDa that is involved with cell adhesion to the ECM as well as wound healing, cell proliferation, and cell differentiation.[63] It is a common protein found in the blood as

well as in the ECM. A number of proteins of the integrin family as well as a number of other biologically important molecules including fibrin, collagen, and heparin are known to interact with FN.[63] A schematic of the protein structure is shown in Figure 2.4. FN is divided into three distinct component regions labeled I, II, and III.[63] Numerous studies have suggested that the RGD peptide sequence located in the 10th type III domain of FN plays a significant role in *T. pallidum* adhesion along with the adjacent PHSRN site found in the FIII9 domain.[64-67] Prior studies have also suggested that the FIII7 and FIII8 domains may influence binding as well.[68] All of these sites fall within what is known as the central cell-binding domain of FN (CCBD).[63] It has also been demonstrated that FN facilitates the binding of different species of bacteria through a number of other sites including the heparin and collagen/gelatin-binding domains.[70, 71]

Studies have shown that *T. pallidum* binds to a number of ECM components, including FN, as a method of adherence and infiltration through tissue.[51-53, 64, 72, 73] One explanation of *T. pallidum's* resistance to antibodies and immune cells is that host proteins bind to exposed antigens and render them inaccessible to host defenses. The ability of a pathogen to interface with components of the host in order to conceal itself from detection is referred to as antigenic disguise as shown in Figure 2.5. The ability to conceal potential antigens combined with the relative paucity of exposed targets in general could account for the considerable immunoevasiveness of the bacteria. FN is a part of the host and thus it exists external to *T. pallidum*. In order for FN to bind to *T. pallidum* and induce antigenic disguise any FN binding proteins must logically be located on the surface of the

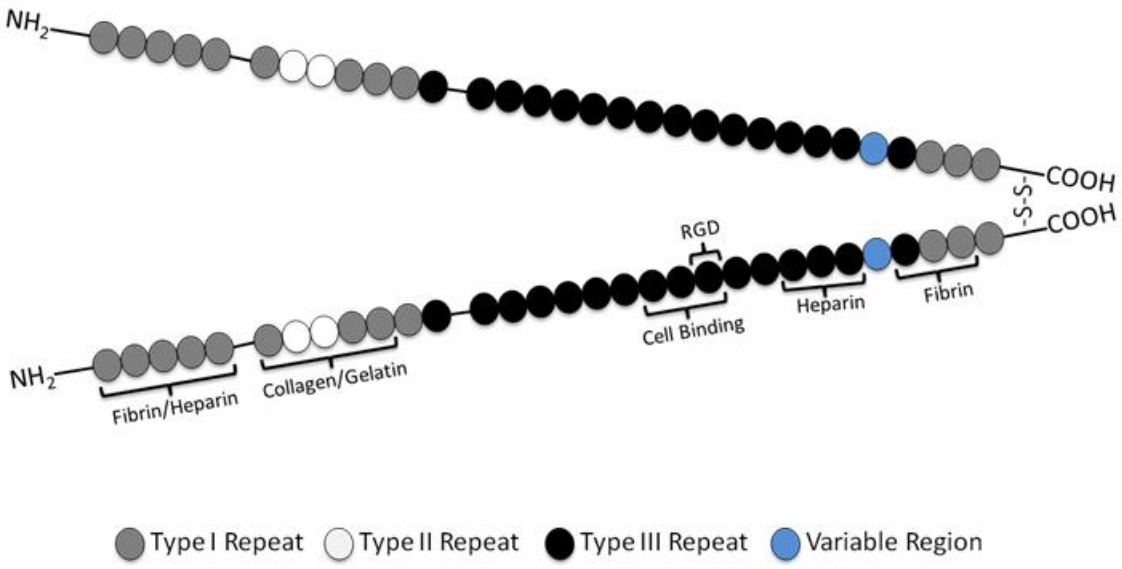

Figure 2.4: Structural diagram of FN. FN is a dimeric protein with two nearly identical subunits capable of binding a wide range of biologically relevant molecules. Important binding domains are indicated above. (Adapted from Zhang *et al.* 2007)[69]

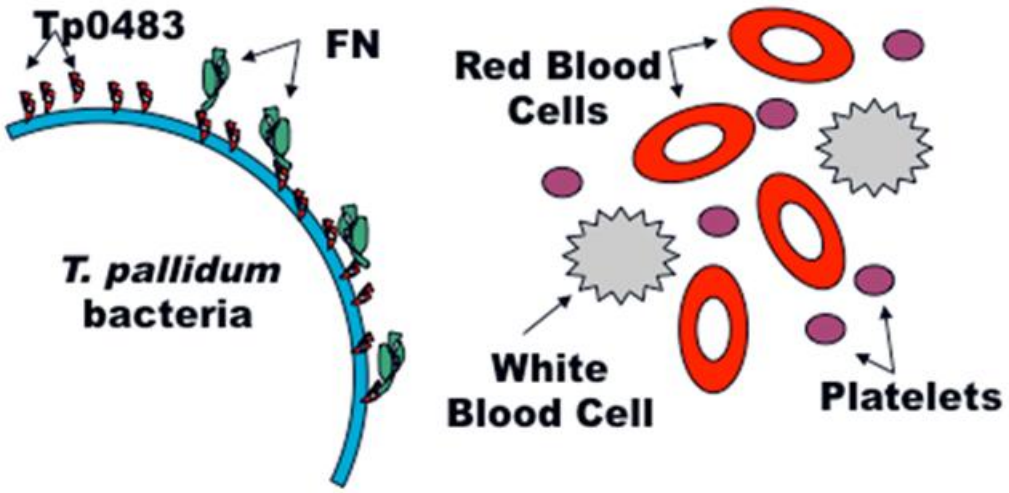

Figure 2.5: Illustration of the ability of *T. pallidum* to coat itself with host FN to circumvent an immune response (antigenic disguise).

bacteria. In a study by Cameron *et al.* two putative outer membrane proteins of *T. pallidum* capable of binding FN, identified as Tp0483 and Tp0155. When expressed in a recombinant system the structure of whole Tp0483 and Tp0155 was unstable. Stability was greatly improved while retaining an affinity for FN when each were expressed as recombinant N-terminal and C-terminal fragments.[53] In addition, work by Brinkman *et al.* identified a third putative membrane protein (Tp0136) that demonstrated similar affinity for the ECM components FN and laminin.[51] While Tp0483, Tp0155, and Tp0136 all bound insoluble ECM FN, only Tp0483 showed an affinity for soluble FN.[53] Binding of ECM FN can be reasonably assumed to be for the purpose of host attachment and tissue infiltration; however, the advantage conferred by soluble FN binding to *T. pallidum* remains unclear. It is postulated that soluble FN is bound for the purpose of obscuring exposed antigenic targets from detection. Such an event was postulated in a study by Lukehart *et al.* as one possible explanation for the resistance to phagocytosis by a subset of *T. pallidum*.[74] Comparable properties have been observed for hepatitis A virus and group A *Streptococcus* where host proteins are used to mask surface antigens.[75, 76] Such an event could help to explain how *T. pallidum* is able to persist after the resolution of the primary infection. Determination of the role of recombinant protein fragment rTp0483 with serum FN in *T. pallidum* antigenic disguise would facilitate a better understanding of the pathophysiology of the bacteria and could potentially aid in the development of a more effective treatment for syphilis. Furthermore, mimicry of *T. pallidum* antigenic disguise may be applied to produce a hemocompatible surface coating. As detailed in Section 2.1.1, hydrophilic polymer coatings do not

entirely prevent protein adsorption and over time their anti-fouling properties degrade. In fact, no coating currently exists that can repel 100% of protein adsorption so it makes more sense to control the type and manner of protein adsorption rather than try and prevent it completely. *T. pallidum* is thought to possess the ability to conceal itself from the host immune response via OMPs that bind host proteins like FN. Based on this, it is postulated that immobilized rTp0483 with FN retains the antigenic disguise property of whole bacteria and using this approach it is possible to reduce or eliminate adverse host reactions to the protein-coated material leading to improved hemocompatibility and biocompatibility.

Chapter 3: EXPERIMENTAL TECHNIQUES AND KINETIC MODELING APPROACHES

3.1. Quartz Crystal Microbalance with Dissipation

A quartz crystal microbalance (QCM) is a sensitive analysis technique used to investigate the adsorption of molecules including proteins, polysaccharides, and DNA at solid-liquid interfaces.[77-80] An electrical voltage is applied to a quartz sensing crystal, which induces the quartz crystal to oscillate at a specific frequency inherent to the crystal. Adsorbed materials shift the resonant frequency, thus by measuring the frequency change it is possible to determine the surface mass density of adsorbed material as seen in Figure 3.1. This overview focuses on the Q-Sense E4 QCM with dissipation (QCM-D) from Biolin Scientific (Linthicum, MD), which is shown in Figure 3.2. The E4 has four independent flow cells than can be analyzed in parallel or separately; however, for the sake of simplicity only one is shown in the illustration. Buffer solution is circulated through the system during operation; a pump allows the flow rate to be controlled. Liquid passes through the system once and is collected in a waste container. Q-sense control software on the linked computer is able to control the temperature inside the flow cells and it records frequency and dissipation energy change as a function of time. To load a sample for analysis the pump is stopped and the tubing moved from the buffer to the sample container and the flow restarted. After the desired time the pump is stopped again and the tubing moved back to buffer.

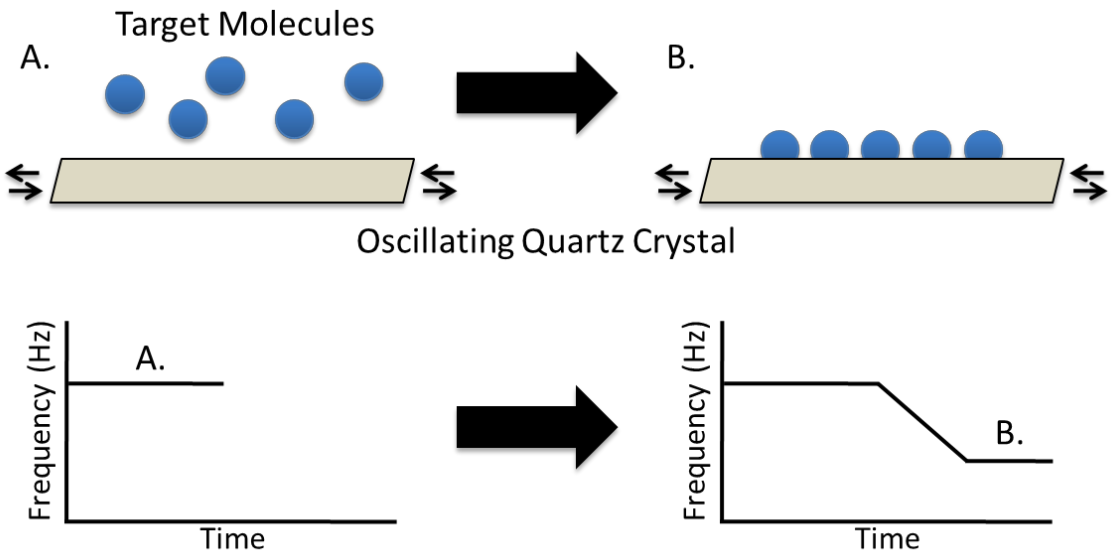

Figure 3.1: Illustration of the frequency shift that accompanies adsorption to the surface of an oscillating quartz crystal. (A) The crystal oscillates at a base frequency, (B) when molecules from solution bind the frequency at which the crystal oscillates decreases.

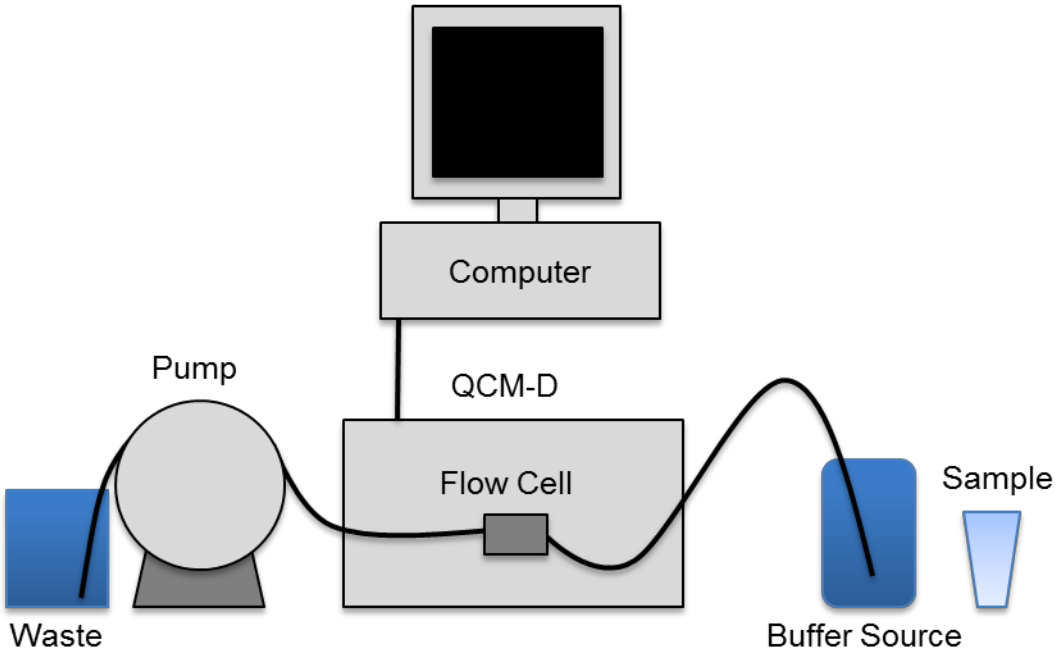

Figure 3.2: Schematic of Q-Sense E4 instrumentation. Buffer and samples are draw through the QCM-D flow cell using a pump while a linked computer controls temperature and records frequency and dissipation energy changes.

In addition to the normal functions of a QCM, a QCM-D system is able to discern the viscoelastic properties of the adsorbed layer by applying voltage in a pulsile manner and measuring the time required for the oscillation to decay.[77-80] Any change in resonant frequency is measured in hertz (Hz) and the viscoelastic properties are determined by measuring dissipation energy (D). Dissipation energy is the sum of all energy lost from the system during a single oscillation divided by the total energy in the system. Physical properties such as hydration and layer fluidity can lead to increases in the dissipation energy of a sample and, based on this, it is possible to compare the binding state of proteins on different surfaces. This process is shown in Figure 3.3. A simple Sauerbrey equation can be employed to estimate the surface mass density of the adsorbed layer by assuming that it is homogeneous and rigid with a no slip condition between the gold layer and adsorbed protein (Equation 1).[77, 78] To fulfill these conditions, dissipation energy of less than 10^{-5} is required.[78]

$$\Gamma = -\frac{C}{n}\Delta f \quad (1)$$

Here, Γ is the surface mass density (pg/mm^2), n is the QCM overtone (n = 1, 3, 5, etc.), and C is a constant for a quartz crystal of a specified resonant frequency. Overtone refers to the oscillation frequency of the QCM crystal relative to its fundamental frequency. The fundamental frequency of a typical quartz crystal is 5 MHz and C = 177 pg/Hz•mm^2. So for example, the 3rd overtone corresponds to three times the fundamental frequency or 15 MHz. Moreover, when dissipation

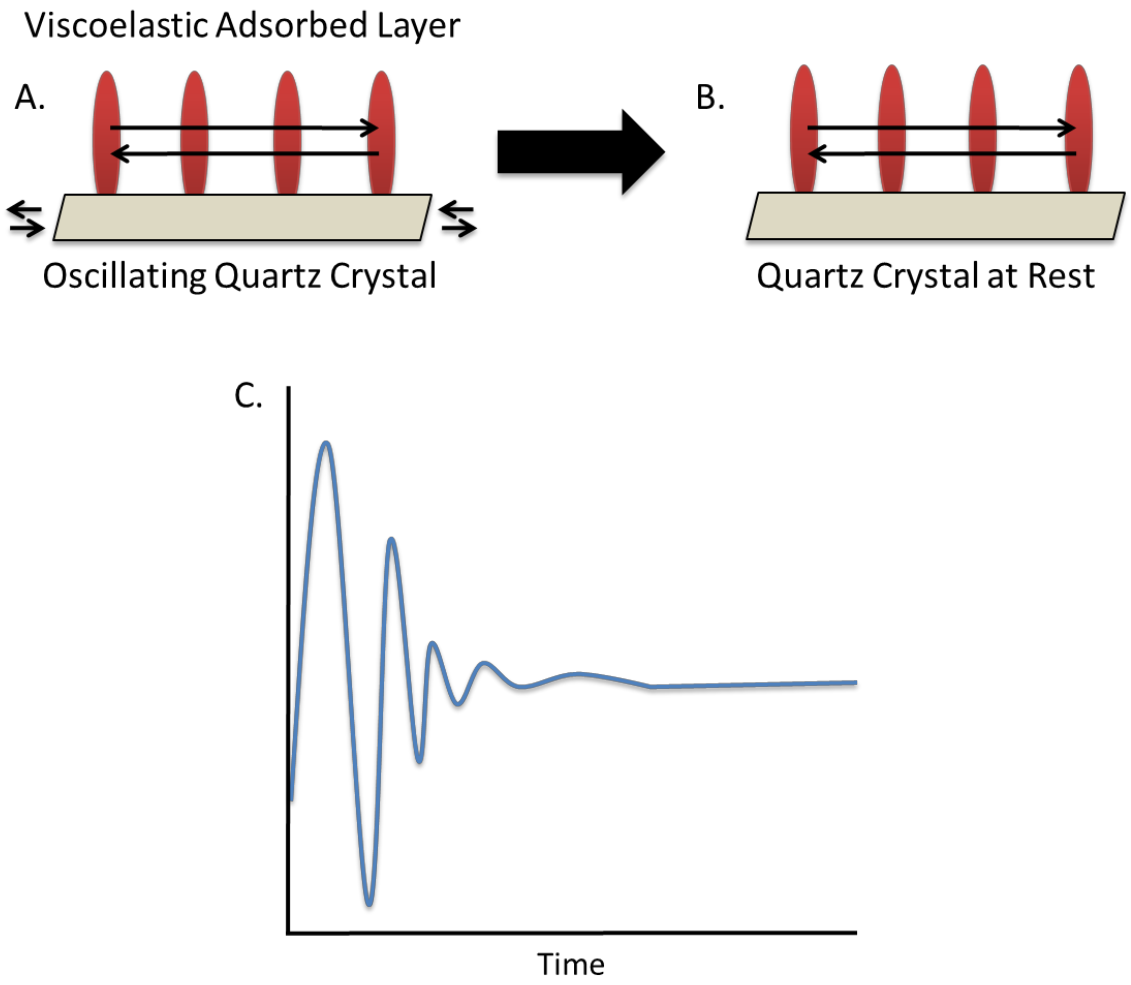

Figure 3.3: Illustration of dissipation energy determination in QCM-D. (A) A viscoelastic layer is adsorbed onto an oscillating quartz crystal, (B) the applied voltage is removed from the quartz crystal allowing it to return to rest, (C) the adsorbed layer continues to oscillate for some time after the crystal returns to rest. This time is measured and used to calculate the dissipation energy of the adsorbed layer.

energy is low, it can be assumed that the deviation between overtones is negligible and data gathered from higher overtones used in place of lower to increase the signal to noise ratio. A diverse range of coated quartz crystals is produced to facilitate the immobilization of molecules on the surface to the crystal. Coated

quartz crystals give the QCM-D technique a great deal of customizability for the user to develop an assay to suit their needs.

3.2. Surface Plasmon Resonance (SPR)

Surface plasmon resonance (SPR) is a refractive index based technique useful in the analysis of binding of an analyte molecule from solution either to an immobilized ligand molecule or directly to a surface in real time. SPR has been employed to analyze a wide variety of biological relevant binding events.[81-83] Because the measurements are in real time it is possible to extract adsorption data and model the kinetics of adsorption and dissociation. A schematic of the process is shown in Figure 3.4.

The principle underlying SPR is based on the reflection of light at the interface of two transparent materials with different refractive indices. A beam of near-infrared (IR) light is focused through a prism, reflected off of a layer of glass in contact with a thin layer of metal (typically gold), and collected at a detector. When the beam of light strikes the metallic surface at a specific angle, known as the SPR angle, electrons located at the interface enter a resonant state, which leads to the propagation of short-range evanescent waves from the surface through any adsorbed materials. As a consequence, there is a measureable decrease in the intensity of reflected light at the SPR angle, which is measured by the detector. The SPR angle is affected by a number of parameters most important of which are the refractive indices of the materials used, the type of metal used to induce

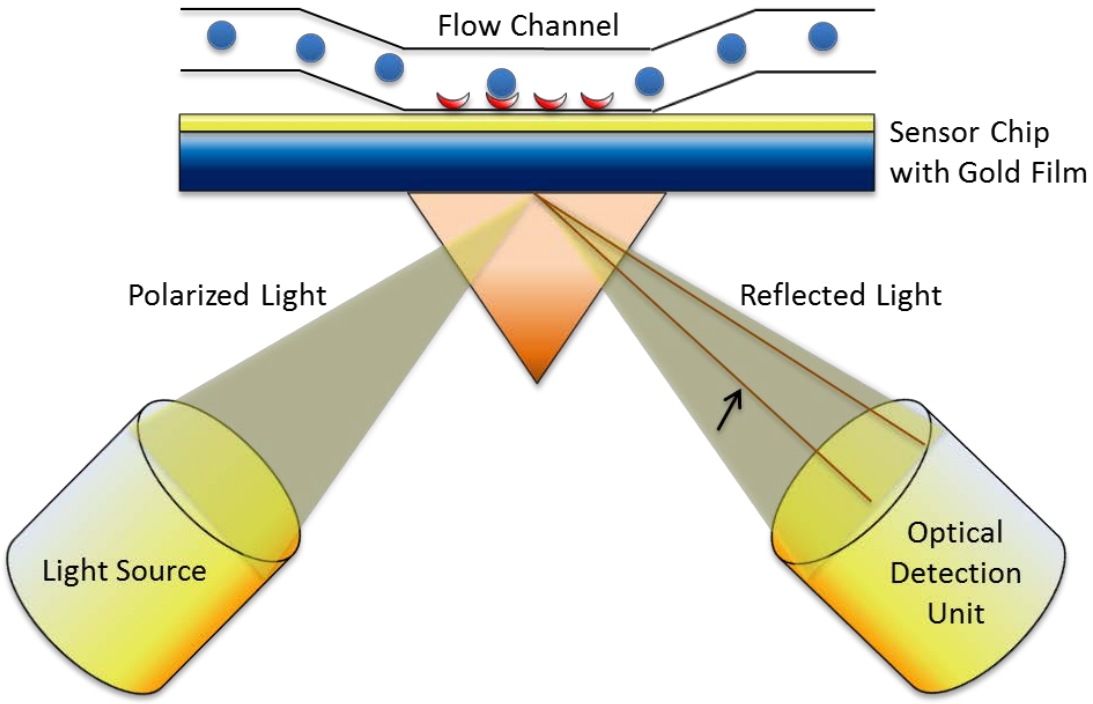

Figure 3.4: Schematic of the SPR process: near-IR light beam focused through a prism, reflected off of a gold-coated surface, and collected for analysis. At the SPR angle, which is dependent on the surface mass density of adsorbed material, there is a measureable loss in light intensity. The change in the SPR angle is measured and related to the change in surface mass density.

plasmon resonance, and the surface mass density of materials adsorbed at the interface. For a specific system the refractive indices and the type of metal are predetermined and unchanging; thus, any change in SPR angle can be directly related to a change in surface mass density.

One of the leading manufacturers of SPR instruments is Biacore AB (Uppsala, Sweden). The instrument used for experimentation was the Biacore X unit, which possesses two individual channels denoted as flow channel 1 (FC1) and flow channel 2 (FC2). This allows for measurement and

subtraction of background noise simultaneously with an experiment and for each surface to be used for two separate trials. Figure 3.5 illustrates the components that compose the Biacore X system while Figure 3.6 shows a schematic of the potential flow patterns the Biacore X is capable of producing. All aspects of the Biacore X are controlled through Biacore software located on the linked computer system. Liquid flow is modulated through a syringe pump while the pressure in the system is regulated by an external pump system. Temperature, flow rate, pressure, and the SPR response of a surface are all monitored in real time by the computer software package.

Prior to testing, the gold-coated glass chips (Biacore) can be functionalized with the ligand of interest much like coated QCM crystals. A number of ligand immobilization strategies exist ranging from chemical bonding to physical adsorption. Once ready for analysis, the gold-coated glass surface is mounted onto a plastic support slide using adhesive tape and inserted into the instrument. After being docked, the chosen analyte solution is introduced at the injection port, passed through one or both flow cells, and the response measured. Any change in SPR signal is measured in response units (RU), where a change of 1 RU was equivalent to a change of 1 pg/mm^2 of protein on the surface.[84] A sample SPR response (sensorgram) is shown in Figure 3.7; by subtracting the response prior to the injection of analyte from the value afterward it is possible to determine the amount of analyte that bound to the immobilized ligand.

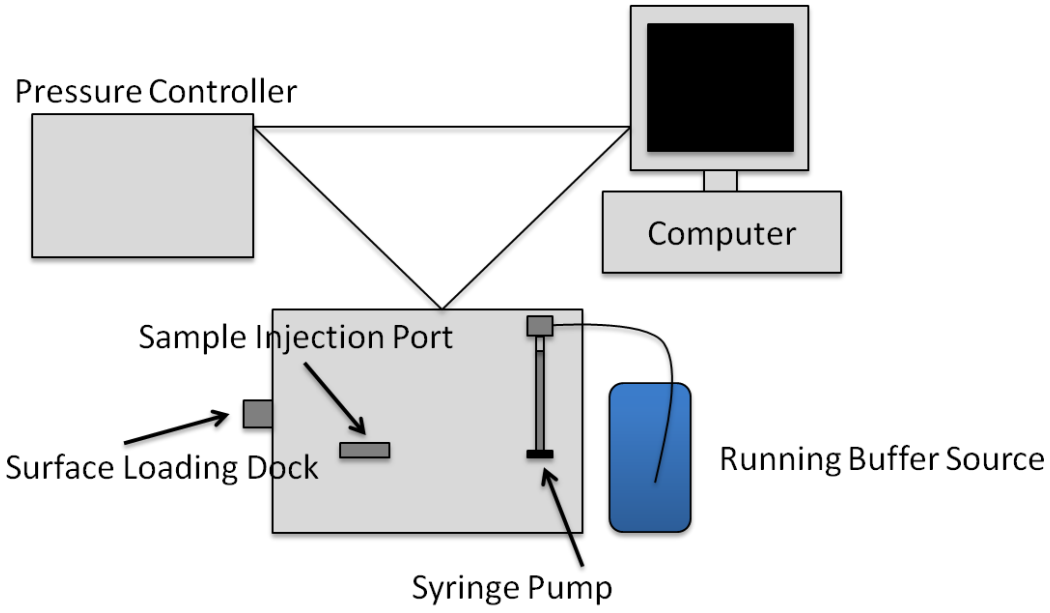

Figure 3.5: Schematic of Biacore X instrumentation. Running buffer constantly circulates through the system. Flow rate, temperature, and pressure are controlled by computer software. A sample is injected into the sample injection port and flow through one or both flow cells. The SPR response is measured in RU and displayed on the computer as a function of time.

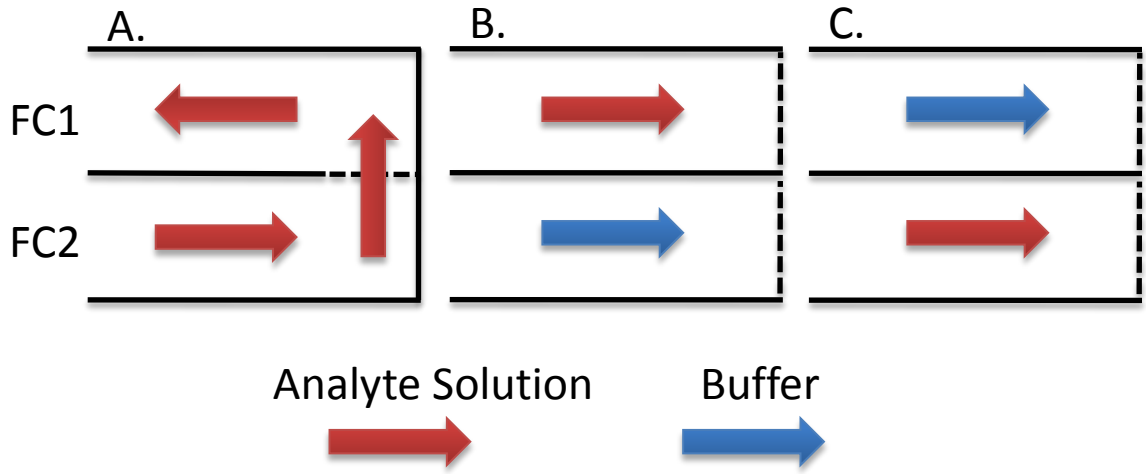

Figure 3.6: Schematic of available BIACORE X flow configurations. (A) FC1-2 (analyte flows through both FCs in series), (B) FC1 (analyte injected into FC1), (C) FC2- (analyte injected into FC2).

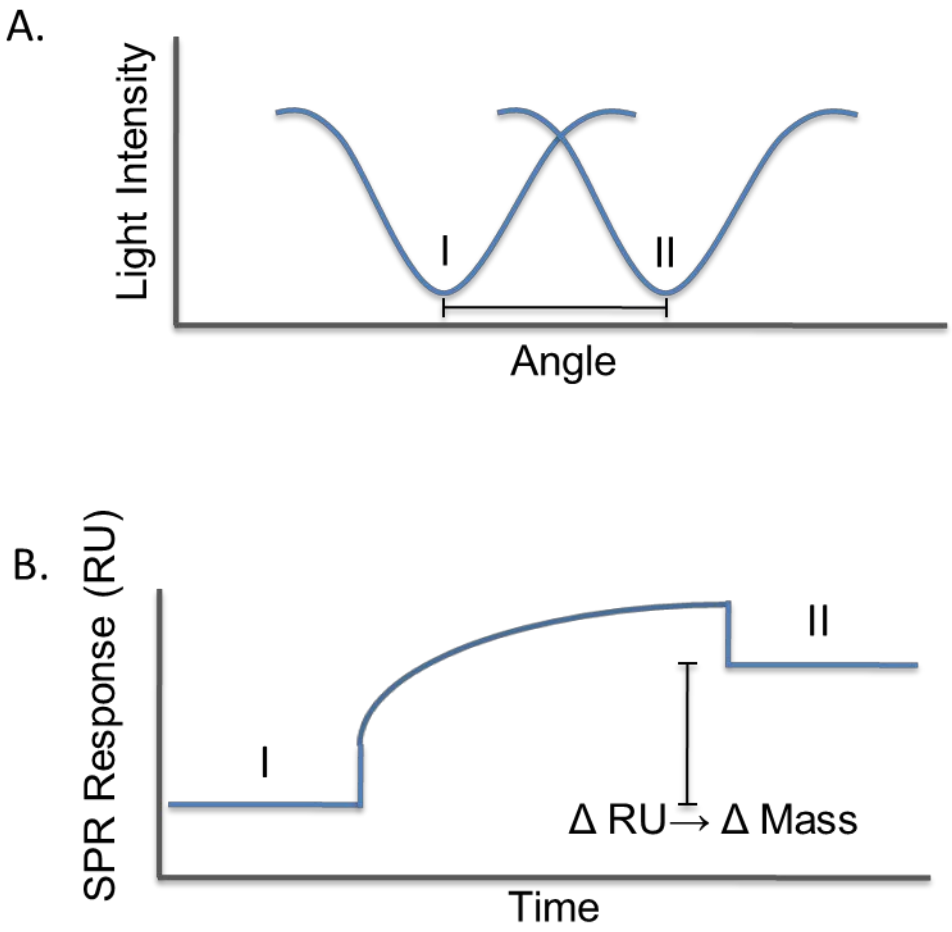

Figure 3.7: Overview of SPR data collection. (A) Schematic illustrating the shift in SPR angle as the surface mass density changes (SPR angle corresponds with the angle where the intensity of reflected light is lowest), (B) Sample sensorgram depicting the change in mass surface density as a function of SPR response in RUs over time. The two quantities are related by the following conversion: 1 RU = 1 pg/mm^2.

3.3. Atomic Force Microscopy

Atomic force microscopy (AFM) is a topographical mapping technique that can be used in a number of different working environments including open atmosphere, vaccum, and in solution.[85-88] AFM is the only technique currently capable of producing resolutions on the sub-nanometer scale in a liquid

environment.[85] For this reason it is an attractive method of mapping the topography of surface adsorbed proteins as well as cells.[69, 88-90] Work by Zhang *et al.* compared the structure of chemically conjugated and physically adsorbed FN on polyethylene terephthalate surfaces.[69] Another study by Ge *et al.* analyzed astrocyte cell monolayers as well as fresh tissue samples using AFM. [88] In AFM a cantilever is moved across a surface and the force between the surface and the cantilever analyzed; a laser is reflected off of the back of the cantilever, as shown in Figure 3.8, in order to determine the deflection of the cantilever. The force between the cantilever and surface can found indirectly from Hook's law (F=-kx), where F is the force between cantilever and surface, k is the cantilever spring constant, and x is the deflection distance. The cantilever can either physically contact the surface, or stop just short of the surface as shown in Figure 3.9. Contact mode applies a constant force as the cantilever moves across the surface. This technique is used when damage to the surface as a consequence of applied forces is not a concern or when the response of a sample to an applied force is being investigated. Non-contacting mode is used when the target is unstable or delicate such as is the case for many biological samples. In some cases, an intermittent contact mode may also be employed by tapping the surface lightly with the cantilever tip. With both approaches the cantilever is vibrated at a selected frequency and forces determined based on the effect the surface has on this resonance. These approaches allow for mapping while preserving the integrity of the materials being examined.

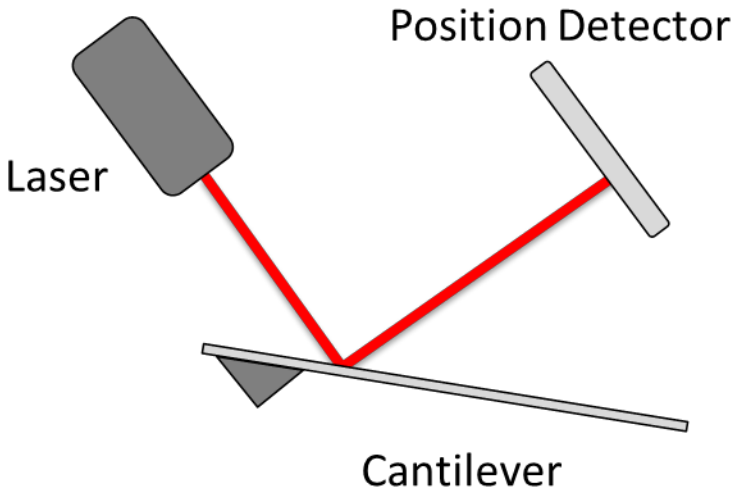

Figure 3.8: Illustration of laser based force measurement during AFM analysis. Force between the cantilever and surface is calculated based on the stiffness of the cantilever and the distance that the cantilever is deflected.

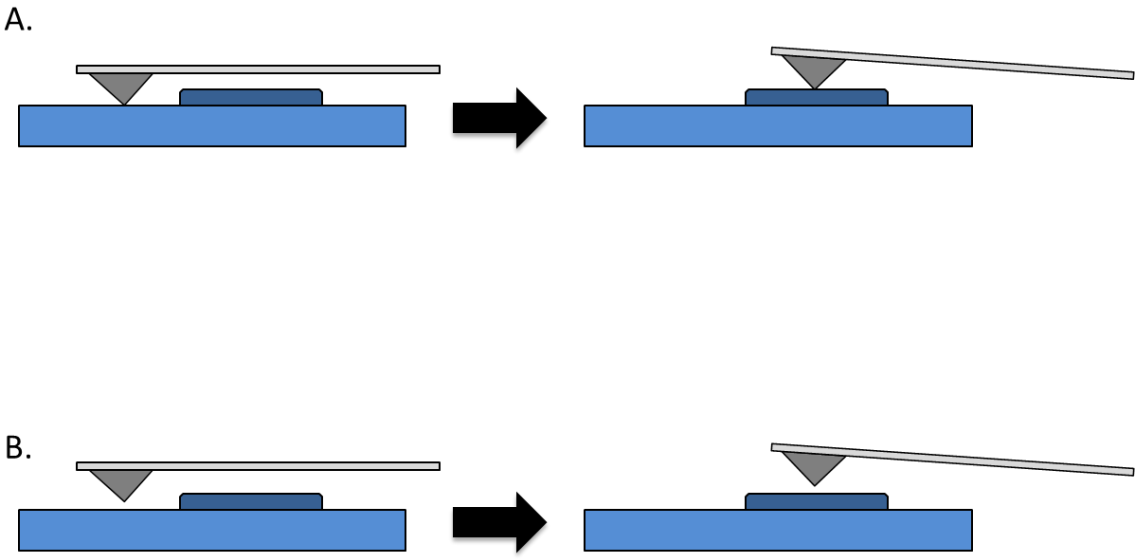

Figure 3.9: Schematic shows the operation of contact and non-contact AFM. (A) In contact AFM the cantilever tip is in direct contact with the surface and deflection is largely in response to topographic features, (B) in non-contact AFM the cantilever never makes contact with the surface and deflection is entirely based on the forces between the tip and surface.

3.4. Flow Cytometry

Flow cytometry is an analysis technique used to investigate multiple physical characteristics of micron sized particles, typically cells, as they flow through a beam of light. Such characteristics as particle size, internal granularity, and fluorescence can be quickly measured for large populations of cells. Figure 3.10 illustrates the general layout of the LSRII flow cytometry unit from BD Sciences (Franklin Lakes, NJ) that is discussed here. BD FACSDiva 6.1.3 software located on a linked computer system controls the system. Collection of side-scattered light (SSC), forward-scattered light (FSC), and fluorescence can be calibrated as well as the number of cells to be analyzed. Samples are prepared in compatible test tubes, which are loaded into the cytometer. An integrated flow system draws the sample from the test tube and through the instrument. Cells are sorted into a single file line that passes through a beam of light where detectors measure SSC, FSC, and any fluorescent light produced by the sample as shown in Figure 3.11. FSC is the portion of light that is diffracted but still travels in a largely straight line; it is an indicator of the size of the sample. SSC is measured at a 90° angle to the beam of light. SSC is the light that is reflected within the sample and is related to the internal granulation and complexity of the sample. Also of note is that that population of cells analyzed needs not be homogenous. Based on the physical characteristics of the sample flow cytometry analysis can differentiate between multiple cell populations within a heterogenous mix. In a study by Autissier *et al.* the relative amounts of monocytes, lymphocytes, and dendritic cells were investigated in a rhesus macaque model in order to better understand how these immune cells react to simian

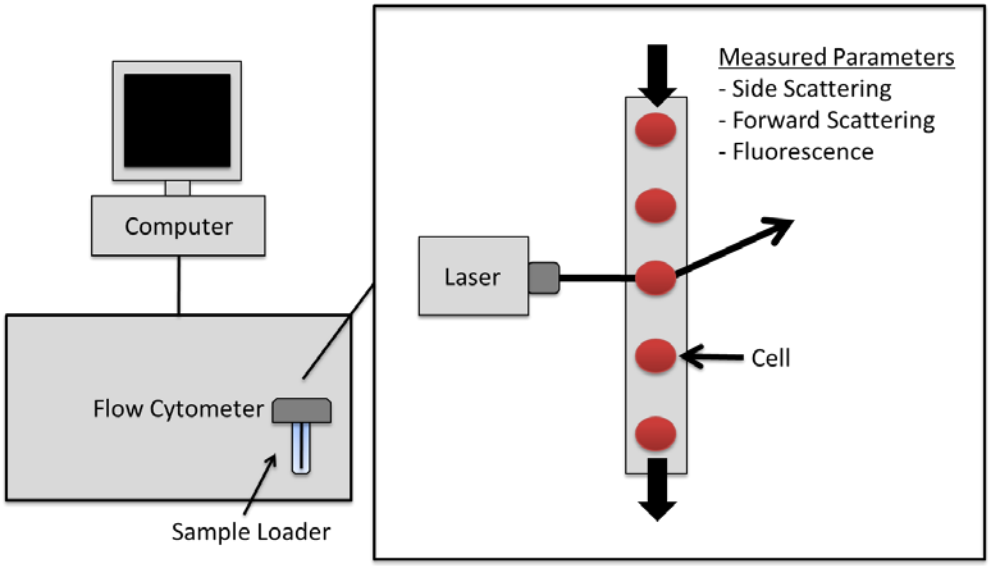

Figure 3.10: Schematic of AFM instrumentation. Sample loaded and the system automatically pulls it through the system. FSC, SSC, and fluorescence detectors calibrated via computer software. In the core cells are organized into a single file line, which passes through a beam of light. Detectors record FSC, SSC, and fluorescence intensity at set wavelengths.

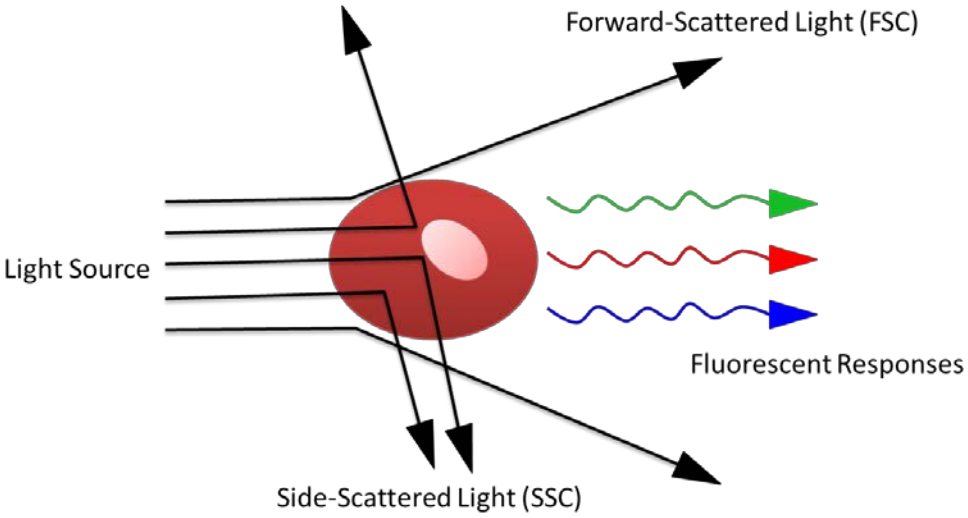

Figure 3.11: Illustration of single cell flow cytometric analysis. A light source is focused on a cell and the response recorded. Some light is refracted but still travels forward (FSC) and is related to the size of the sample. Other light is reflected within the sample (SSC) and can be used to determine the relative internal complexity of the sample. Fluorescent excitation of the sample can also be recorded, which can be used to track biological events and detect biomolecules using fluorescent labels.

immunodeficiency virus (SIV) with the hope of extending the findings to the treatment of AIDS.[91] Flow cytometry can also be used to identify biomolecules on the surface of cells using fluorescent labeling and to visualize biological responses like cell cytotoxicity and phagocytosis. A study by Dyer *et al.* used flow cytometry to identify eosinophils in mouse tissues using fluorescent antibodies specific to a surface receptor.[92] Eosinophils are cells recruited by inflammatory agents and which plays a role in allergic and hypersensitivity responses.[92] In another work by Kim *et al.* flow cytometry was used to track the cytotoxicity of NK cells toward cancer cells by loading the cancer cells with a dye then tracking its release as a consequence of apoptosis by NK cells.[93] At the same time, Kim *et al.* investigated the expression of biomarkers on the surface of the NK cells associated with cell lysis.[93]

3.5. Protein Adsorption Kinetics

The kinetics of protein adsorption play an important role in the function of the protein once bound. Often, protein activity is affected due to changes in the conformation of the adsorbed protein or non-optimal orientation.[94] This is especially important when an adsorbed protein is expected to elicit a biological response or interact in a specific fashion with another molecule. An understanding of adsorption kinetics allows for the intelligent design of materials that result in optimal protein function. For the purposes of this work a Biacore X SPR spectrometer was employed in the investigation of protein adsorption kinetics. This platform provides a controlled environment with consistent environmental conditions in order to accurately determine kinetic parameters. For determination

of adsorption kinetics a high flow rate across the surface is suggested along with a relatively low amount of protein in solution.[95] When the affinity between a protein and a surface is very high it is possible that the mass transport of protein from bulk solution to the liquid-solid interface may be slower than adsorption. This can also be the case when there are a large number of active binding sites located on the surface. Increasing the flow rate over the surface increases the rate of mass transfer while reducing the amount of protein in solution decreases the rate of adsorption. Alteration of one of both of these parameters is often enough to eliminate mass transport effects; however, if they persist there are methods to account for the effects, which are detailed in the modeling overview below.

Three models of protein adsorption kinetics will be reviewed. The first of the three is a simple 1:1 Langmuir binding model of a protein to a surface. The second is a 1:1 Langmuir model that takes into account potential mass transport effects. The third model is a bivalent analyte model, which assumes a two step binding event.

3.5.1. 1:1 Langmuir Binding

The binding kinetics for 1:1 Langmuir binding are represented in Equation 2 and the related rate equations are summarized in Equations 3 and 4. *A* is a molecule in solution, *B* is a binding site on the surface, and *AB* is a protein *A* bound to site *B* on the surface. In a 1:1 Langmuir binding event a single protein molecule binds with a single binding site on the surface. The bulk concentration of *A* is assumed to be

constant thus the rate equations are written with respect to the change in the number of occupied sites on the surface.

$$A + B \Leftrightarrow AB \quad (2)$$

$$\frac{\partial[B]}{\partial t} = -\left(k_a[A][B] - k_d[AB]\right) \quad (3)$$

$$\frac{\partial[AB]}{\partial t} = k_a[A][B] - k_d[AB] \quad (4)$$

The injected concentration of *A* is known, and the number of occupied sites is assumed to be zero initially ($[AB]_0$=0). The maximum binding capacity (R_{max}) is determined empirically for each surface and assumed to be equal to the number of sites *B* initially ($[B]_0$=R_{max}). The forward reaction is regulated by the rate constant k_a while the reverse reaction is regulated by the rate constant k_d. BIAevaluation software v3.0.2 program is then used to calculate adsorption and dissociation kinetics by fitting experimentally obtained SPR adsorption data.

3.5.2. 1:1 Langmuir Binding with Mass Transport Limitations

In this model, the basic 1:1 Langmuir model is modified to account for limitations in the transfer of *A* from bulk solution to the surface. Equations 5 and 6 illustrate the modified process. When mass transport limitations are accounted for adsorption becomes a two-step process. First, *A* moves from the bulk solution to the surface and once it arrives it binds to *B.* The impact on adsorption kinetics is accounted for through the addition of an extra term in Equation 7 including a mass

transfer coefficient (k_t) along with a term for the bulk concentration of *A* in solution ($[A]_s$), which is assumed to be constant. The remaining rate equations are shown in Equations 8 and 9.

$$A_s \Leftrightarrow A \quad (5)$$

$$A + B \Leftrightarrow AB \quad (6)$$

$$\frac{\partial[A]}{\partial} = k_t\left([A]_s - [A]\right) - \left(k_a[A][B] - k_d[AB]\right) \quad (7)$$

$$\frac{\partial[B]}{\partial} = -\left(k_a[A][B] - k_d[AB]\right) \quad (8)$$

$$\frac{\partial[AB]}{\partial} = k_a[A][B] - k_d[AB] \quad (9)$$

As previously discussed, the injected concentration of *A* is known, all sites are assumed to be empty initially ($[AB]_0$=0), and the total number of sites is determined empirically for each surface that is analyzed ($[B]_0$=R_{max}). Additionally, the concentration of *A* is assumed to be zero initially ($[A]_0$=0). BIAevaluation software v3.0.2 is then used to determine the binding and dissociation kinetics for both reactions.

3.5.3. Bivalent Analyte

A bivalent analyte adsorption model represents a system where a molecule in solution (*A*) adsorbed to a binding site on a surface (*B*) as described above; however, once *AB* is formed, it reacts with a second ligand *B* resulting in the

complex AB_2. Like 1:1 Langmuir binding, the concentration of A is assumed to be constant, and the equations solved with respect to sites on the surface occupied by either AB or AB_2. These reactions are represented below in Equations 10 and 11 and the corresponding rate equations are shown in Equations 12-14. The forward reactions are regulated by the rate constants k_{a1} and k_{a2} while the reverse reactions are regulated by the rate constants k_{d1} and k_{d2}.

$$A + B \Leftrightarrow AB \quad (10)$$

$$AB + B \Leftrightarrow AB_2 \quad (11)$$

$$\frac{\partial[B]}{\partial t} = -\left(k_{a1}[A][B] - k_{d1}[AB]\right) - \left(k_{a2}[AB][B] - k_{d2}\left[AB_2\right]\right) \quad (12)$$

$$\frac{\partial[AB]}{\partial t} = \left(k_{a1}[A][B] - k_{d1}[AB]\right) - \left(k_{a2}[AB][B] - k_{d2}\left[AB_2\right]\right) \quad (13)$$

$$\frac{\partial[AB_2]}{\partial t} = k_{a2}[AB][B] - k_{d2}\left[AB_2\right] \quad (14)$$

The same assumptions are made for this model as detailed above. In addition, the initial concentration of AB_2 is assumed to be zero ($[AB_2]_0=0$). BIAevaluation software v3.0.2 is then used to determine the binding and dissociation kinetics for both reactions based on adsorption sensorgrams.

Chapter 4: EXPRESSION AND PURIFICATION OF RECOMBINANT *T. PALLIDUM* PROTEIN FRAGMENT rTP0483

4.1. Introduction

Tp0483 is a FN binding protein believed to reside on the surface of *T. pallidum* and is thought to play a role in the antigenic disguise of the bacteria.[53] This protein has been successfully expressed and purified by Cameron and a similar procedure is used here to express a 22 kDa, recombinant fragment of Tp0483 (rTp0483) in an *E. coli* system.[96] Once rTp0483 had been expressed and purified its purity and concentration were determined using a combination of sodium dodecyl sulfate polyacrylamide gel electrophoresis (SDS-PAGE), western blot, and bicinchoninic acid (BSA) assay.

SDS-page is a technique developed for the separation of biomolecules based on molecular weight. SDS is an anionic detergent that is added to the protein solution; it binds to and unfolds the protein giving it a uniform negative charge. This is necessary because the charge of proteins with similar molecules weights often varies greatly. The denatured protein is loaded into a porous polyacrylamide gel and a current applied between a cathode and anode. All proteins possess an equivalent negative charge as a result of treatment with SDS, thus their rate of migration through the polyacrylamide gel toward the cathode is completely dependent on the molecular weight of the protein. Smaller proteins move more rapidly through the porous gel while larger proteins become constricted and move more slowly. Protein ladders with known proteins with ranges of molecular

weights are commercially available and by comparing the migration distance of an unknown protein it is possible to determine molecular weight.

Using SDS-PAGE the size of rTp0483 was confirmed; however, a more specific test was required to verify that the protein was without a doubt rTp0483 and not an unrelated protein with a similar molecular weight. Western blotting is an immunoblotting technique that exploits the specificity of antibody-antigen interactions. Proteins are treated with SDS, separated using gel electrophoresis, and transferred to a polyvinylidene difluoride (PVDF) membrane. The transfer of protein from gel to membrane is accomplished in a manner similar to separation of proteins during SDS-PAGE. The gel and membrane are sandwiched together between a cathode and an anode with the gel being closer to the anode. When a current is applied the negatively charged proteins migrate toward the cathode going from gel to membrane. Once the target protein is successfully immobilized on the membrane an antibody specific to the target (primary antibody) is added and allowed to react. After the immobilized proteins have reacted with the primary antibody a second antibody specific to the primary antibody (secondary antibody) is added. The secondary antibody is conjugated with a detection molecule, which can be activated in order to visually confirm the presence of the secondary antibody-primary antibody-protein complex. Western blot in combination with SDS-PAGE confirmed the presence of rTp0483.

The concentration of rTp0483 was determined with a BCA assay, which utilizes a modified Biuret reaction to measure protein concentration in solution. In the Biuret reaction Cu^{2+} is reduced to Cu^{1+} by proteins in an alkaline solution. The

Cu^{1+} ions that are produced form a complex with bicinchoninic acid, which results in the production of a deep violet color. The absorbance of this solution is then measured and compared to a standard curve with known concentrations to determine an unknown concentration.

4.2. Experimental Procedures

4.2.1. Tp0483 Expression Vector and Maintenance Strain Preparation

A pRSETc plamid vector containing the rT0483 expression gene along with an N-terminal 6xHIS tag was provided by Caroline Cameron at the University of Victoria (Victoria, British Columbia). Immediately upon receipt, the plasmid was reconstituted in deionized water (diH_2O) and transformed into a TOP10 chemically competent *E. coli* cell line from Invitrogen (Carlsbad, CA). One 50 µL vial of TOP10 cells was thawed on ice. Once thawed, 5 µL of plasmid solution was added to the TOP10 vial, mixed by gently tapping, and incubated on ice for 30 minutes. The cells were heat shocked in a 42°C water bath for 30 seconds and returned to ice. Once cooled, 250 µL of super optimal broth with catabolite repression (SOC) media from Invitrogen at room temperature was added to the vial, the vial sealed with paraffin, and shaken on its side at 225 RPM and 37°C for 1 hour. The cell solution was added to pre-warmed (37°C) LB agar plates (Sigma (St. Louis, MO)) inoculated with 100 µg/mL ampicillin (Sigma) in volumes of 20, 50, or 100 µL and incubated overnight at 37°C. The next day, single *E. coli* colonies were selected and transferred to 5 mL of LB broth (Sigma) inoculated with 100 µg/mL ampicillin and incubated overnight

at 225 RPM and 37°C. Finally, 15% (v/v) glycerol (Sigma) was added to the TOP10 cell stock, the solution divided into 1 mL aliquots, and stored at -80°C.

4.2.2. rTp0483 Expression Vector Transformation

A vial of TOP10 cells with the rTp0483 expression vector was thawed at room temperature. TOP10 cells were transferred from the stock sample into 5 mL of freshly prepared LB broth inoculated with 100 µg/mL ampicillin. The cells were grown overnight at 37°C while shaking the sample at 225 RPM, then the cells were recovered by centrifugation at 6000 x G for 15 minutes at 4°C. The rTp0483 expression vector was extracted using a QIAGEN plasmid mini kit from QIAGEN (Hilden, Germany) as per manufacturer instructions.

The rTp0483 expression vector was transformed into a BL21(DE3)pLysS chemically competent *E. coli* line from Invitrogen. One 50 µL vial of BL21(DE3)pLysS cells was thawed on ice. Once thawed, 5 µL of plasmid solution was added to the vial, mixed by gently tapping, and incubated on ice for 30 minutes. The cells were heat shocked in a 42°C water bath for 30 seconds and returned to ice. Once cooled, 250 µL of SOC media was added to the vial, the vial sealed with paraffin, and shaken on its side at 225 RPM and 37°C for 1 hour. The cell solution was added to pre-warmed LB agar plates inoculated with 100 µg/mL ampicillin and 34 µg/mL chloramphenicol (Sigma) in volumes of 20, 50, or 100 µL and incubated overnight at 37°C. The next day, single isolated *E. coli* colonies were selected and transferred to 5 mL of LB broth inoculated with 100 µg/mL ampicillin and 34 µg/mL chloramphenicol and incubated overnight at 225 RPM and 37°C.

4.2.3. *E. coli* Amplification and rTp0483 Expression

The 5 mL overnight cell cultures were transferred to 1 L baffled flasks and combined with 500 mL of LB broth inoculated with 100 µg/mL ampicillin and 34 µg/mL chloramphenicol and incubated at 225 RPM and 37°C. The optical densities of the cell suspensions were measured periodically at a wavelength of 600 nm using a Spectronic GENSYS 5 photospectrometer until they reached a value between 0.4 and 0.6, which corresponds to the exponential growth phase of *E. coli*. Once in the exponential growth phase, isopropyl β-D-1thiogalactopyranoside (IPTG) (Sigma) was added to a final concentration of 0.5 mM in order to induce the expression of rTp0483. After the addition of IPTG the cell samples were incubated at 225 RPM and 30°C for 3 hours. The *E. coli* were pelleted by centrifugation at 4000 RPM and 4°C for 15 minutes, the LB broth poured off, and the cells stored at -20°C until purification was carried out.

4.2.4. rTp0483 Purification and Refolding

The frozen cell pellets were thawed on ice then resuspended and lysed by sonication in 20 mL of cold binding buffer (20 mM Tris-base (Fisher), 5 mM imidazole (Sigma), 0.5 M NaCl (Sigma), pH 7.9) with 0.1% NP-40 (Sigma) and 1% (v/v) EDTA free, Halt protease inhibitor cocktail (HPIC) from Thermo Scientific (Rockford, IL). Sonication was carried out on ice and was cyclic with a 10 second interval of sonication followed by a 5 second interval of rest for a total of 6 cycles. Lysed cell contents were recovered by centrifugation at 13,000 RPM for 15 minutes. The pellet was resuspended in 20 mL of binding buffer with 1% (v/v) HPIC,

sonicated, and recovered by centrifugation twice. Insoluble rTp0483 in the pellet was solubilized by resuspending the pellet in 5 mL of binding buffer with 6 M urea (Sigma) by sonication and incubating for 1 hour at 4°C on a rotating test tube rack. The remaining insoluble material was pelleted by centrifugation at 13,000 RPM for 15 minutes while solubilized rTp0483 was filtered through 0.45 μm syringe filters (Millipore (Bedford, MA)) and mixed with 2 mL of Ni-NTA superflow resin from QIAGEN. This suspension was incubated at 4°C for 1 hour on a rotating test tube rack then centrifuged at 2,000 RPM for 5 minutes and the liquid removed. The resin was washed twice with 10 mL of binding buffer with 6 M urea and 5 mM imidazole and once with 10 mL of binding buffer with 6 M urea and 20 mM imidazole, each time for 10 minutes at 4°C on a rotating test tube rack. After the third wash was removed, rTp0483 was eluted with the addition of 1 mL of elution buffer (20 mM Tris-base, 0.5 M NaCl, 1 M imidazole, pH 7.9) and incubation for 1 hour at 4°C on a rotating test tube rack. The resin was removed by centrifugation at 2,000 RPM for 5 minutes at 4°C and the protein solution filtered through 0.45 μm syringe filters to remove any remaining resin. A process for protein renaturation was adapted from Zhang *et al.*[97] Zwittergent 3-12 (Sigma) was added to final concentration of 0.5% (w/v) and the protein solution was injected into a 10,000 MW Slide-a-Lyzer dialysis cassette from Invitrogen. The sample was dialyzed for 3 hours then overnight in renaturation buffer 1 (100 mM Tris-base, 200 mM NaCl, 10 mM EDTA (Sigma), pH 8.0) at 4°C. Then, the sample was dialyzed for 6 hours then overnight in renaturation buffer 2 (50 mM Tris-base, 200 mM NaCl, 0.5 mM EDTA) at 4°C. The

solution was removed from the dialysis cassette, filtered through 0.45 μm syringe filters, and stored at 4°C until protein analysis was complete.

4.2.5. SDS-PAGE

rTp0483 solution was combined in a 1:1 ratio with 5x SDS loading buffer (10% (w/v) SDS (Bio Rad (Hercules, CA)), 30% (v/v) glycerol, 5% (v/v) β-mercapitalethanol (Sigma), and 0.02% bromophenol blue (Sigma) (w/v) in 250 mM Tris-HCl (Sigma), pH 6.8). The solution was loaded into a 10-20% tris-glycine polyacrylamide gel (Invitrogen) along with a Mark12 unstained protein ladder (Invitrogen) while any empty lanes were loaded with 5x SDS loading buffer alone. Gel electrophoresis was carried out in a Novex mini cell (Invitrogen) at 120 V and a starting current of 35 mA. Once electrophoresis was complete the gel was incubated 3 hours in protein fixing solution (50% (v/v) methanol (Sigma), 10% (v/v) acetic acid (Sigma), and 40% (v/v) diH_2O). The fixing solution was removed and replaced with staining solution (2 g/L Coomassie brilliant blue (Sigma), 45% (v/v) methanol, 45% (v/v) diH_2O, and 10% (v/v) acetic acid) and the gel incubated overnight. The gel was rinsed twice with fixing solution and then incubated in destaining solution (25% (v/v) methanol, 10% (v/v) acetic acid, and 65% (v/v) diH_2O) for 5 hours. The destaining solution was removed and the gel was washed well with diH_2O. The diH_2O was removed and replaced with drying solution (5% glycerol, 30% methanol, and 65% diH_2O). The gel was sandwiched between 2 pieces of cellophane and allowed to dry.

4.2.6. Western Blot

rTp0483 and the protein ladder were separated by gel electrophoresis as in Section 4.2.5. Transfer of proteins from gel to a PVDF membrane (Invitrogen) was carried out in an XCell II blotting module (Invitrogen) at 25 V for 90 minutes. The membrane was incubated in Tris-buffered saline (TBST) (8 g/L NaCl, 0.2 g/L KCl (Sigma), and 3 g/L Tris-base in diH_2O, pH 7.4) with 0.1% Tween 20 (Sigma) for 5 minutes. The solution was replaced with fresh TBST and incubated 5 minutes. TBST was removed and the membrane was incubated in 5% blocking solution (5% dried milk in TBST) for 1 hour at room temperature. The blocking solution was removed and the membrane was washed twice with TBST. An antibody specific to rTp0483 was diluted 1:1000 in 5% blocking solution and the membrane was incubated overnight in the solution at 150 RPM at room temperature. The antibody solution was removed and the membrane was washed twice with TBST. A secondary, alkaline phosphatase conjugated antibody specific to the rTp0483 primary antibody was diluted 1:1500 in 5% blocking solution and the membrane was incubated in the solution for 1 hour. The antibody solution was removed and the membrane was washed in TBST for 10 minutes. The membrane was washed 2 more times with TBST for a total of 3 washes. The final TBST wash was removed and the membrane was incubated in nitro-blue tetrazolium chloride (NBT) and 5-bromo-4-chloro-3'-indolyphosphate p-toluidine (BCIP) (Thermo Scientific), which reacts with alkaline phosphatase to form a dark purple precipitate.

4.2.7. BCA Assay

Bovine serum albumin (BSA) standards were prepared in Dulbecco's phosphate buffered saline (DPBS) (137 mM NaCl, 2.7 mM KCl, 8 mM Na_2HPO_4 (Sigma), and 1.5 mM KH_2PO_4 (Sigma) in diH_2O, pH 7.4) and the BCA working reagent was prepared as per manufacturer instructions. 100 µL of each sample was combined with 2 mL of working reagent; BSA standards were analyzed in duplicate while rTp0483 was analyzed at a number of concentrations (100% rTp0483 solution, 50% rTp0483 solution in DPBS, and 25% rTp0483 solution in DPBS). The samples were sealed with paraffin, incubated 30 minutes in a water bath at 37°C, and allowed to cool to room temperature. The absorbance was then measured at 562 nm using a photospectrometer. BSA standards at known concentrations were used to generate a calibration curve for the determination of rTp0483 concentration. Based on this curve the concentration of rTp0483 was found for each sample and an average value determined.

4.2.8. Protein Storage

Once the purity and concentration of rTp0483 was determined, the protein solution was aliquoted and stored at -20°C.

4.3. Results

Figure 4.1 shows the results of SDS-PAGE and western blot analysis for rTp0483. A protein of the same size as rTp0483 (~22 kDa) was observed on the SDS-PAGE gel and NBT-BCIP reacted with alkaline phosphatase conjugated

secondary antibody indicating the presence of rTp0483. Thus, the presence and purity of recombinantly expressed rTp0483 was confirmed. The concentration of rTp0483 varied from batch to batch ranging from 400-700 μg/mL

4.4. Conclusions

The selected method of vector transformation, cell culture, protein expression, and protein purification were successful in producing recombinant rTp0483 protein. Generated protein was of sufficient purity and concentration to move forward with further studies.

A.

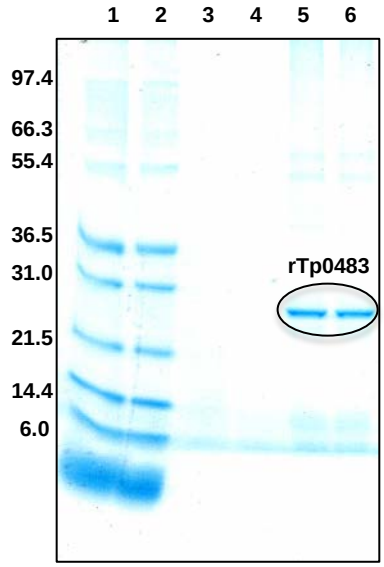

B.

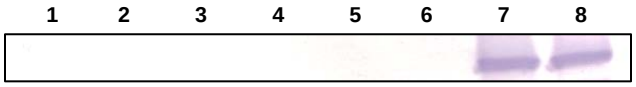

Figure 4.1: (A) SDS-PAGE analysis for rTp0483. Lanes 1 and 2 are Mark12 protein ladder, lanes 3 and 4 are empty, and lanes 5 and 6 are rTp0483. A strong band was observed at the appropriate position for rTp0483 (~22 kDa). (B) Western blot analysis of rTp0483. Lanes 1 and 2 are Mark12 protein ladder, lanes 3-6 are empty, and lanes 7 and 8 are rTp0483. NBT-BCIP precipatate was observed for rTp0483 but not in the other lanes indicating a specific interaction with rTp0483.

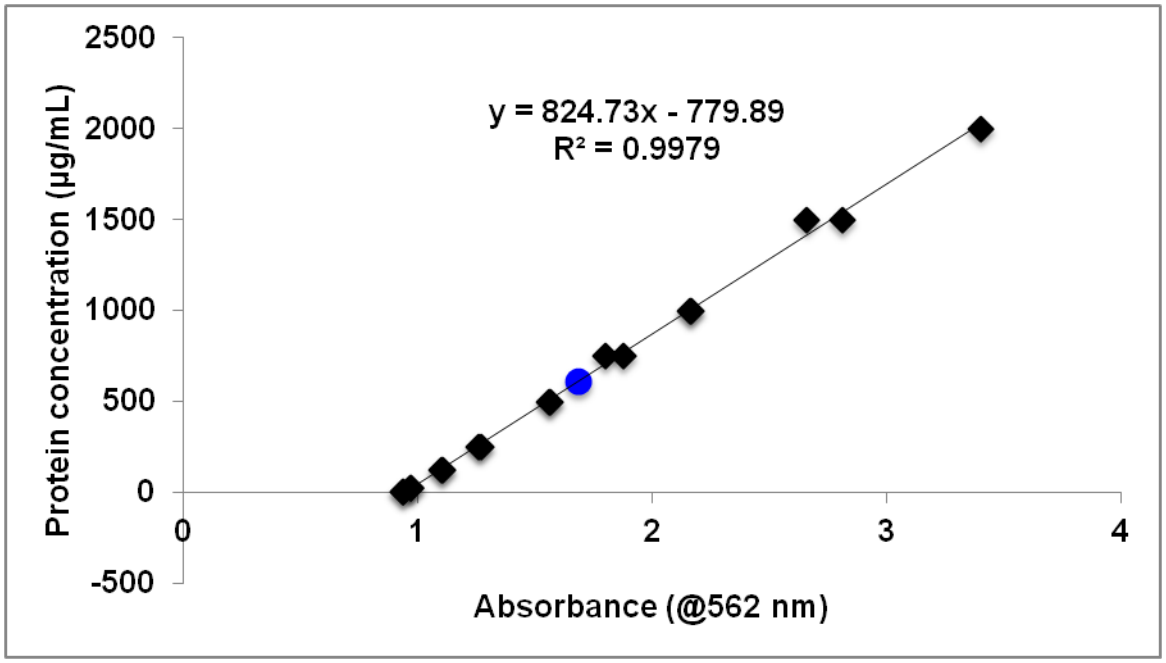

Figure 4.2: Representative BSA calibration curve for BCA assay. Absorbance measured at 562 nm is proportional to the concentration of protein in solution. Linear regression of BSA standards allows for the determination of rTp0483 concentration. (◆)- BSA standards and (●)- rTp0483.

Chapter 5: SELF-ASSEMBLED MONOLAYER FORMATION AND VALIDATION

5.1. Introduction

The chemisorption of organosulfur compounds onto gold surfaces has been demonstrated to be an effective method in the analysis of a wide range of surface interactions including protein adsorption, blood coagulation, and biomineralization of apatite.[98-104] These organosulfur compounds are composed of a functional head group with a hydrocarbon tail, which terminates with a thiol group. The thiol groups spontaneously coordinate with a gold surface leading to the formation of a tightly packed layer with uniform surface chemistry known as a self-assembled monolayer (SAM). This method can be employed to quickly and efficiently assemble surfaces with diverse chemical and physical properties. Chung *et al.* generated SAMs with phospholipid head groups in order to assess their hemocompatilibilty.[98] In another study by Keslowsky *et al.* the effect of surface charge on FN binding strength and binding site availability was investigated.[99]

The four SAM surface chemistries shown in Figure 5.1 were analyzed to determine the effect of charge and hydrophobic interactions on the adsorption behaviors of rTp0483 and FN. Carboxyl, hydroxyl, methyl, and amino-terminated SAMs were produced to investigate negatively charged, hydrophilic, hydrophobic, and positively charged surfaces respectively. SAM formation was verified with contact angle measurement accompanied by X-ray photoelectron spectroscopy (XPS).

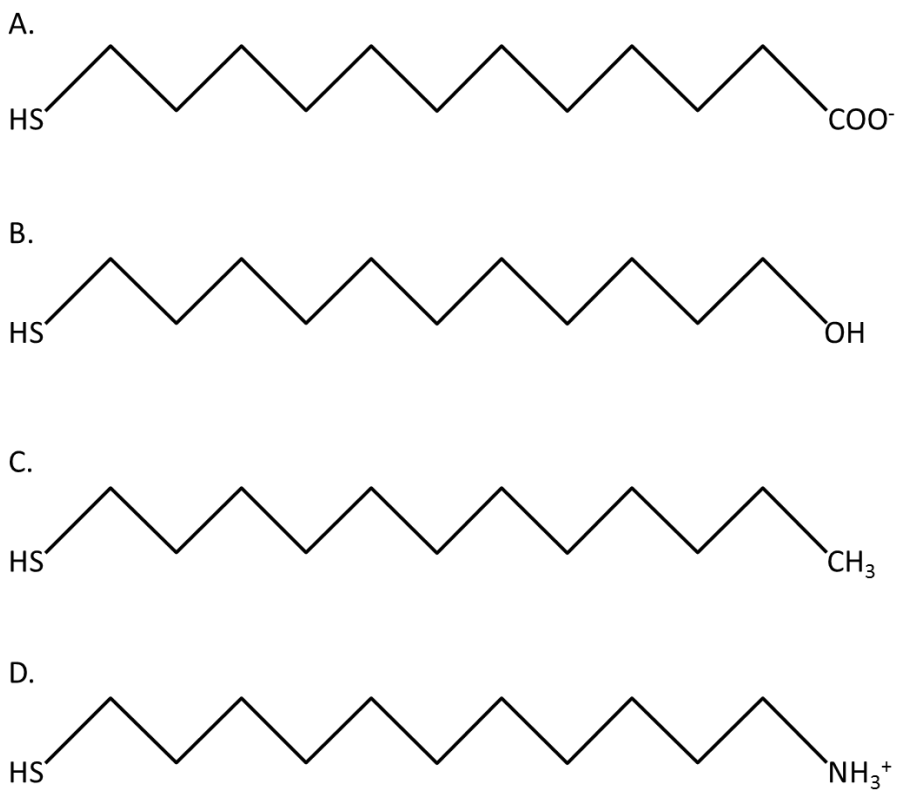

Figure 5.1: Structure of selected alkanethiol SAM precursors. (A) 11-mercapto-undecanoic acid (-COO^-) produces a negative surface charge, (B) 11-hydroxy-1-undecanethiol (-OH) produces a hydrophilic surface, (C) 1-dodecanethiol (-CH_3) produces a hydrophobic surface, (D) and 11- amino-1-undecanethiol (-NH_3^+) produces a positive surface charge.

5.2. Experimental Procedures

5.2.1 SAM Formation

The SAMs were assembled on gold QCM and SPR surfaces by incubation overnight in selected 1 mM alkanethiol solutions; 11-mercapto-undecanoic acid (-COO^-) was purchased from Sigma; 11-hydroxy-1-undecanethiol (-OH), 1-dodecanethiol (-CH_3), and 11- amino-1-undecanethiol hydrochloride (-NH_3^+) were purchased from Asemblon (Redmond, WA). Gold QCM surfaces were purchased

from Biolin Scientific and gold SPR surfaces were purchased from Biacore AB. Prior to analysis surfaces were washed for 15 seconds in ACS grade ethanol (Sigma) followed by 15 seconds in diH_2O then dried with N_2 gas (Scott-Gross (Lexington, KY)).

5.2.2. Contact Angle Analysis

Analysis of the angle of contact between a drop of liquid on a surface is an effective method for the determination of the hydrophobicity of the surface. The contact angle of liquid on a surface depends on the thermodynamic equilibrium between the liquid, the surface, and the environment surrounding them. This relationship is illustrated in Figure 5.2 and is represented by Young's equation below (Equation 15). At equilibration the three phases are in balance and as a result the sum of the surfaces energies add up to zero. The energy at the interface of the liquid with the atmosphere is denoted as γ_{AL}, at the interface of the surface and the atmosphere as $\gamma_{SA,}$ and at the interface between the liquid and the surface as γ_{SL}. As the hydrophobicity of the surface increases the surface energy at the interface between the liquid and the surface increases along with the contact angle. Static and advancing contact angles for water on SAM surfaces were measured. A single drop of water was added to each surface then the contact angle measured for static detection. For advancing contact angle analysis water was slowly added to the surface while simultaneously measuring the contact angle as it spread across the SAMs. Contact angle studies were conducted using diH_2O on a Future Digital Scientific Contact Angle Goniometer (Long Island, NY).

$$\gamma_{SA} = \gamma_{SL} + \gamma_{AL} \cos \theta \quad (15)$$

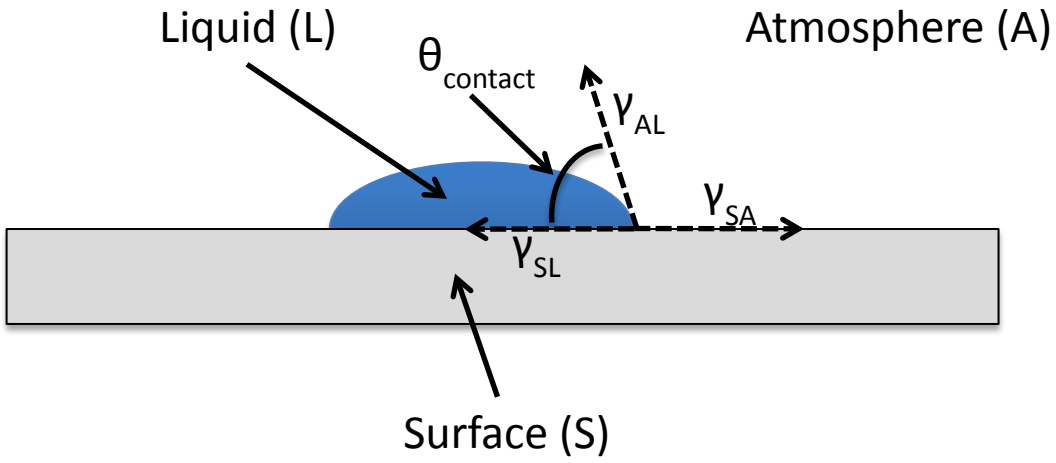

Figure 5.2: Illustration of the thermodynamic balance of surface energies associated with liquid spreading on a surface.

5.2.3. X-ray Photoelectron Spectroscopy

X-ray photoelectron spectroscopy (XPS) is a technique used for the determination of the chemical composition of a surface. The sample surface is bombarded with X-rays while the number and binding energy of liberated electrons is measured. All elements have unique binding energy signals so by measuring the number of each event the chemical composition and relative amounts of materials located from 1-10 nm inside of a material can be determined. XPS data were gathered using Mg from a twin anode XR3E2 X-ray source and the CLAM4MCD analyzer from Thermo VG Scientific (Waltham, MA).

5.2.4. Gold Surface Regeneration

Gold coated QCM and SPR surfaces are costly, thus a method for removing all adsorbed materials, including SAMs, was required so that the surfaces could be reused. Surfaces were regenerated by either 5 minute immersion in a 5:1:1 mixture of d_iH2O, ammonium hydroxide (VWR (Radnor, PA)), and hydrogen peroxide (VWR) at 75 °C followed by 10 min exposure to UV/ozone or a 20 min exposure to O_2 plasma at a flow rate of 1 standard ft^3/h (SCFH) and a pressure of 700 mTorr in a PDC-002 (230 V) plasma cleaner with Plasmaflo unit from Harrick Plasma (Ithaca, NY) followed by immersion in ACS grade ethanol for at least 14 h. Success of regeneration was determined by assembling a fresh SAM layer on the cleaned gold surface and comparing the baseline response to that of a SAM layer assembled new gold surface in the Biacore X SPR spectrometer

5.3. Results

Functionalized SAMs displaying $-COO^-$, -OH, $-NH_3^+$, and $-CH_3$ groups were prepared as previously described. Contact angle and XPS data were determined and compared with literature values.[98-104] The contact angles shown in Figure 5.3 corresponded well with literature values, and XPS data shown in Table 5.1 relating surface composition indicated SAM formation. SAMs formed on regenerated gold surfaces produced an SPR response equivalent to SAMs formed on new gold surfaces indicating successful regeneration.

5.4. Conclusions

Based on contact angle and XPS analysis SAM formation was confirmed. Organic materials including SAMs were successfully removed from the gold surfaces allowing for them to be reused. The functionalized SAMs formed allow for the analysis of rTp0483 and FN adsorption behavior as well as other biological responses as a function of surface chemistry.

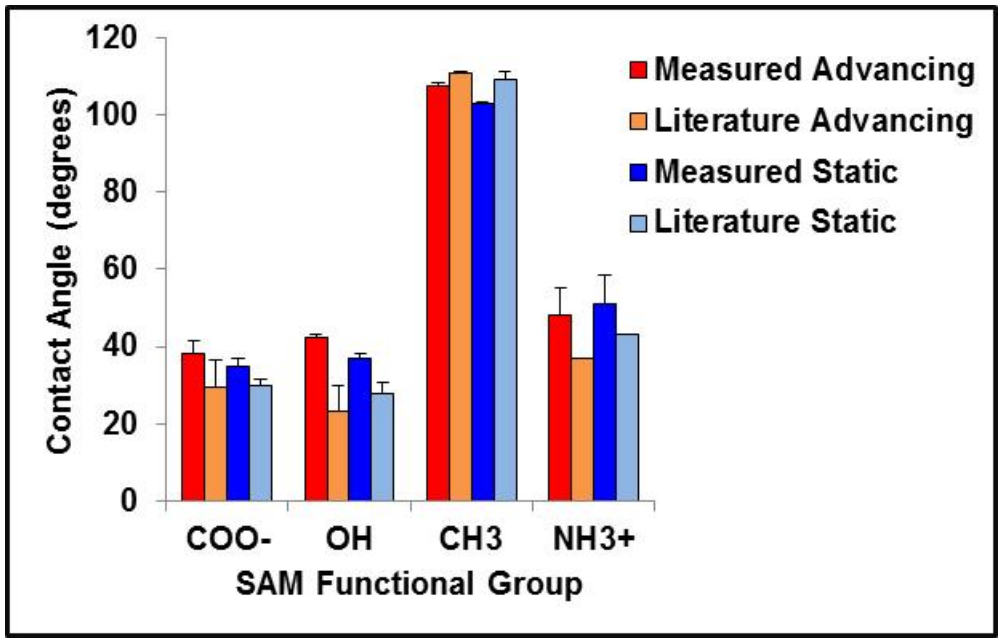

Figure 5.3: Comparison of experimental and literature values for the advancing and static contact angles of water on each functionalized SAM

Table 5.1: X-ray photoelectron spectroscopy (XPS) values. Experimentally determined values from literature as well as theoretical values given for comparison.

XPS Measurements					
Surface		C1s (%)	O1s (%)	N1s (%)	S2p (%)
	Experimental	99.5	----	----	0.5
$-CH_3$	Literature	97.6	----	----	2.4
	Theoretical	92.3	----	----	7.7
	Experimental	90.5	6.6	----	2.9
-OH	Literature	83.2	13.3	----	3.5
	Theoretical	84.6	7.7	----	7.7
	Experimental	94.6	3.3	----	2.1
$-COO^-$	Literature	79.4	18.9	----	1.8
	Theoretical	79.0	14.0	----	7.7
	Experimental	88.9	----	6.6	3.5
$-NH_3^+$	Literature	86.6	----	11.9	1.5
	Theoretical	86.0	----	7.0	7.0

Chapter 6: FIBRONECTIN BINDING TO THE *TREPONEMA PALLIDUM* ADHESIN PROTEIN FRAGMENT RTP0483 ON FUNCTIONALIZED SELF-ASSEMBLED MONOLAYERS

6.1. Introduction

A number of studies have demonstrated the FN binding capacity of *T. pallidum* and work by Cameron *et al.* further implicated the putative surface protein Tp0483 in FN adhesion.[51-53, 64, 72, 73] A stable Tp0483 fragment known as rTp0483 was expressed and purified by Cameron *et al.* that retained the FN binding affinity of whole Tp0483.[53] Because rTp0483 has been shown to bind soluble plasma FN and insoluble ECM FN it was chosen for the investigation of rTp0483 adsorption to functionalized SAMs and plasma FN adsorption to rTp0483. This chapter is based on Dickerson *et al.* (in press).

Physical adsorption of rTp0483 was investigated on a number of functionalized SAMs in order to ascertain the effect of surface chemistry on rTp0483 adsorption and FN binding affinity. Adsorption of rTp0483 and subsequently FN was analyzed with QCM-D while SPR was used to measure the binding/dissociation kinetics of rTp0483 and FN adsorption. The physical character of the adsorbed protein layers was also investigated using QCM-D. Atomic force microscopy (AFM) was used to examine the distribution of rTp0483 on the functionalized SAM surfaces. Two segments of the whole Tp0483 protein sequence located on the expressed rTp0483 fragment were identified as potential FN binding sites, then peptides and antibodies matching these regions were produced to test their involvement in FN binding. Numerous studies have suggested that the RGD cell-

binding sequence located in the 10th type III domain of FN plays a significant role in *T. pallidum* adhesion.[64-67] In addition, a number of other binding domains exist on FN including binding sites specific for heparin and collagen/gelatin.[63] It has been shown that the binding of certain species of bacteria are modulated by these heparin or collagen/gelatin-binding domains of FN.[70, 71] In order to elucidate a more complete profile of rTp0483 FN binding, anti-RGD, heparin, and gelatin binding were studied to determine their involvement in the binding of FN on surfaces coated with rTp0483 compared to unmodified -COO^- SAMs.

6.2. Experimental Procedures

6.2.1. Biomolecules and Reagent

DPBS was prepared as specified in Section 4.2.7. Human plasma fibronectin (FN) and all other chemicals not specifically mentioned were purchased from Sigma. An antibody against the RGD (Arginine-Glycine-Aspartate) cell-binding site of FN was purchased from Chemicon International (Temecula, TN) and later from Abcam (Cambridge, MA). The protein fragment rTp0483 was expressed and purified as per the protocol provided in Section 4.2.4.

Aves Labs (Tigard, OR) identified two possible FN binding peptide sequences on rTp0483 using a combination of Hopp-Woods and Kyte-Doolittle (hydrophilicity), Emini (surface probability), Karplus-Shulz (chain flexibility), and Jameson-Wolf (a combination of attributes) methods. Peptides corresponding to residues 274-289 (D1- QMHSDSKQVDVKLDGN) and 316-333 (D2-

QRKEDDSMYSYVTGTMKY) of the complete Tp0483 sequence were prepared along with monoclonal antibodies (anti-Tp0483#1 IgY, chicken # 5507-5508 - against residues 274-289 and anti-Tp0483#2 IgY, chicken # 5509-5510 - against residues 316-333) by Aves Labs. Two other peptides (A3 - AYSSGAPPMPPF and P1 - HSSYWYAFNNKT) were provided for use as negative controls.

6.2.2. QCM

A Q-Sense E4 QCM unit was used for rTp0483 and FN adsorption studies. SAMs were prepared as described in Section 5.2.1 before they were mounted in the QCM sample chamber. DPBS was employed as a running buffer and used to dilute all proteins to the desired concentration for analysis. A constant flow rate of 50 µL/min was employed. Once a sample surface was mounted it was primed with DPBS until the QCM response was stable. Samples were introduced by stopping buffer flow, moving the inlet tube from the buffer reservoir to the sample vial, and resuming flow. Once the sample had been introduced flow was stopped again, the inlet tube moved back to buffer, and flow restarted. After an injection the signal was allowed to stabilize for 10 minutes, then changes in signal as a result of protein adsorption were measured as a frequency drop (Δf) in hertz (Hz). Changes in dissipation energy (D) were also recorded.

6.2.3. rTp0483 Adsorption to SAMs and FN Adsorption to rTp0483

To investigate protein adsorption, 20 µg rTp0483/mL was introduced into the system for 2 minutes at a flow rate of 50 µL/min. After rTp0483 adsorption, 2

mg BSA/mL was introduced for 2 minutes at a flow rate of 50 μL/min to block the surface not covered by rTp0483 and, hence, prevent nonspecific binding of FN to exposed SAMs. Finally, 100 μg FN/mL was introduced into the QCM for 2 minutes at a flow rate of 50 μL/min.

6.2.4. rTp0483 Monolayer Dissipation Energy Analysis

The Q-Sense E4 was employed for the analysis of rTp0483 monolayer dissipation energy. For dissipation energy studies, 100 μg rTp0483/mL was introduced into the QCM for 2 minutes at a flow rate of 50 μL/min. The higher concentration of rTp0483 was used in this study to produce a more complete protein monolayer. The change in dissipation energy for each surface was divided by the frequency change in order to calculate the dissipation energy as a function of protein surface mass density.

6.2.5. SPR

A Biacore X SPR unit was used for all kinetic studies. SAMs were prepared as described in Section 5.2.1. DPBS was employed as a running buffer and was used to dilute all proteins to the desired concentrations. A constant flow rate of 50 μL/min was employed. Once a sample surface was docked, it was primed with DPBS until the response signal in both flow channels was stable. Buffer was circulated through FC1 and FC2 in series in order to monitor signal stability. After the response had stabilized buffer flow was changed to single channel flow (either FC1 or FC2) for kinetic testing and the other channel was used to monitor background noise.

Protein samples were introduced through an injection port and after each injection the signal was allowed to stabilize before changes in the SPR signal were recorded. After the first flow channel was used flow was reversed and the other was used in a similar fashion.

6.2.6. Kinetic Analysis of rTp0483 and FN Adsorption

To investigate the kinetics of rTp0483 binding, 100 µL of rTp0483 was injected at concentrations of 5, 10, and 20 µg rTp0483/mL at a flow rate of 50 µL/min. The corresponding adsorption sensorgrams were analyzed using Biacore BIAevaluation software v3.0.2 to model kinetic parameters based on the models presented in Section 3.5.

For FN kinetic analysis, 100 µL of rTp0483 was injected at 5 and 20 µg rTp0483/mL at a flow rate of 50 µL/min. A volume of 100 µL of 2 mg BSA/mL was injected to block the surface not covered by rTp0483 at a flow rate of 50 µL/min. Finally, 100 µL of FN was injected at concentrations of 10, 20, and 40 µg FN/mL at a flow rate of 50 µL/min. These lower FN concentrations were used in order to limit the potential of mass transport effects. The corresponding adsorption sensorgrams were analyzed using Biacore BIAevaluation software v3.0.2 in order to model kinetic parameters based on the models presented in Section 3.5.

6.2.7. AFM Imaging of rTp0483 on SAMs

A Molecular Imaging PicoSPM from Agilent Technologies (Tempe, AZ) using Tap300 Intermittent Contact Tips from Budget Tips (Sofia, Bulgaria) was used to

provide images of rTp0483 adsorption on each of the SAMs. Data analysis was completed using PicoScan Software (Agilent Technologies) and Gwyddion Software 2.5 (General Public License, development supported by the Czech Metrology Institute, Brno, Czech Republic). Functionalized SAMs were incubated in a solution of 10 μg rTp0483/mL for 15 minutes at room temperature. Surfaces were rinsed with diH_2O, dried with N_2 gas, and imaged immediately.

6.2.8. rTp0483 Binding Domain Analysis

The Biacore X SPR spectrometer was used for all rTp0483 antibody and rTp0483 peptide studies. The selected rTp0483 antibodies (aTp) were prepared at a concentration of 200 μg antibody/mL. Initially, 100 μL of 20 μg rTp0483/mL was injected and adsorbed onto a surface at a flow rate of 50 μL/min. After stabilization, 100 μL of 2 mg BSA/mL was injected to block the surface not covered by rTp0483 at a flow rate of 50 μL/min. To test the effect of FN on antibody binding, 100 μL of 100 μg FN/mL was injected at a flow rate of 50 μL/min and, once the SPR signal was stable, 100 μL of aTp#1 or aTp#2 were injected at a flow rate of 50 μL/min. Nonspecific antibody binding on the BSA blocked portion of the surface was analyzed by injecting 100 μL of 2 mg BSA/mL at 50 μL/min followed by 100 μL of aTp#1 or aTp#2 at a flow rate of 50 μL/min.

To determine the effect of rTp0483 antibodies on FN binding rTp0483 was injected followed by BSA as detailed above. This was followed by 100 μL of aTp#1 or aTp#2 at a flow rate of 50 μL/min, then 100 μL of 100 μg FN/mL at a flow rate of 50 μL/min.

The peptide sequences analogous to the selected antibodies were examined along with random, negative control peptides. Because the corresponding rTp0483 antibodies bound to rTp0483 only on negatively charged SAMs, only -COO^- terminated SAMs were examined here. Samples containing a 20:1 molar ratio of a specific rTp0483 peptide or a negative control peptide and were prepared with FN. First, 100 µL of 20 µg rTp0483/mL was injected and adsorbed to each surface at a flow rate of 50 µL/min. After stabilization, 100 µL of 2 mg BSA/mL was injected to block the surface not covered by rTp0483 at a flow rate of 50 µL/min. After the SPR signal stabilized, 100 µL of one of the 20:1 peptide/FN solutions was injected at a flow rate of 50 µL/min. Alternately, after rTp0483 had been adsorbed and blocked with BSA, 100 µL of 100 µg FN/mL was injected for comparison at a flow rate of 50 µL/min. Binding inhibition was determined using Equation 16:

$$\%\ FN\ binding = \frac{FN + peptide\ on\ rTp0483\left(\frac{pg}{mm^2}\right)}{FN\ on\ rTp0483\left(\frac{pg}{mm^2}\right)} x\ 100\% \quad (16)$$

6.2.9. FN Binding Domain Analysis

The Biacore X SPR spectrometer was used for all FN binding domain studies. Because FN bound preferentially to rTp0483 adsorbed on negatively charged surfaces, only -COO^- terminated SAMs were analyzed in these tests. First, 100 µL of 100 µg rTp0483/mL was injected and adsorbed onto -COO^- terminated SAMs at a flow rate of 50 µL/min. After the SPR signal stabilized, 100 µL of 100 µg FN/mL was

injected at a flow rate of 50 µL/min. The signal was again allowed to stabilize, and then 50 µL of 2 mg heparin/mL was injected at a flow rate of 50 µL/min. Alternately, 100 µL of 100 µg FN/mL was injected and adsorbed onto a -COO^- terminated SAM without rTp0483 at a flow rate of 50 µL/min followed by 50 µL of 2 mg/mL heparin at a flow rate of 50 µL/min. This process was repeated for anti-RGD (20 µg/mL) and type A gelatin (1 mg/mL).

As the RGD peptide sequence had previously been implicated in the adhesion of *T. pallidum* to FN, the interaction via this site was further characterized. The Biacore X was used to analyze the involvement of the RGD peptide sequence in the binding of FN to surface-adsorbed rTp0483 on -COO^- functionalized SAMs. A 100 µL of 20 µg rTp0483/mL was injected at a flow rate of 50 µL/min. Then, 100 µL of 2 mg BSA/mL was injected to block the surface not covered by rTp0483 at a flow rate of 50 µL/min. After signal stabilization, 50 µL of 10 µg FN/mL blocked with 20 µg anti-RGD/mL or 50 µg anti-RGD/mL was injected at a flow rate of 50 µL/min. Alternately, 50 µL of 10 µg FN/mL was injected alone onto adsorbed rTp0483 at a flow rate of 50 µL/min. Nonspecific antibody adsorption was measured by injecting 50 µL of anti-RGD alone at 20 µg anti-RGD/mL and 50 µg anti-RGD/mL at a flow rate of 50 µL/min. The mass of adsorbed anti-RGD+FN complex was adjusted to account for the added mass of any bound antibodies. Because FN is dimeric, it was assumed that each FN bound two molecules of anti-RGD. This added mass was accounted for multiplying the observed SPR response by a correction factor as shown in Equations 17 and 18.

$$Correction\ Factor = \frac{FN\ M_W}{FN + antibody\ M_W} = \frac{440{,}000\ Da}{440{,}000\ Da + \left(2\ x\ 150{,}000\ Da\right)} = 0.595 \quad (17)$$

$$Fibronectin\ concentration = Observed\ concentration\ x\ 0.595 \quad (18)$$

6.2.10. Statistical Analysis

Statistical analysis was carried out using the Microsoft Excel addon StatPlus to conduct multiple pair-wise comparisons between each sample group. One-way analysis of variance (ANOVA) was employed for this analysis. The maximum p-value considered for significance was 0.05; all data are reported as mean values ± standard error. All reported values are n=3+ with the exception of the aTp studies, which are n=2.

6.3. Results

6.3.1. rTp0483 Adsorption to SAMs and FN Adsorption to rTp0483

Adsorption results for rTp0483 onto functionalized SAMs are shown in Figure 6.1A. Results for -COO^- SAMs indicated an average surface mass density of 782 ± 46 pg/mm^2 while -OH, -NH_3^+, and -CH_3 SAMs were 358 ± 80 pg/mm^2, 453 ± 73 pg/mm^2, and 442 ± 30 pg/mm^2, respectively. ANOVA indicated that adsorption on the -COO^- SAMs was significantly greater than the other three surfaces ($p<0.05$) and that all of the other surfaces were indistinguishable.

The adsorption of FN onto rTp0483 on functionalized SAMs is shown in Figure 6.1B. As previously mentioned, the portion of each surface not covered by

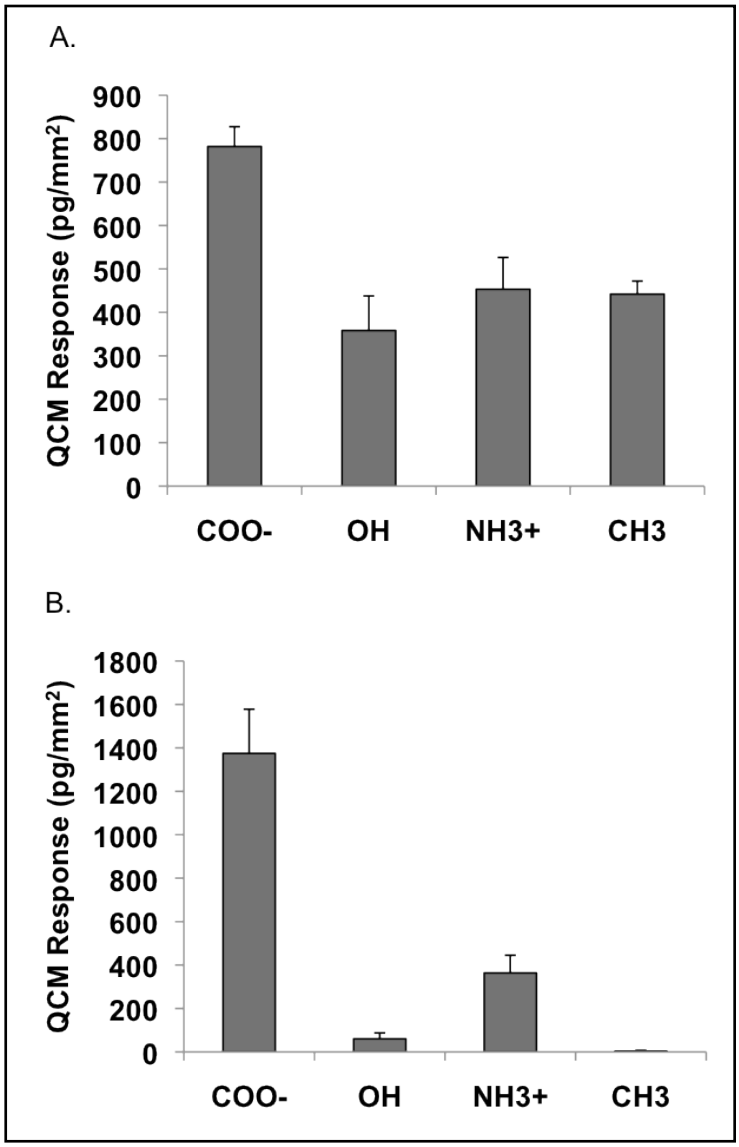

Figure 6.1: (A) Average rTp0483 binding on SAMs determined by QCM and (B) average FN binding to adsorbed rTp0483 on SAMs determined by QCM. ANOVA indicates higher rTp0483 and FN binding on -COO^- SAMs ($p<0.05$). Data is reported as a mean (n=3) for all sample groups with error bars representing standard error. From Dickerson *et al* (2011).[105]

rTp0483 was blocked with BSA, hence, any FN adsorption observed is onto rTp0483. Minimal binding of FN was observed to rTp0483 on the -OH (60 ± 28 pg/mm^2), -NH_3^+ (363 ± 82 pg/mm^2), and -CH_3 (3.5 ± 3.5 pg/mm^2) surfaces,

however, -COO^- SAMs demonstrated significantly higher binding (1380 ± 200 pg/mm^2, $p<0.05$) than the other three surfaces, which were not significantly different from one another. Because there was significantly more FN binding to rTp0483 adsorbed to -COO^- functionalized SAMs, it was the only surface employed for further study of FN binding to adsorbed rTp0483.

6.3.2. rTp0483 Monolayer Dissipation Energy Analysis

The changes in dissipation energy divided by the frequency shift for adsorbed rTp0483 are shown in Figure 6.2. SAM terminal groups were found to have a measureable effect on the relative dissipation energy. Adsorption of rTp0483 on -OH SAMs produced the largest value ($(0.220 \pm 0.013) \times 10^{-6}$ Hz^{-1}) while adsorption of rTp0483 on -CH_3 SAMs produced the lowest value ($(0.105 \pm 0.011) \times 10^{-6}$ Hz^{-1}). The values for -COO^- ($(0.1432 \pm 0.0085) \times 10^{-6}$ Hz^{-1}) and -NH_3^+ ($(0.1675 \pm 0.0035) \times 10^{-6}$ Hz^{-1}) were located between the two. ANOVA analysis indicated that the ratio of dissipation energy to frequency change for -OH SAMs was higher than the other three groups ($p<0.05$), that the value for -CH_3 SAMs was lower than the other three groups ($p<0.05$), and that the values for -COO^- and -NH_3^+ SAMs were not statistically significant.

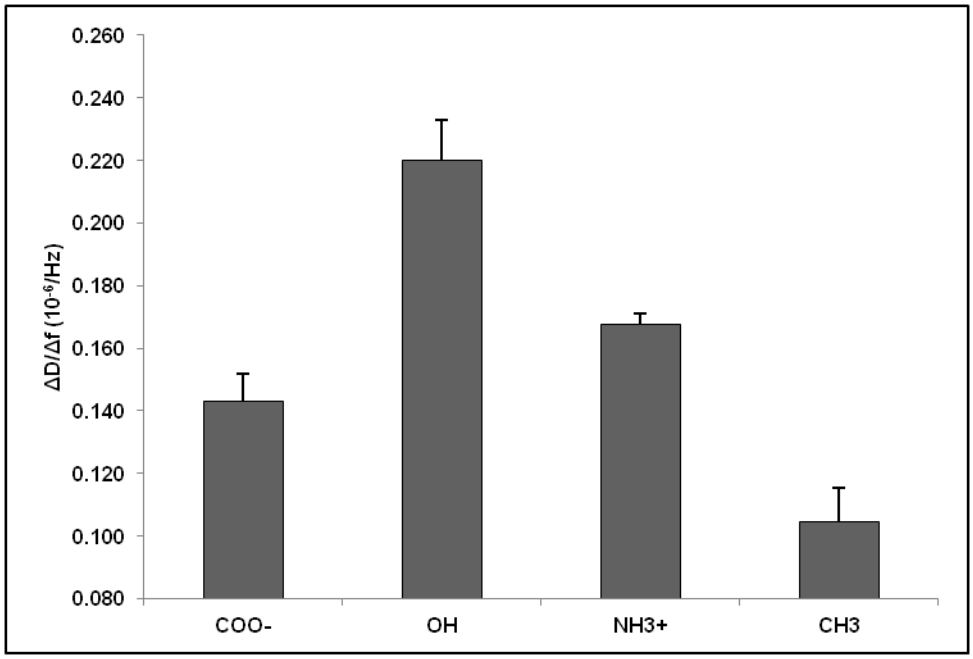

Figure 6.2: Ratio of QCM dissipation energy change (ΔD) to frequency shift (Δf) for rTp0483 adsorption at 100 µg rTp0483/mL on functionalized SAMs. ANOVA indicates a difference between the groups with -OH being the highest, $-CH_3$ being the lowest, and $-COO^-$ and $-NH_3^+$ being statistically indistinguishable. Data are reported as a mean (n=3) for all sample groups with error bars representing standard error. From Dickerson *et al* (2011).[105]

6.3.3. Kinetic Analysis of rTp0483 and FN Adsorption

rTp0483 was injected into the Biacore X SPR and adsorbed onto functionalized SAMs over a range of concentrations as previously described and the adsorption sensorgrams used to model the kinetics of rTp0483 adsorption. rTp0483 adsorption data was fit to a 1:1 Langmuir model as well as a 1:1 Langmuir model with mass transfer limitations. The Chi^2 parameter (mean square of signal noise) was used as a gauge of how well each adsorption model corresponded to experimental results. The lower the Chi^2 value, the more closely a model correlated to the experimental data. In general, Chi^2 should be of the same magnitude as the

noise inherent in a fit to be considered acceptable.[95] The best fit was chosen based on the lowest Chi^2 value and, after being chosen, the Chi^2 value was compared to the range of noise in the model versus the experimental data. A 1:1 Langmuir binding model with mass transfer limitations produced the best fit for rTp0483 adsorption. Chi^2 values ranged from 2.5-4.7 RU, while noise deviated from 0 RU up to 10 RU compared to experimental data. Model rTp0483 adsorption and experimental results for each of the selected functionalized SAMs are shown in Figure 6.3, and the corresponding values for K_A are included in Table 6.1. The K_A for rTp0483 adsorption to functionalized SAMs was found to be $(13.10 \pm 0.19) \times 10^7$ 1/M for $-COO^-$ SAMs, $(7.23 \pm 0.21) \times 10^7$ 1/M for -OH SAMs, $(5.12 \pm 0.25) \times 10^7$ 1/M for $-NH_3^+$ SAMs, and $(4.93 \pm 0.08) \times 10^7$ 1/M for $-CH_3$ SAMs. ANOVA analysis indicated significant differences between these values ($p<0.05$) except for $-NH_3^+$ and $-CH_3$ SAMs, which were the same.

Using the Biacore X unit, rTp0483 was injected and adsorbed onto $-COO^-$ SAMs followed by BSA in order to block any uncoated area against nonspecific adsorption. This was followed by the injection and adsorption of FN at a range of concentrations detailed previously. The resulting adsorption sensorgrams were employed to model the kinetics of FN adsorption onto rTp0483. A bivalent analyte model was found to fit best the adsorption behavior of FN onto rTp0483 immobilized on $-COO^-$ SAMs. Chi^2 values for the bivalent analyte model were 4.0 RU and 4.8 RU for 5 μg rTp0483/mL and 20 μg rTp0483/mL respectively, while noise deviated from 0 RU up to 15 RU compared to experimental data. The experimental results for FN adsorption onto rTp0483 immobilized on $-COO^-$ surfaces along with

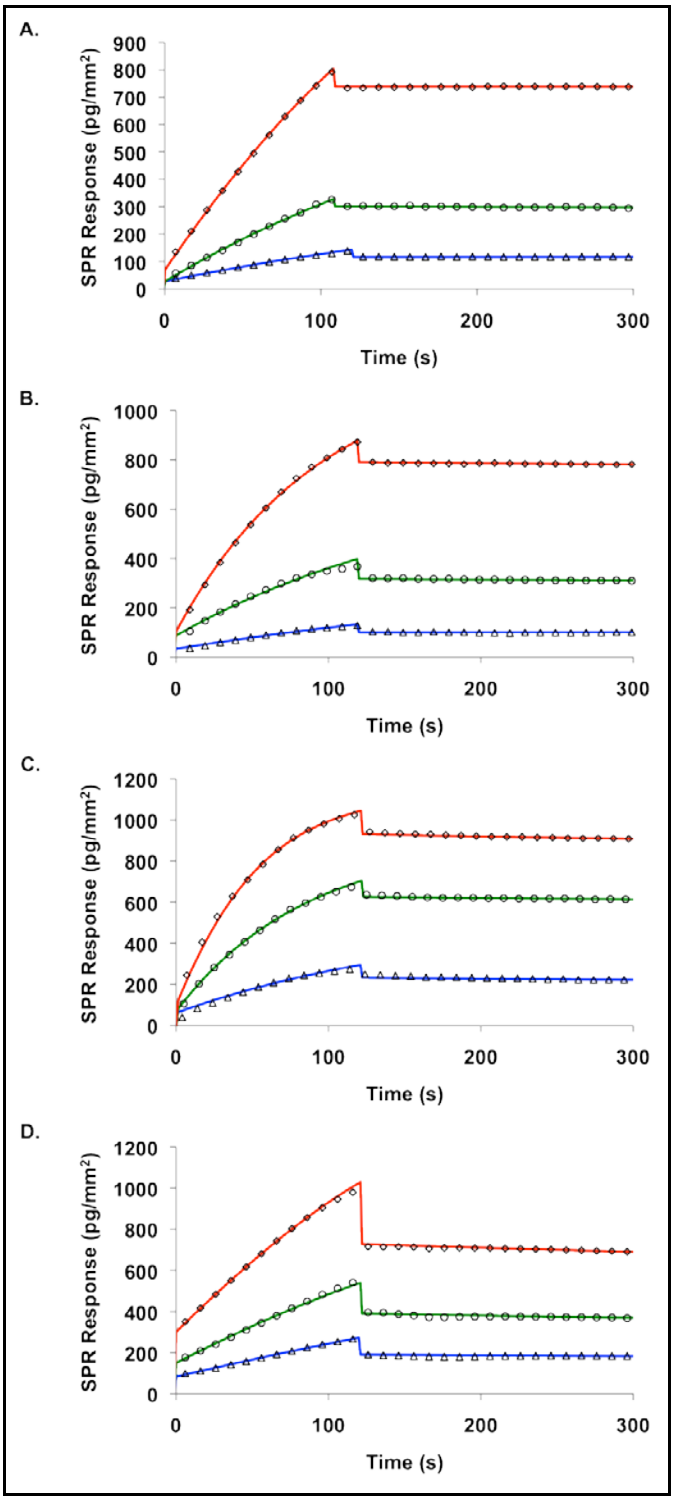

Figure 6.3: 1:1 Langmuir binding with mass transport limitations for rTp0483 adsorption onto SAMs at 5 (△), 10 (○), and 20 (◇) μg rTp0483/mL with surfaces functionalized with (A) $-COO^-$, (B) -OH, (C) $-CH_3$, and (D) $-NH_3^+$. Solid lines are predicted fits based on 1:1 Langmuir binding with mass transport limitations for 5 (—), 10 (—), and 20 (—) μg rTp0483/mL. From Dickerson *et al* (2011).[105]

Table 6.1: Kinetic constants for 1:1 Langmuir binding with mass transport limitations for rTp0483 binding on functionalized SAMs. [c]

SAM type	K_A (1/M) [a]	chi^2 (RU) [b]
$-COO^-$	$(13.10\pm0.19)\times10^7$	2.5
-OH	$(7.23\pm0.21)\times10^7$	2.4
$-CH_3$	$(4.93\pm0.08)\times10^7$	3.7
$-NH_3^+$	$(5.12\pm0.25)\times10^7$	4.7

(a) K_A- affinity constant; (b) Chi^2- goodness of fit; (c) K_A was significantly different between surfaces ($p<0.05$) except for $-CH_3$ and NH_3^+, which were the same (n=3). From Dickerson *et al* (2011).[105]

the model fit are shown in Figure 6.4. The corresponding values for K_{A1} and K_{A2} are included in Table 6.2. K_{A1} was found to be slightly higher with 5 μg rTp0483/mL adsorbed to the surface ($(1.53 \pm 0.13) \times 10^9$ 1/M) compared to the value with 20 μg rTp0483/mL adsorbed to the surface ($(1.03 \pm 0.08) \times 10^9$ 1/M). However, K_{A2} for FN adsorption to rTp0483 was higher when 20 μg rTp0483/mL was adsorbed to the surface ($(4.03 \pm 0.47) \times 10^{-2}$ 1/RU) compared to the value when 5 μg rTp0483/mL was adsorbed ($(2.25 \pm 0.21) \times 10^{-2}$ 1/RU). The second reaction was expressed as a function of surface mass density rather than concentration because it is purely a surface reaction. The dissociation constants (K_{D1}) were calculated by taking the inverse of the first K_A value at each concentration; for 5 μg rTp0483/mL the K_{D1} was 0.65 ± 0.05 nM and for 20 μg rTp0483/mL the K_{D1} was 0.97 ± 0.07 nM, both of which indicate very strong interactions between rTp0483 and FN.

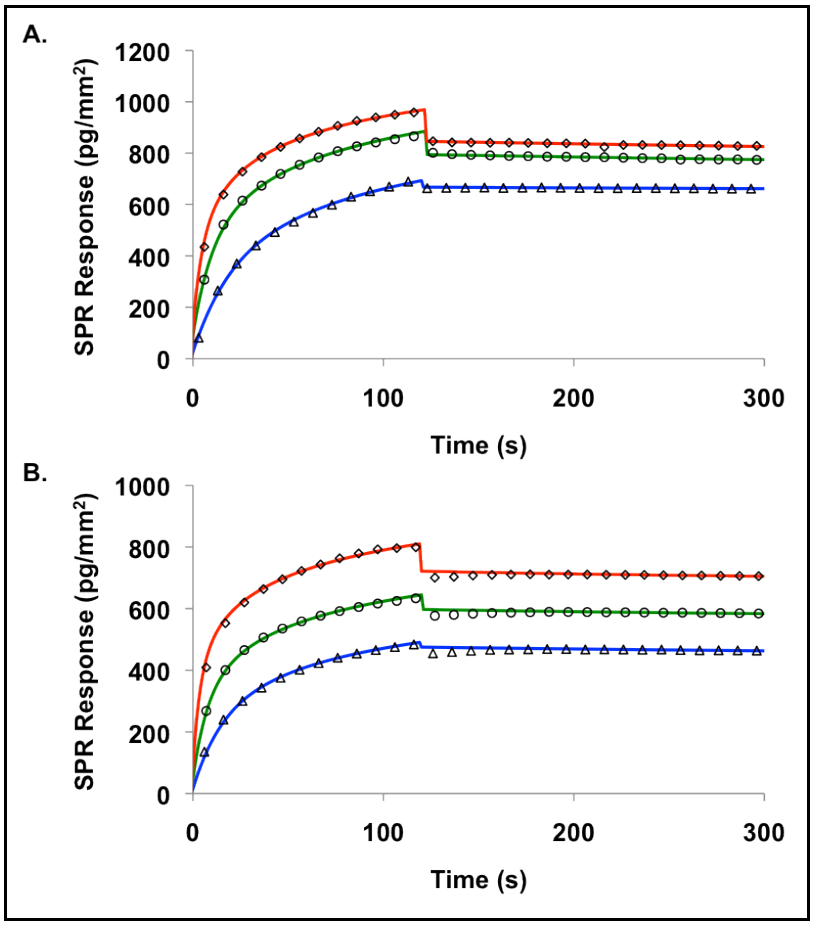

Figure 6.4: Bivalent FN binding to adsorbed rTp0483 on -COO^- SAMs at 10 (△), 20 (○), and 40 (◇) µg FN/mL with (A) 5 µg rTp0483/mL and (B) 20 µg rTp0483/mL rTp0483 adsorbed. Solid lines are predicted fits based on a bivalent analyte model for 10 (—), 20 (—), and 40 (—) µg FN/mL. From Dickerson *et al* (2011).[105]

Table 6.2: Kinetic constants for bivalent FN binding to rTp0483 on -COO^- SAMs. [c]

rTp0483 (µg/mL)	K_{A1} (1/M) [a]	K_{A2} (1/RU) [b]	Chi^2 (RU)
5	$(1.53\pm0.13)\times10^9$	$(2.25\pm0.21)\times10^2$	4.8
20	$(1.03\pm0.08)\times10^9$	$(4.03\pm0.47)\times10^2$	4.0

(a) K_{A1}- affinity constant for reaction 1; (b) K_{A2}- affinity constant for reaction 2; (c) K_{A1} and K_{A2} were significantly different between 5 and 20 µg/mL adsorbed rTp0483 ($p<0.05$) (n=3). From Dickerson *et al* (2011).[105]

6.3.4. AFM Imaging of rTp0483 on SAMs

AFM was employed to investigate the surface distribution of rTp0483 on functionalized SAMs. Figure 6.5 shows representative AFM images of rTp0483 binding on each of the functionalized SAM layers and compares them to an unfunctionalized gold surface and to a model SAM ($-CH_3$). Based on its molecular weight the average area occupied by a rTp0483 molecule would be expected to be considerably less than the observed area. This suggests that rTp0483 aggregates as it adsorbs onto a surface. Aggregation was less pronounced on the $-COO^-$ SAM, where the protein was more evenly spread across the entire area. Also, the size of rTp0483 aggregates appeared larger on the $-NH_3^+$ SAM than the other three.

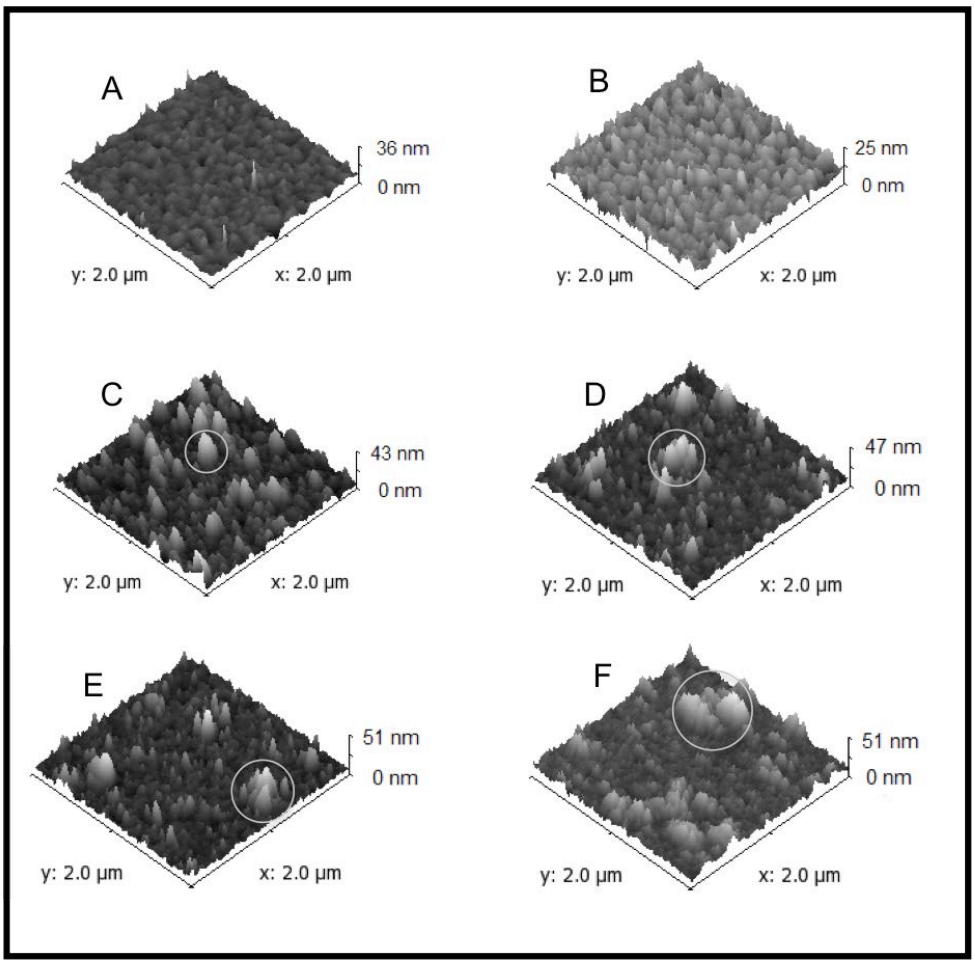

Figure 6.5: AFM comparison of gold, a model -CH_3 SAM and 10 µg rTp0483/mL coated SAMs. (A) Unmodified gold surface, (B) model SAM (-CH_3), (C) rTp0483 on -COO^- SAM, (D) rTp0483 on -CH_3 SAM, (E) rTp0483 on -OH SAM, and (F) rTp0483 on -NH_3^+ SAM. Representative areas with aggregated proteins are noted. From Dickerson *et al* (2011).[105]

6.3.5. rTp0483 Binding Domain Analysis

SPR was used to probe two potential FN binding sites located on rTp0483. Polyclonal antibodies were raised against two amino acid sequences of rTp0483, which were predicted to be surface-exposed and used to determine if they play a role in FN binding to rTp0483. Antibody binding onto rTp0483 adsorbed on -CH_3, -OH, and -NH_3^+ SAMs was indistinguishable from binding to the respective SAMs in

the absence of protein indicating that the targets were inaccessible when bound on these surfaces (results not shown). When considering the -COO^- SAM, significantly more of both antibodies bound to the adsorbed rTp0483 than directly to the unmodified surface ($p<0.05$).

Figure 6.6A shows that when adsorbed onto rTp0483, FN significantly decreased the binding of both antibodies ($p<0.05$). The binding of aTp#1 decreased from 540 ± 28 pg/mm^2 to 341 ± 19 pg/mm^2, and aTp#2 decreased from 465 ± 49 pg/mm^2 to 204 ± 16 pg/mm^2.

Figure 6.6B shows that when adsorbed rTp0483 on the -COO^- surface was blocked with aTp#1 or aTp#2, FN adsorption was significantly reduced ($p<0.05$). FN originally bound to rTp0483 at 846 ± 40 pg/mm^2, which decreased to 373 ± 71 pg/mm^2 in the presence of aTp#1 and to 270 ± 73 pg/mm^2 in the presence of aTp#2.

Figure 6.6C shows the results of blocking of FN with the peptide sequences corresponding to the selected antibodies. Binding of FN blocked with D1 was indistinguishable from FN alone (92% ± 10%). D2 was shown to have a measurable effect on FN binding, reducing FN binding to 88.0% ± 4.5% of FN alone ($p<0.05$). No inhibition of FN binding was observed for either negative control (A3- 101.9% ± 7.7% and P1- 110% ± 12%).

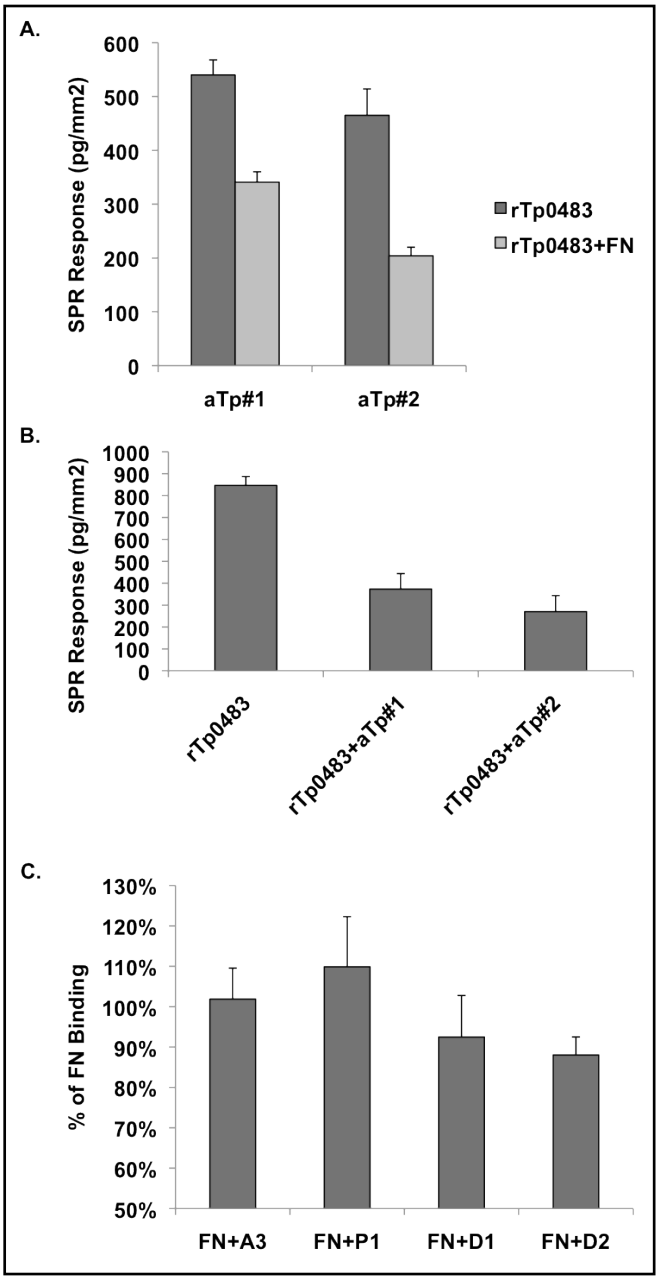

Figure 6.6: rTp0483 binding site studies. (A) anti-rTp0483 antibody binding on surfaces with adsorbed rTp0483 or rTp0483+FN, (B) FN binding on surfaces with adsorbed rTp0483 with and without antibodies, (C) FN binding when blocked with peptide sequences compared to FN alone on surfaces with adsorbed rTp0483. Binding of FN to rTp0483 reduced the binding of aTp#1 and aTp#2 ($p<0.05$). Data represent mean (n=2) with error bars representing standard error. Binding of FN onto rTp0483 and aTp#1 or aTp#2 was lower than binding of FN on rTp0483 alone ($p<0.05$). Data represent mean (n=2) with error bars representing standard error. Peptide D2 reduced FN binding ($p<0.05$). Data represent mean (n=6) with error bars representing standard error. From Dickerson *et al* (2011).[105]

6.3.6. FN Binding Domain Analysis

Figure 6.7 shows a comparison of binding of selected molecules to adsorbed FN or rTp0483+FN on -COO^- SAMs. The difference in heparin binding was not statistically significant on FN (61.3 ± 7.0 pg/mm^2) and rTp0483+FN (25 ± 13 pg/mm^2). Binding of anti-RGD antibody on FN (540 ± 72 pg/mm^2) was significantly higher than rTp0483+FN (267 ± 46 pg/mm^2) ($p<0.05$). Binding of gelatin on FN (940 ± 120 pg/mm^2) was significantly greater than on rTp0483+FN (211 ± 12 pg/mm^2) ($p<0.05$).

Figure 6.8 shows the binding of FN that had been pre-incubated with anti-RGD and alone to rTp0483 on -COO^- SAMs. The surface mass density bound was 91 ± 25 and 47 ± 33 pg/mm^2 for FN with 20 µg/mL and 50 µg/mL anti-RGD, respectively. The amount of FN alone that bound was 282 ± 15 pg/mm^2. ANOVA indicated that when blocked with anti-RGD at either ratio, FN binding was significantly reduced ($p<0.05$) suggesting the involvement of the RGD peptide sequence in rTp0483 binding. The same test indicated that the difference in binding between the two blocking concentrations was negligible.

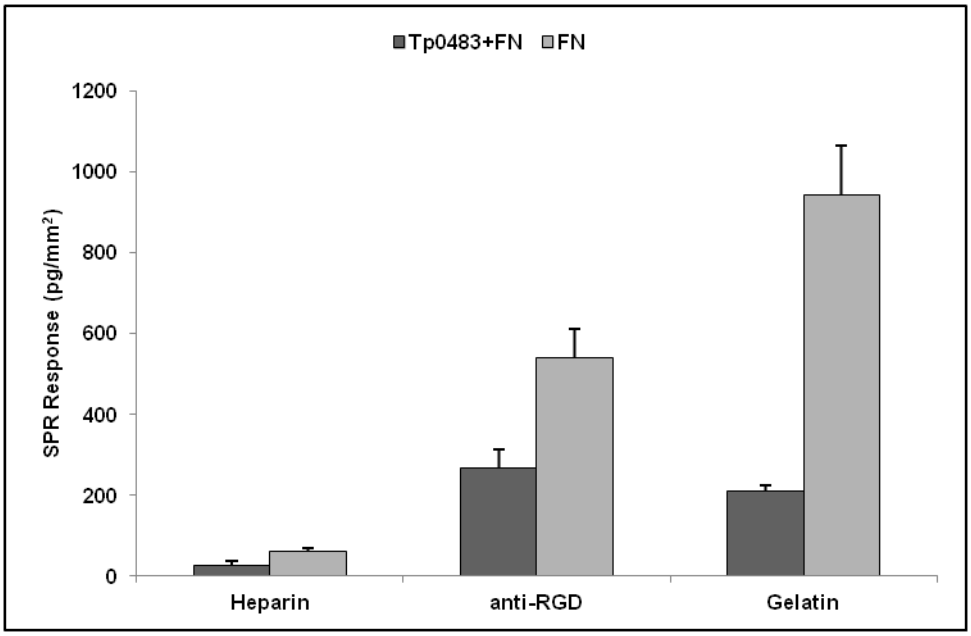

Figure 6.7: Binding of heparin, anti-RGD antibody, and gelatin to FN or rTp0483+FN on -COO^- SAMs. Binding to Tp0483+FN was determined to be significantly less than to FN for anti-RGD and gelatin ($p<0.05$). Data represent mean ($n=3$) with error bars representing standard error. From Dickerson *et al* (2011).[105]

6.4. Discussion

The goal of the studies presented in this chapter was to determine the effect that surface chemistry plays in the adsorption of rTp0483 and its ability to bind human plasma FN. Functionalized SAMs presenting positively charged, negatively charge, hydrophobic, and hydrophilic motifs were used to probe these interactions. Binding of rTp0483 to the SAM surfaces was investigated as well as binding of FN to adsorbed rTp0483.

QCM analysis indicated that all selected functionalized SAMs bound equal quantities of rTp0483 with the exception of -COO^-, which bound significantly more than the other groups, as seen in Figure 6.1A. Likewise, Figure 6.1B shows that adsorbed rTp0483 on -COO^- SAMs bound significantly more FN than the other three

under the selected conditions. The rTp0483 kinetic data shown in Table 6.1 indicated the affinity of rTp0483 for -COO^- SAMs was significantly higher than the other functionalized surfaces. Interestingly, under the conditions employed in the adsorption studies, rTp0483 binding on -OH, -NH_3^+, and -CH_3 SAMs was similar; however, a kinetic analysis revealed that the K_A was slightly higher on -OH SAMs than the other two. The apparent similarity in rTp0483 binding was likely due to a combination of mass transport effects and sub-saturation conditions. These results suggest that -COO^- functionalized SAMs provide the best conditions for rTp0483 binding, which is likely due to the high isoelectric point (pI) of the protein. The pI of rTp0483 is 9.3 and since all studies were conducted at a physiological pH (7.4), the protein would possess a net positive charge. This in turn should lead rTp0483 to interact most strongly with the negatively charged SAM via electrostatic interactions.

This idea can also be seen in the dissipation energy data shown in Figure 6.2. Dissipation energy is a measure of the total energy lost per cycle during QCM operation.[77, 78] The amount of energy lost is related to the physical properties of the material adsorbed on the quartz sensing crystal. A soft, fluid layer deforms while oscillating, which leads to high dissipation energy while a rigid, closely packed layer does not deform and as a result has low dissipation energy. rTp0483 adsorption on -CH_3 SAMs resulted in the lowest energy configuration, while adsorption on -OH SAMs resulted in the highest energy configuration. This indicates that on a hydrophobic surface rTp0483 forms a more tightly packed layer with low fluidity, and on a hydrophilic surface rTp0483 forms a much more deformable, fluid layer.

The dissipation energy for rTp0483 on -COO^- and -NH_3^+ SAMs was similar; however, there was a clear difference in both rTp0483 and FN adsorption. This difference can be explained as a combination of hydrophobic and charge effects. The observed trend is that the dissipation energy of rTp0483 is inversely proportional to hydrophobicity. By this logic, it would follow that rTp0483 adsorption on -COO^- SAMs would result in a dissipation energy value close to that of an -OH SAM and slightly higher than an -NH_3^+ SAM, which in turn should be higher than a -CH_3 SAM. This, however, does not take into consideration the ionic properties of -COO^- and -NH_3^+ SAMs. rTp0483 possesses a net positive charge under experimental conditions so it would be expected to bind more tightly to a negatively charged, hydrophilic surface than to a hydrophilic surface with no charge. By the same reasoning, binding to a positively charged surface would be looser than to an uncharged surface with similar hydrophobicity. It is also possible that this charge interaction contributes to the FN binding capacity of rTp0483 adsorbed onto -COO^- SAMs. The observation that FN binds to -COO^- SAMs but not onto -OH SAMs, which have higher dissipation energy, hints that rTp0483 must undergo a change in order to bind FN. The high energy of rTp0483 on -OH SAMs indicates a weak surface interaction and as a result rTp0483 is likely to have a conformation closely related to rTp0483 in solution. This fact may mean that FN binding by adsorbed rTp0483 is at least partially a surface mediated event. It is possible that the binding orientation of rTp0483 differs based on surface chemistry, and that the FN binding site is only displayed when it is bound to -COO^- SAMs or that the FN binding site of rTp0483 is normally concealed within a fold of the protein, and when rTp0483 encounters a -

COO^- SAM a change in conformation occurs exposing the binding site and allowing FN to bind.

FN binding with rTp0483 adsorbed on -COO^- SAMs was analyzed at two rTp0483 concentrations in order to gain more information about the mechanism of binding. Initial analysis at 20 μg rTp0483/mL suggested a bivalent analyte mechanism as stated above. Since FN is a dimeric protein with two nearly identical units, each should be able to bind rTp0483, thus a bivalent analyte mechanism is reasonable. Assuming this convention, one unit of a FN molecule encounters and binds rTp0483 on the surface, followed by the second unit binding to an additional rTp0483 protein to complete the AB_2-type complex. Following this study, it was of interest to determine whether with decreasing rTp0483 surface mass density there existed a point where the distance between proteins became too great for adsorbed FN to reach the second rTp0483 required for AB_2 formation. For this purpose, the concentration of rTp0483 was reduced to 5 μg rTp0483/mL and FN adsorption was evaluated. Interestingly, K_{A1} for FN adsorption was higher for 5 μg rTp0483/mL, while K_{A2} was higher for 20 μg rTp0483/mL. FN (440kDa) is significantly larger than rTp0483 (22kDa), so complete coverage of the surface by rTp0483 is not necessary and according to these results may actually lead to a lower surface mass density of FN. rTp0483 and FN adsorption studies along with AFM analysis suggested that protein aggregation on the surface may play a role. The most significant FN binding correlated to rTp0483 adsorbed on -COO^- SAMs, which also displayed the smallest and most evenly distributed aggregate formation. As the rTp0483 concentration increases, the size of the protein aggregates also likely

increases. It is possible that as the aggregate size increases, the affinity for FN of proteins within the aggregate becomes limited due to steric hindrance. This agrees with the minimal FN binding to rTp0483 adsorbed on the other SAM surfaces, which displayed larger rTp0483 aggregates when compared to -COO^- SAMs. Thus, at the lower concentration of 5 μg rTp0483/mL protein aggregates would be smaller, and likewise K_{A1} for FN greater. Conversely, at a concentration of 20 μg rTp0483/mL the size of protein aggregates would increase to limit the binding of a portion of rTp0483 proteins, leading to a smaller K_{A1}. The spacing of aggregates on each surface can help account for differences in K_{A2}. Once bound to rTp0483, FN would be stationary, and as a consequence, the chance of interacting with a second rTp0483 limited to the range of motion of the unbound FN unit. While the initial affinity of FN for rTp0483 was less at 20 μg rTp0483/mL than at 5 μg rTp0483/mL, for the secondary binding event the distance between aggregates becomes important. At 20 μg rTp0483/mL the distance between aggregates is likely less than at 5 μg rTp0483/mL, and accordingly the chance that a bound FN is able to reach a second rTp0483 increases.

Unfortunately, the crystal structure of rTp0483 has not been elucidated; however, an estimation of its size can be made. The partial specific volume (υ) of a large number of globular proteins was determined experimentally to fall within a tight range from 0.70-0.75 cm^3/g.[106] Using this value as a starting point, an estimate of protein volume was made based on the rTp0483 molecular weight using Equation 19. Here υ was assumed to fall in the middle of the range (0.73 cm^3/g), M_W

(g/mol) was the molecular weight of rTp0483, and N_A was Avogadro's number ($6.02x10^{23}$ molecules/mol).

$$\frac{\upsilon \, x \, 10^{24} \, \frac{A^3}{cm^3} \, x \, M_W}{N_A} \, x \, 0.001 \frac{nm^3}{A^3} = 1.21x10^{-3} \, x \, M_W \, \frac{nm^3}{molecule} \quad (19)$$

The molecular weight of rTp0483 is 22kDa, and the estimated volume is 27 nm^3. If surface adsorbed rTp0483 molecules are approximated as spheres the average surface area occupied by a single rTp0483 molecule can be estimated. Based on this approximation the surface area occupied by an rTp0483 molecule is 11.3 nm^2.

The shape of rTp0483 likely varies from surface to surface based upon dissipation energy data; however, this is not as apparent in Figure 6.5 because the surfaces were dried prior to imaging, which may have impacted protein shape; however, based on Figure 6.5, it is apparent that for all surfaces the elevated areas have an area greater than 11.3 nm^2, which supports the theory that rTp0483 binds in aggregate form rather than as single proteins. The size of these protein islands was found to vary with surface chemistry. On -NH_3^+ SAMs, protein islands were larger compared to the other surfaces. For -OH and -CH_3 surfaces, rTp0483 islands were smaller than for -NH_3^+, while the distance between each island was similar. Adsorbed rTp0483 aggregates were the smallest on -COO^- SAMs and were spread evenly across the entire surface. The size of the rTp0483 aggregates can be correlated to FN binding capacity. The -COO^- SAMs displayed the least aggregation

and the most uniform binding of rTp0483 across the surface. Because rTp0483 molecules are more spread out, it is probable that a greater number are able to take on an ideal binding configuration. As aggregates form, nearby rTp0483 may become restricted and thus access to potential binding sites could be inhibited.

Two peptide sequences of rTp0483 were identified as possible binding sites, and antibodies toward each were produced. The data show that aTp#1 and aTp#2 were able to inhibit FN binding to rTp0483 ($p<0.05$). When FN was added to rTp0483 prior to the antibodies, there was also a significant drop in antibody binding ($p<0.05$). Additionally, the two antibodies only bound to rTp0483 when immobilized on $-COO^-$ SAMs, which supports the idea that the targeted sites are obscured on all SAMs except for $-COO^-$.

Peptides matching the proposed FN binding sites on rTp0483 were synthesized and used to block FN. Peptides were evaluated because their small size eliminates the possibility of steric effects, which could result from blocking with the larger antibodies. Only D2 resulted in a significant decrease in FN binding ($p<0.05$). Based on this study, it appears that D1 did not play a direct role in FN-rTp0483 binding. It is probable that D2 plays some role; however, the observed reduction is not large enough to account for the entire binding event. The fact that significant inhibition was observed for both antibodies while little inhibition was seen for the specific peptides may indicate that the active FN binding sites of rTp0483 are located near the expressed sequences but do not coincide perfectly with them. Further characterization of the tertiary structure of Tp0483 is required to reach a conclusion.

FN domain studies were conducted to determine the regions of FN that are involved in rTp0483 binding. This was done based on changes in binding to FN when it was bound to rTp0483 compared to on unmodified -COO^- SAMs. In a native environment, the RGD binding site of FN enables the protein to bind to cells and cellular components throughout the body, thereby modulating cell processes such as attachment, migration, growth, and differentiation.[63] It is also thought to play some role in the binding of FN by *T. pallidum,* which helps the bacteria to infiltrate the body via interactions with cells and the ECM.[51-53, 64, 72, 73] Further, it has been theorized that the adhesion of various host proteins, including FN, to the outer surface of *T. pallidum* partially contributes to the bacterium's ability to remain in the body for long periods of time between outbreaks. When FN was bound to rTp0483 adsorbed on -COO^- SAMs, a 50% reduction in anti-RGD binding was observed compared to when FN was adsorbed on unmodified -COO^- SAMs. To investigate further the involvement of the RGD site, an antibody specific to the cell-binding domain of FN was used to block the RGD peptide sequence in an effort to determine whether this site plays a role in rTp0483 binding. This study demonstrated a significant decrease in FN binding when blocked with 20 μg/mL anti-RGD, which agrees with previous reports that indicated a measureable inhibition of *T. pallidum* binding to FN when it was incubated with anti-RGD.[64-67]

The heparin-binding domains of FN were also examined as they have been implicated previously as potential bacterial targets on FN.[71] Results did not show strong heparin binding on either of the prepared protein coatings. One possible explanation lies in the location of the major heparin-binding sites. The stronger

heparin II site is very close to the central cell-binding domain (CCBD), thus if there is an interaction in this region, it is reasonable to expect low binding on rTp0483+FN due to steric effects.[63] Low binding on FN can be accounted for based on electrostatic interactions. Heparin is strongly negative, and conversely, its binding site is strongly positive. When FN was adsorbed onto -COO^- SAMs, the positively charged binding site could have been attracted to the negatively charged surface resulting in minimal binding. The balance of heparin binding can be accounted for by the weaker heparin I site; since it is located farther away from the cell-binding domain, it would remain unaffected by the binding of rTp0483 and FN.

Lastly, gelatin binding was examined. Gelatin is a denatured form of collagen; therefore, the gelatin-binding domain also serves as a binding domain for collagen. Like the CCBD and heparin-binding domains, certain species of bacteria have been shown to interact with FN through this domain.[70] Studies revealed an 80% reduction in gelatin binding when FN was bound to rTp0483 adsorbed on -COO^- SAMs compared to FN bound to unmodified -COO^- SAMs. This outcome suggests that the gelatin/collagen-binding domain of FN may play a role in rTp0483 binding.

6.5. Conclusions

Binding of *T. pallidum* recombinant protein fragment rTp0483 was shown to be greatest on negatively charged -COO^- SAMs, while FN only bound in significant quantities to rTp0483 adsorbed on these surfaces. QCM analysis of dissipation energy to frequency shift ratio of rTp0483 adsorption to functionalized SAMs

suggested different binding configurations based on surface chemistry. Kinetic analysis of rTp0483 adsorption revealed that the strength of the bond between the protein and surface was dependent on surface chemistry. Also, kinetic analysis of FN binding on adsorbed rTp0483 demonstrated that the surface mass density of rTp0483 affects the strength of FN binding. Decreasing the concentration of adsorbed rTp0483 from 20 to 5 μg/mL increased K_{A1} and decreased K_{A2} for FN binding. Also, AFM analysis illustrated that rTp0483 binds as protein aggregates rather than single proteins. A blocking study toward the RGD sequence of FN demonstrated an involvement in rTp0483 binding, and through the use of antibodies and peptides, rTp0483 amino acids 316-333 were observed to play a role in FN binding. FN binding domain studies reinforced the importance of the RGD sequence and pointed toward the association of the collagen/gelatin-binding domain in rTp0483 binding. Through the development of an rTp0483 surface coating capable of binding FN with high affinity it will be possible to analyze the effect of rTp0483 on various aspects of the host response with and without FN in a manner resembling natural Tp0483 on the surface of *T. pallidum*. In the future this may lead to a better understanding of *T. pallidum* as well as potential applications in development of materials with antigenic disguise properties.

Chapter 7: HEMOCOMPATIBILITY ANALYSIS OF FIBRONECTIN BINDING, RECOMBINANT PROTEIN FRAGMENT RTP0483 ON CARBOXYLATE TERMINATED SELF-ASSEMBLED MONOLAYERS

7.1 Introduction

In order to explore the potential protective capacity of the putative surface protein fragment rTp0483 in conjunction with soluble plasma FN a number of tests were conducted to quantify any effect on surface hemocompatibility. The recombinant protein fragment rTp0483 was used because of its ability to bind plasma FN.[53] Surface chemistry often plays a role in the activity of adsorbed proteins.[99, 101, 107] The study of FN adsorption onto rTp0483 on functionalized SAMs in Chapter 6 indicated that binding was highest when rTp0483 was adsorbed on negatively charged -COO^- SAMs and so they were selected for hemocompatibility analysis. Plasma protein adsorption is the first response of the body to a foreign material and type and amount play a large role in the resulting hematological and immune response. Adsorption and activation of one such protein, FXII, initiates the intrinsic clotting pathway summarized in Section 2.3 and Figure 2.3. The positive feedback loop from kallikrein resulting from FXII activation is also relevant to this process. Because the intrinsic pathway is the primary clotting pathway on biomaterials it is key in understanding surface hemocompatibility. Platelet activation is another indicator of hemocompatibility. Activated platelets participate in the formation of blood clots by releasing clotting factors and acting as a catalyst for other events such as FXII activation.

Moments after exposure of a foreign body to blood, a mix of circulating proteins begin to adsorb to the surface. Fibrinogen (Fg) adsorbs to biomaterial surfaces and active platelets, is converted to insoluble fibrin by thrombin, and becomes cross linked to form a fibrin network that stabilizes blood clots. FXII becomes active FXIIa when it adsorbed to a negatively charged surface and leads to thrombin production and ultimately fibrin network formation through the intrinsic pathway. Human serum albumin (HSA) is the most plentiful protein in the blood and is commonly used to model protein adsorption. For these reasons Fg, FXII, and HSA were chosen to model this adsorption event based on their relevance to hemocompatibility quantification.[34-45] Intrinsic pathway activity as a result of FXII and kallikrein activation was examined along with platelet activation. Both have previously been employed for measurement of surface hemocompatibility.[35, 37-43, 45, 47, 48]

SPR was used to observe protein binding on functionalized SAMs. Intrinsic activity was quantified in solution and at the material interface using UV/Vis spectroscopy to measure p-nitroaniline (pNA) liberation from an H-D-Prolyl-L-phenylalanyl-L-arginine-p-nitroaniline dichloride (H-D-Pro-Phe-Arg-pNA•2HCl) substrate as a function of the conversion of prekallikrein to kallikrein by FXIIa. This reaction is illustrated in Figure 7.1. Phospholipids known as phosphatidylserines are exposed on the surface of activated platelets, which bind strongly with annexin-V proteins. Platelet activation was quantified based on phosphatidylserine presentation using FITC labeled annexin V (FITC-AXV). Binding of FITC-AXV was determined using fluorescence microscopy.

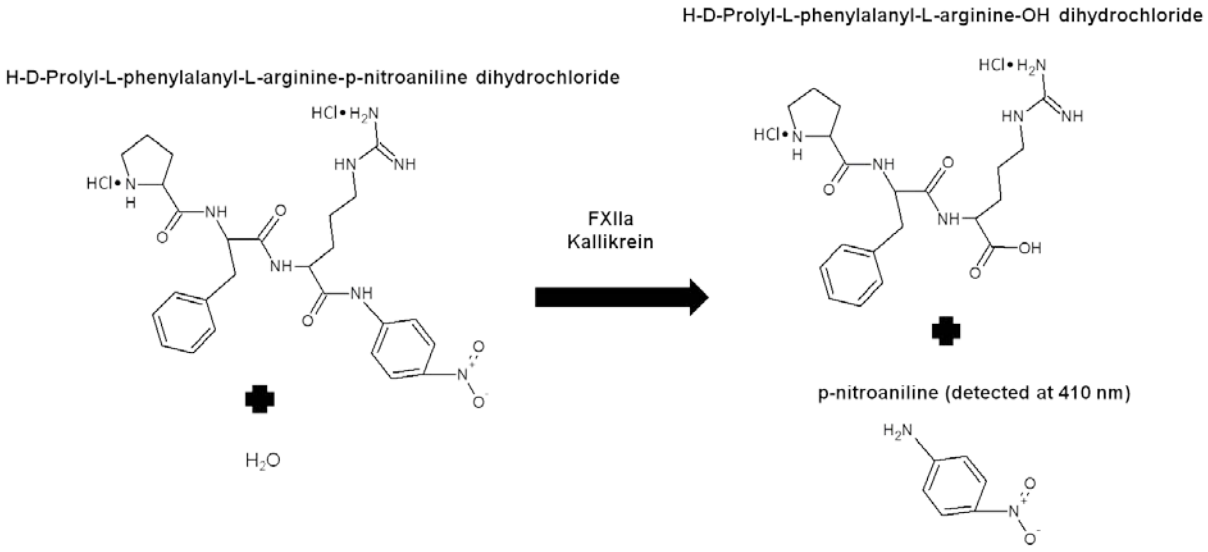

Figure 7.1: Overview of the method used to determine intrinsic pathway activity. H-D-Prolyl-L-phenylalanyl-L-arginine-p-nitroaniline dichloride (H-D-Pro-Phe-Arg-pNA•2HCl) is degraded by FXIIa and kallikrein in the presence of water to liberate pNA, which can be quantified by measuring the absorbance at 410 nm.

7.2 Experimental Procedures

7.2.1. Biomolecules and Reagents

DPBS was prepared as specified in Section 4.2.7, H-D-Pro-Phe-Arg-pNA•2HCl was purchased from Chromogenix (Milano, Italy) and fresh human platelets and plasma were obtained from the Central Kentucky Blood Center (Lexington, KY). Annexin V-FITC (AXV-FITC) was purchased from Invitrogen and diluted 1:50 in Tyrodes buffer (TB) (10 mM HEPES, 137 mM NaCl, 12 mM $NaHCO_3$, 5.5 mM glucose, 2.8 mM KCl, 1 mM $MgCl_2$, 0.4 mM Na_2HPO_4, pH 7.4) with 5 mM $CaCl_2$. Unless specified all proteins were purchased from Sigma. FXII was purchased from Haemtech (Essex Junction, VT). The protein fragment rTp0483 was expressed and purified as per the protocol provided in Section 4.2.4.

7.2.2. SPR

A Biacore X SPR unit was used for all plasma protein binding studies. SAMs were prepared as described in Section 5.2.1. DPBS was employed as a running buffer and was used to dilute all proteins to the desired concentrations. A constant flow rate of 50 μL/min was employed. Once a sample surface was docked it was primed with DPBS until the response signal in both flow channels was stable. Buffer was circulated through FC1 and FC2 in series in order to monitor signal stability. After the response had stabilized buffer flow was changed to single channel flow (either FC1 or FC2) for observation of protein binding and the other channel was used to monitor background noise. Protein samples were introduced through an injection port and after each injection the signal was allowed to stabilize before changes in the SPR signal were recorded. After the first flow channel was used flow was reversed and the other was used in a similar fashion.

7.2.3. Plasma Protein Adsorption

Plasma proteins were prepared in DPBS at physiological concentrations of 3 mg/mL fibrinogen (Fg), 45 mg/mL human serum albumin (HSA), and 20 μg/mL FXII while rTp0483 and FN were prepared at a concentration of 100 μg/mL in DPBS. Protein binding was analyzed on negatively charged -COO^- SAMs. Once the SPR signal was stable 100 μL of 100 μg rTp0483/mL was injected at a flow rate of 50 μL/min. The signal was allowed to stabilize then 100 μL of 100 μg FN/mL was injected at a flow rate of 50 μL/min. Alternately, either 100 μL of 100 μg rTp0483/mL or 100 μL of 100 μg FN/mL was injected alone at a flow rate of 50

μL/min. For each case, 50 μL of one of the plasma protein solutions was injected at a flow rate of 50 μL/min after the signal stabilized. Nonspecific plasma protein adsorption was determined by injection of 50 μL of each plasma protein solution onto unmodified -COO^- SAMs at a flow rate of 50 μL/min. Data is presented as a reduction in plasma protein adsorption compared to nonspecific adsorption on an unmodified SAM as shown in Equation 20.

$$Percent\ Inhibition = \left(\frac{\left(\frac{pg}{mm^2}\ protein\ on\ SAM - \frac{pg}{mm^2}\ protein\ on\ coated\ SAM \right)}{\frac{pg}{mm^2}\ protein\ on\ SAM} \right) x\ 100\% \quad (20)$$

7.2.4. Intrinsic Pathway Activation Study

Functionalized -COO^- SAM surfaces were prepared as detailed in Section 5.2.1 and equilibrated in 1 mL of DPBS for 30 min in a 24 well plate. The DPBS was removed and 300 μL of 100 μg rTp0483/mL, 300 μL of 100 μg FN/mL, or 300 μL of 2 mg/mL BSA was added to an equal number of wells and incubated 40 minutes at room temperature. At the same time 300 μL of 100 μg rTp0483/mL was added to an equal number of wells and incubated 40 minutes at room temperature then removed, washed twice with 1 mL of DPBS, then incubated with 300 μL of 100 μg FN/mL for 40 minutes at room temperature. After incubation all surfaces were washed twice with 1 mL of DPBS.

All tests were conducted with a single unit of plasma derived from a single donor. The second DPBS wash was removed and 200 μL of plasma was added to

each protein coated sample surface as well as to 3 empty wells, hereafter referred to as control plasma, and incubated at room temperature for 1 minute to allow FXII to activate and for prekallikrein to be converted to kallikrein. Then, 20 µL of plasma from each well was transferred into separate wells to determine intrinsic activity in the plasma; the remaining plasma was discarded. Next, 300 µL of 0.3 mM H-D-Pro-Phe-Arg-pNA•2HCl was added to each surface and plasma sample and reacted for 30 minutes at room temperature. The reaction was stopped by adding 75 µL of 20% (v/v) acetic acid from Sigma. 200 µL of each sample was transferred to a 96 well plate and the absorbance analyzed at 410 nm using a UV-Vis spectrophotometer equipped with a Cary 50 MPR microplate reader from Varian (Santa Clara, CA). The absorbance change of all sample groups was normalized to the change for control plasma

7.2.5. Platelet Activation Study

All tests were conducted with a single unit of plasma and platelets, each derived from a single donor. Protein coated -COO^- SAM surfaces were prepared as detailed in Section 7.2.4. Platelets were stored at room temperature and used within 3 days of arrival while plasma was aliquoted and stored at -20°C upon arrival. Platelets were diluted 1:6 in plasma and used immediately. Platelet activation experiments closely followed a protocol previously reported by Berrocal *et al.*[108] The second DPBS wash was removed from the surfaces and 500 µL of diluted platelet solution was added and incubated 2 hours at 37°C, 5% CO_2. The platelet solution was removed and the surfaces washed 3 times with 1 mL TB. 500

μL of FITC-AXV solution was added to each surface and incubated in the dark for 20 minutes at room temperature to allow the FITC-AXV to bind with surface exposed phosphatidylserine. The FITC-AXV solution was removed and the surfaces washed 3 times with 1 mL TB. Samples were imaged immediately.

Imaging was completed at 5X magnification using a Nikon Eclipse LV100 microscope with a FITC filter set (Melville, NY). Images were taken with a Nikon DS Qi1Mc camera. Data compilation and analysis were done using NIS-elements BR 3.0 software. Each image was analyzed based on the fluorescent intensity of each individual pixel. The lowest intensity value for each image was set to zero then the % fluorescence of the image was calculated based on all pixels with intensity greater than this background value. Data were normalized to the values for unmodified SAMs. Observed fluorescence was related to the amount of phosphatidylserine presented on the surface of active platelets thus it is possible to compare the relative platelet activity on each surface.

7.2.6. Statistical Analysis

Statistical analysis was performed using the Microsoft Office Excel Data Analysis tool, StatPlus. Multiple pair-wise comparisons were made using one-way analysis of variance (ANOVA) with a maximum p-value of 0.05. All data are reported as a mean $\pm$ standard error. Plasma protein adsorption and intrinsic pathway activation tests were n=3 and platelet activation experiments were n=5.

7.3 Results

7.3.1. Plasma Protein Adsorption

Percent inhibition of Fg, HSA, and FXII adsorption on rTp0483+FN, rTp0483, and FN coated SAMs is shown in Figure 7.2. The adsorption of Fg to each of the three coatings was significantly different ($p<0.05$) where rTp0483+FN resulted in a 79.0 ± 2.4% reduction, rTp0483 resulted in a 69.92 ± 0.76% reduction, and FN resulted in a 60.3 ± 1.8% reduction compared to adsorption onto unmodified $-COO^-$ functionalized SAMs. The inhibition of HSA adsorption was significantly higher on rTp0483+FN than on rTp0483 or FN ($p<0.05$), which were indistinguishable. Adsorbed rTp0483+FN resulted in a reduction in HSA adsorption of 90.2 ± 2.5% while rTp0483 resulted in a reduction of 75.0 ± 1.2% and FN resulted in a reduction of 69.8 ± 5.7%. The inhibition of FXII adsorption was similar for rTp0483+FN and FN where the reduction was 73.1± 5.6% and 73.7 ± 2.2% respectively. Adsorption on rTp0483 was lower than the other two groups ($p<0.05$) where adsorption was reduced by 52.5 ± 3.1%).

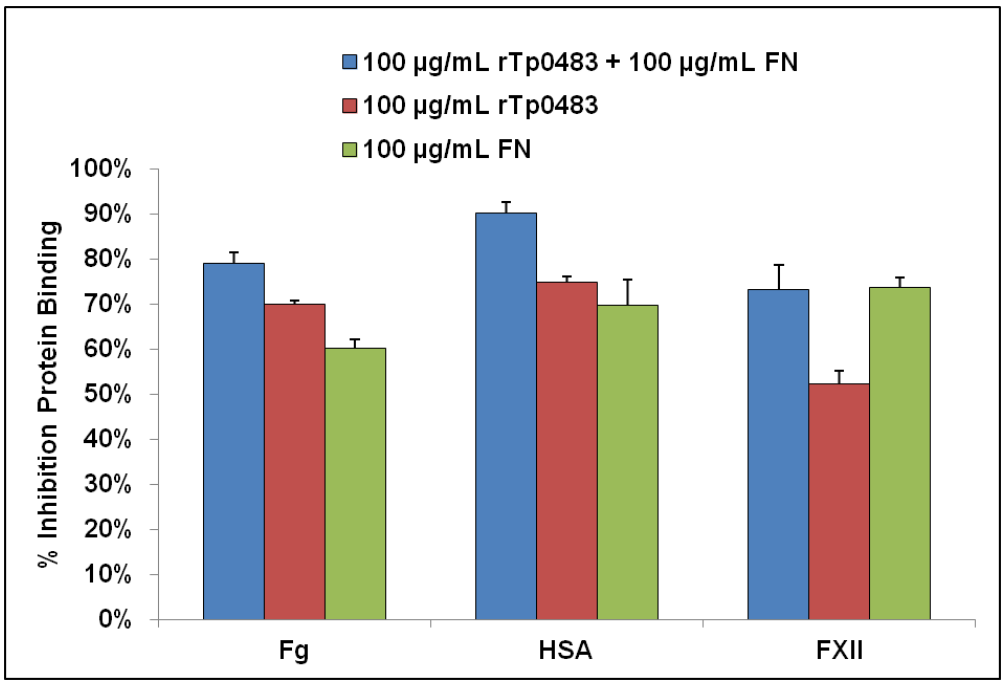

Figure 7.2: Comparison of plasma protein adsorption to rTp0483+FN, rTp0483, and FN on -COO^- functionalized SAMs. Percent inhibition was determined by subtracting the plasma protein adsorption on rTp0483+FN, rTp0483, or FN coated -COO^- functionalized SAMs from adsorption on unmodified -COO^- functionalized SAMs, dividing by the protein adsorbed to the unmodified -COO^- functionalized SAMs, and multiplying by 100. Fg and HSA onto rTp0483+FN less than rTp0483 or FN ($p<0.05$) and FXII onto rTp0483+FN less than rTp0483 ($p<0.05$). Data is reported as a mean (n=3) with error bars representing standard error.

7.3.2. Intrinsic Pathway Activation Study

Activation of the intrinsic clotting pathway at the surface and in plasma is shown in Figure 7.3. The absorbance of sample groups was measured after 30 min and the values were normalized to control plasma. Liberation of pNA as a result of FXII activation and conversion of prekallikrein to kallikrein was used as a measure of the relative intrinsic activity in each of the sample groups. Activity in plasma samples with rTp0483+FN (1.03 ± 0.02), FN (1.02 ± 0.02), and BSA (1.06 ± 0.02) coatings were indistinguishable from control plasma while activity in plasma for

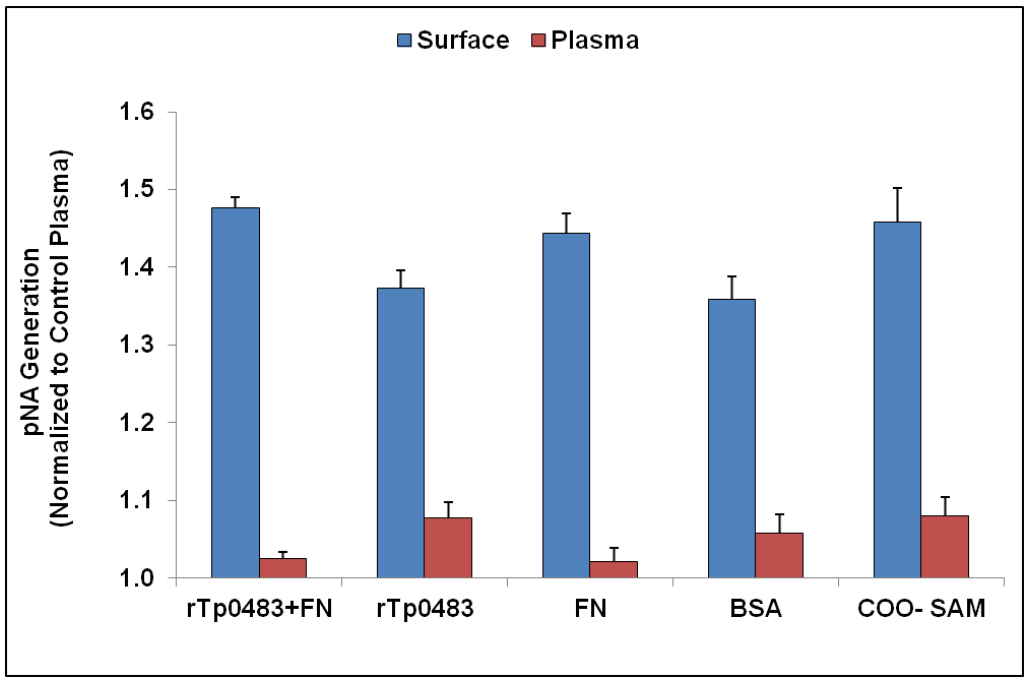

Figure 7.3: Comparison of intrinsic pathway activation on rTp0483+FN, rTp0483, and FN coated -COO^- functionalized SAMs as well as unmodified COO^- functionalized SAMs compared to control plasma. Samples were taken at the material interface and in solution and activity measured as the absorbance at 410 nm after 30 min. Intrinsic activity at the surface was elevated for all sample groups ($p<0.05$). rTp0483+FN was higher than rTp0483 and BSA ($p<0.05$), which were indistinguishable, and was indistinguishable from FN and unmodified -COO^- SAMs. Intrinsic activity in plasma higher than control plasma for rTp0483 and unmodified -COO^- SAMs ($p<0.05$). Data reported as a mean (n=3) with error bars representing standard error.

rTp0483 (1.08 ± 0.3) and unmodified -COO^- SAMs (1.08 ± 0.02) was slightly elevated ($p<0.05$). Alternately, activity at the surface was elevated for all test groups with rTp0483+FN (1.48 ± 0.02), rTp0483 (1.37 ± 0.02), FN (1.44 ± 0.02), BSA (1.36 ± 0.02), and unmodified -COO^- SAMs (1.46 ± 0.03) respectively compared to control plasma ($p<0.05$). The intrinsic activity of surface adsorbed FN was higher than adsorbed rTp0483 or BSA ($p<0.05$) and equal to unmodified -COO^- functionalized SAMs. At the same time, rTp0483 showed similar activity to BSA coated -COO^-

functionalized SAMs until FN was added at which point the intrinsic activity increased to a rate indistinguishable from FN alone.

7.3.3. Platelet Activation Study

Sample images of platelet activation are shown in Figure 7.4. Both the FN coated and unmodified -COO^- functionalized SAMs visually appeared to display more fluorescence than the other surfaces. Quantitative comparison of the platelet activation on each of the coated surfaces normalized to unmodified -COO^- functionalized SAMs is summarized in Figure 7.5. Platelet activity on FN coated SAMs was 1.38 ± .23 times that of the activity on unmodified -COO^- functionalized SAMs , on rTp0483 it was 0.26 ± .06 times that of activity on unmodified -COO^- functionalized SAMs, and on rTp0483+FN it was 0.18 ± .03 times that of activity on unmodified -COO^- functionalized SAMs. ANOVA indicated that platelet activation on FN coated and unmodified -COO^- SAMs was indistinguishable and that activation on rTp0483 and rTp0483+FN coated SAMs was indistinguishable. The same ANOVA showed that platelet activation on FN coated and unmodified -COO^- SAMs was significantly higher than activity on rTp0483 and rTp0483+FN coated SAMs ($p<0.05$).

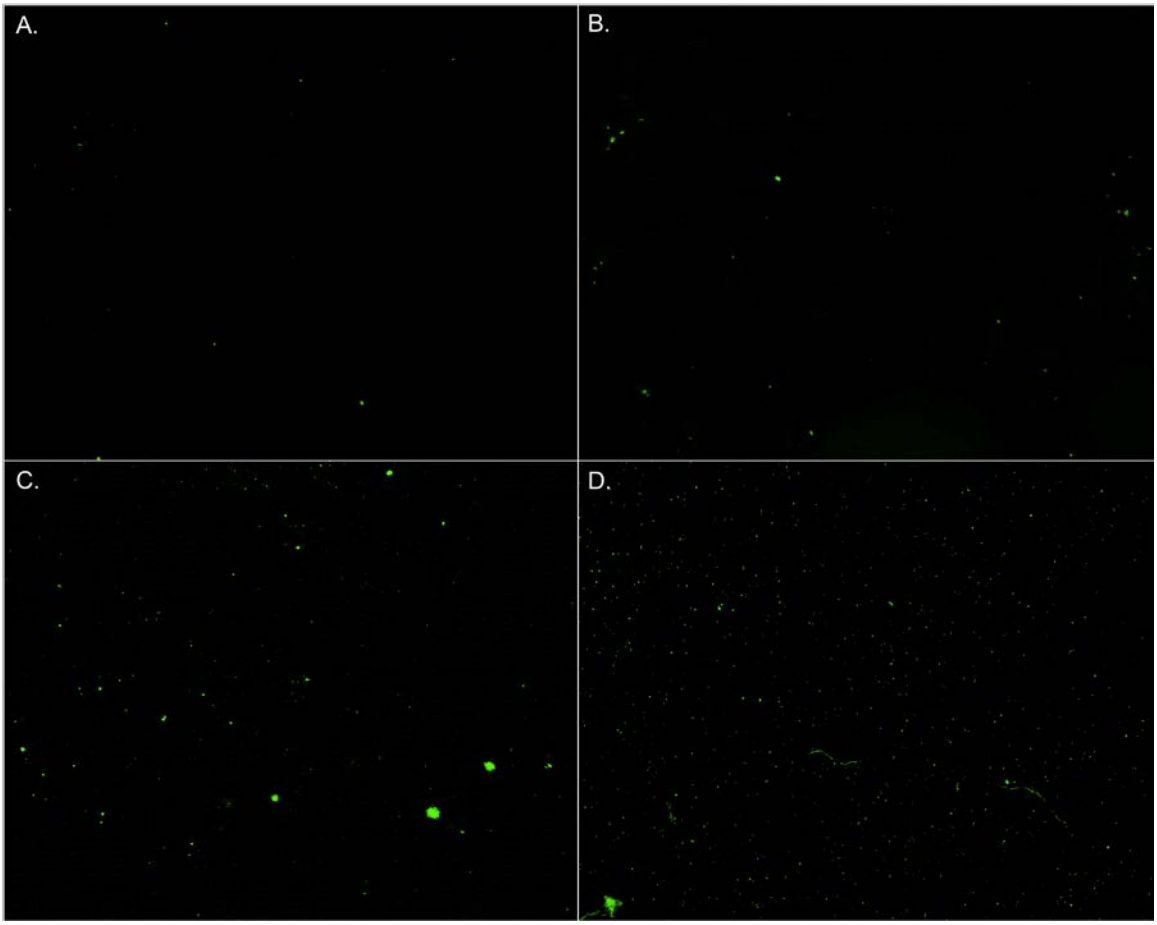

Figure 7.4: Sample fluorescence microscope images of platelet activation on rTp0483+FN, rTp0483, and FN coated -COO^- functionalized SAMs. Activation on an unmodified -COO^- functionalized SAM is shown as well. Platelet activation was quantified by the use of FITC labeled annexin-V (FITC-AXV). A) rTp0483+FN coated SAM, B) rTp0483 coated SAM, C) FN coated SAM, and D) unmodified -COO^- functionalized SAM.

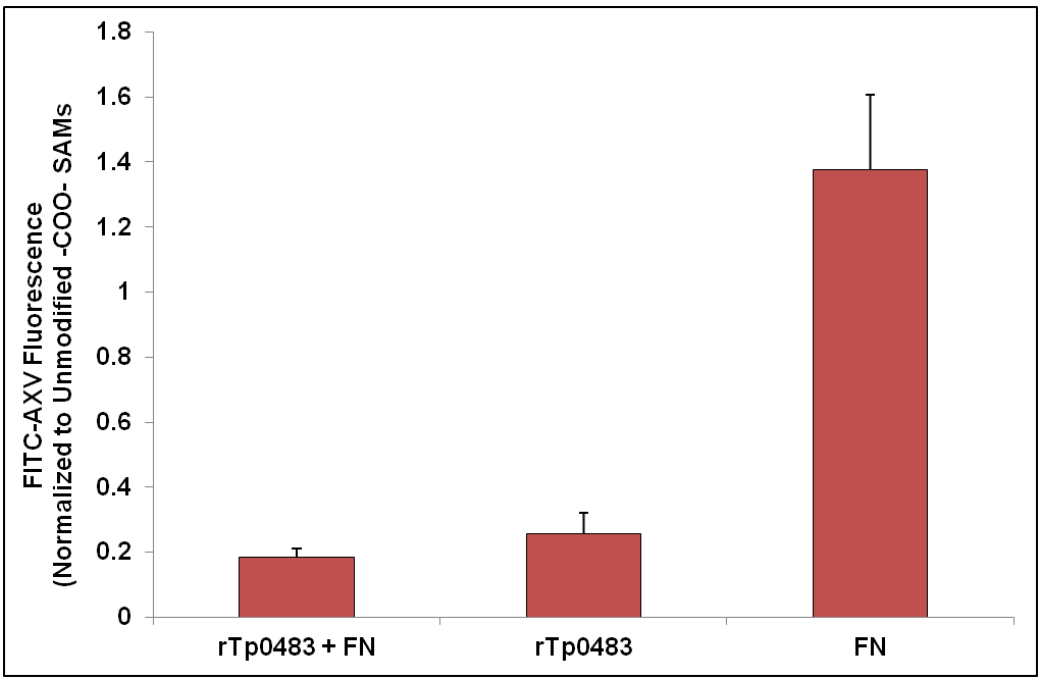

Figure 7.5: Comparison of platelet activation on rTp0483+FN, rTp0483, and FN coated -COO^- functionalized SAMs normalized to unmodified -COO^- functionalized SAMs. Platelet activation on FN indistinguishable from activation on unmodified -COO- SAMs while activation on rTp0483+FN and rTp0483 was significantly lower ($p<0.05$) and indistinguishable from one another. Data is reported as a mean (n=5) with error bars representing standard error.

7.4. Discussion

A number of outer membrane proteins (OMPs) found on the surface of *T. pallidum* are believed to act as antigens for immune response as well as facilitate bacteria interactions with the ECM.[51-58, 64, 72-74] Despite the existence of such proteins, *T. pallidum* exhibits an ability to evade the host immune response and lie latent for extended periods of time. A putative *T. pallidum* OMP called rTp0483 was isolated that shows an ability to bind soluble FN. Here it is theorized that soluble FN may be bound in order to increase the hemocompatibility of *T. pallidum*

The adsorption of Fg, HSA, and FXII to SAMs coated with rTp0483+FN, rTp0483, or FN was investigated. In all cases, protein binding was reduced by more than 50% compared to unmodified SAMs. Adsorption of rTp0483+FN resulted in the largest reduction in Fg and HSA adsorption while adsorption of rTp0483 resulted in a moderate decrease in Fg binding compared to FN. Adsorption of rTp0483+FN and FN produced similar results for FXII adsorption while adsorption of rTp0483 was less effective. These results indicate that for Fg, HSA, and FXII at physiological concentrations adsorption of rTp0483+FN reduces further protein adsorption as well as or more effectively than FN or rTp0483 alone.

Fg plays an important role in the coagulation cascade; it is known to activate platelets and is converted to fibrin by thrombin in order to form a fibril network, which aids in thrombus stabilization.[34, 38-45] It is interesting that significant Fg binding was observed on all coated -COO^- SAMs. A study by Makogonenko *et al.* found that FN and Fg bound only after Fg had been converted to fibrin.[109] One difference that may account for this is that here Fg binding to surface adsorbed FN was observed whereas in the study by Makogonenko *et al.* FN binding to surface adsorbed Fg was examined. The same manuscript indicated that the conformation of Fg is quite labile, which would be even more apparent while free in solution.[109] The binding activity of Fg may have been affected by immobilization, which could account for low FN binding. Reduction of Fg binding when FN was added to an rTp0483 coated SAM may indicate access to Fg specific domain(s) is being restricted. As a result of this effect the thrombogenic potential of a surface with

adsorbed rTp0483+FN may be attenuated by reducing the Fg binding ability of bound FN.

HSA while not an adhesin protein, is found in normal plasma at a concentration of 30-50 mg/mL making it the most prevalent protein in the blood; its high concentration makes it a common model for protein adhesion.[37, 40] Thus, the observed reduction in binding suggests an overall decrease in protein binding, which may be indicative of fouling resistance. As with Fg, rTp0483+FN was more effective in reducing adsorption of HSA when compared to rTp0483 or FN alone.

FXII is a precursor of the intrinsic clotting pathway.[34, 35, 38, 39, 41, 43-45] Adsorption of this factor to a material surface and subsequent conversion to an active form (FXIIa) begins a cascade of biochemical events that result in the conversion of Fg to fibrin. FXII binding onto adsorbed rTp0483 was reduced when FN was added prior to the introduction of FXII. Also, binding of FXII to FN on rTp0483 was the same as binding on FN alone. Conversion of circulating FXII to active FXIIa is a surface mediated process; therefore, if less FXII is bound it stands to reason that intrinsic activity could lessen as well.[38, 41, 45] These results point toward a possible connection between soluble FN binding by rTp0483 and the reduction of plasma protein binding.

In addition to plasma protein adhesion, intrinsic clotting pathway activation was studied at the interface of protein coated -COO^- functionalized SAMs as well as in solution. This coagulation pathway is controlled by a number of precursors including surface mediated activation of FXII. In the plasma protein inhibition study a significant drop in FXII binding was observed when FN was added to adsorbed

rTp0483, which suggested that there might be a reduction in intrinsic pathway activation as well; however, the opposite was observed. Though adsorbed rTp0483+FN bound less FXII, it led to increased intrinsic activity compared to rTp083 alone. In solution the only group other than unmodified -COO^- functionalized SAMs that showed a significant increase in activity was rTp0483. The SPR adsorption study considered only the adsorption of FXII to the protein coated SAMs; however, other components of the intrinsic cascade must be considered to get the complete picture. The intrinsic pathway is initiated by the spontaneous conversion of FXII into an active FXIIa form when it interacts with a negatively charged surface; however, the involvement of kallikrein is also important.[38] All test groups generated significant intrinsic activity at the surface. Unreactive prekallikrein is activated by FXIIa and in turn kallikrein activates FXII. The intrinsic activity assay measures the overall response, which includes the contributions of FXIIa and kallikrein. Thus, the differences between FXII adsorption and intrinsic activity are likely due to the effects of kallikrein. Another possibility is that simply binding to a surface is not sufficient to initiate FXII activation. rTp0483 alone bound 20% more FXII than either FN or rTp0483+FN; however, intrinsic activity was significantly lower. With an isoelectric point of 9.3 at physiological pH 7.4 rTp0483 possesses a net positive charge. Conversely, FN has an isoelectric point of 6.1 meaning it possesses a net negative charge. The positive charge of rTp0483 could potentially be slowing the autoactivation of FXIIa. Subsequently, when FN is added to rTp0483 the negative charge of FN allows for the activation of FXII to proceed and as a result the rate of intrinsic activity increases. The increase in intrinsic

activity in solution for rTp0483 may be related to the higher surface concentration as well. One possible explanation might be that FXII is so tightly packed on adsorbed rTp0483 that as it converts into FXIIa a small amount is forced from the surface and leads to activity in the surrounding plasma. *In vivo* this would be less of a concern as any FXII or FXIIa that detaches would be carried away by blood flow.

Platelet activation is one of the most commonly studied events in the quantification of hemocompatibility.[35, 37, 39, 40, 42, 43, 47, 48] Activated platelets play a major role in clot formation through the secretion of clotting factors and proteins as well as facilitating other key biological events.[39] In general, low platelet activation was observed for all surfaces as can be seen in Figure 7.4; this is partially due to the negative charged -COO^- functionalized SAMs that the selected proteins were adsorbed onto. Prior studies saw a decrease in platelet activation when a surface was functionalized with -COO^- groups.[43, 48] Adsorption of 100 μg rTp0483/mL appeared to be sufficient to further reduce platelet activation. Adsorption of 100 μg FN/mL was indistinguishable from an unmodified SAM initially; however, when added to SAMs that were incubated with 100 μg rTp0483/mL it resulted in platelet activation equivalent to 100 μg rTp0483/mL alone. These results suggest that rTp0483 adsorbed on a -COO^- functionalized SAM surface is an effective method to reduce platelet activation. Furthermore, the data suggest that platelet activation as a result of exposure to FN on a -COO^- SAM can be reduced significantly by adsorbing rTp0483 onto the surface prior to the adsorption of FN.

The role of soluble FN in platelet activation and aggregation remains a debated topic. Work by Reheman *et al.* and Cho *et al.* reported conflicting outcomes;

one study found that soluble FN inhibited platelet activation while the other found that it accelerated it.[110, 111] Addition of the RGDS cell-binding peptide from FN had been shown to inhibit FN binding for platelets.[112] Likewise, the RGD peptide was able to inhibit *T. pallidum* adhesion to human endothelial cells and surface adsorbed FN.[64] These observations suggest that rTp0483 may interact with FN in a way similar to *T. pallidum* by binding to the cell-binding sites of FN and inhibiting platelet adhesion. This property would be highly desirable for a blood contacting biomaterial. FN will eventually adsorb to the surface irrespective of the material and this will lead to platelet adhesion, which in turn leads to blood clotting on the biomaterial; however, if a layer of rTp0483 were applied prior to implantation, FN would still bind but according to these results it would be unable to facilitate platelet adhesion.

7.5. Conclusions

Plasma protein adsorption, intrinsic pathway activation, and platelet activation were examined as indicators of hemocompatibility for $-COO^-$ functionalized, alkanethiol SAMs coated with rTp0483 and/or human plasma FN. Studies showed significant plasma protein inhibition and minimal platelet activation on $-COO^-$ functionalized SAMs with adsorbed rTp0483+FN. These results indicate that binding of soluble plasma FN by rTp0483 may help to reduce further interactions with plasma proteins as well as inhibit FN mediated platelet activation.

Chapter 8: PHAGOCYTIC RESPONSE OF MOUSE MACROPHAGES TO FN BINDING RECOMBINANT PROTEIN FRAGMENT RTP0483

8.1. Introduction

The implantation of a biomaterial into the body elicits a complex immune reaction.[113, 114] As detailed in Section 2.2 the response of phagocytic cells, such as macrophages, to the implantation of a biomaterial plays a key role in the overall biocompatibility of the implant.[115] Soon after entry into the body macrophages adhere to the surface of a biomaterial; once adsorbed these cells regulate the immune response toward the implant by excreting inflammatory chemicals, producing reactive species, and potentially engulfing the material.[116-118] For larger implants the possibility exists that macrophages will fuse into multinucleated giant cells that results in a chronic immune response.[119] Attenuating this response is critical in the development of new biomaterials. Common methods of assessing macrophage response to biomaterials include the measure of cytokine secretion and reactive species, examination of phagocytosis, and extent of macrophage adhesion to a surface.[120-127]

In Section 2.4 the unique structure of *T. pallidum's* outer membrane was discussed. The outer surface of the bacteria lacks LPS found on other gram-negative bacteria and also displays less than 1% of the number of proteins typically found on *E. coli*. The lack of antigenic targets is thought to play a role in the immunoevasiveness of *T. pallidum*; however, the defenses of the bacteria are not perfect and over time an effective immune response is mounted and the majority of the bacteria are eliminated. The immune response to *T. pallidum* is believed to be in

response to OMPs found on the surface of the bacteria.[55] The FN binding protein fragment rTp0483 was chosen for study because it is believed to play a role in *T. pallidum's* ability to circumvent the host immune response. The immune response to rTp0483 before and after FN adsorption was investigated by examining the response of macrophage cells.

Two cell systems were employed; CRL-2449 cells are a nonadherent mouse macrophage tumor cell line and RAW 264.7 cells are an adherent mouse macrophage tumor cell line. The effect of FN added to adsorbed rTp0483 on surfaces small enough to be engulfed by macrophages was examined by coating plain and carboxyl functionalized (COO^-) polystyrene microspheres (PSMs) with the proteins and observing the phagocytic response of CRL-2449 cells in solution. Responses to rTp0483 and FN on rTp0483 were compared to the response of FN coated, BSA coated, and unmodified PSMs. The effect of FN added to adsorbed rTp0483 on large surfaces was determined by coating COO^- well plates (WPs) with the proteins and observing the phagocytic response of adsorbed RAW 264.7 cells. Responses to rTp0483 and FN on rTp0483 were compared to the response to FN coated, BSA coated, and unmodified surfaces. In each case, the response of macrophages stimulated directly with the proteins in solution was also observed.

The response of CRL-2449 cells was determined by measuring the production of the inflammatory cytokine tumor necrosis factor α (TNF-α), the generation of the antimicrobial nitric oxide (NO), and by examining the phagocytosis of protein coated, fluorescent PSMs using flow cytometric analysis.

The response of RAW 264.7 cells was determined through measuring the generation of TNF-α and NO and calculating the number of adherent macrophage cells.

8.2. Experimental Procedures

8.2.1. Biomolecules and Reagents

CRL-2449 mouse tumor macrophages were purchased from the American Type Cell Collection (ATCC (Manassas, VA)) and RAW 264.7 mouse tumor macrophages were purchased from Sigma. Complete CRL-2449 medium (CM_{CRL}) was prepared with 1% (v/v) penicillin-streptomycin from Lonza (Walkersville, MD) and 10% heat-inactivated, iron supplemented bovine calf serum (Lonza) in Dulbecco's Modified Eagle Medium (DMEM) purchased from ATCC. Complete RAW 264.7 medium (CM_{RAW}) was prepared with 1% (v/v) penicillin-streptomycin and 10% heat-inactivated fetal bovine serum (Lonza) in DMEM. Mouse TNF-α enzyme-linked immunosorbent assays (ELISAs) were purchased from Thermo Scientific and assays for NO_2^- detection were purchased from Cayman Chemicals (Ann Arbor, MI). Plain and COO^-, 200 nm diameter, fluorescent (fluorescein core) and non-fluorescent PSMs were purchased from Polysciences (Warrington, PA). DPBS was prepared as specified in Section 4.2.7. All proteins were purchased from Sigma unless otherwise specified. The protein fragment rTp0483 was expressed and purified as per the protocol provided in Section 4.2.4.

8.2.2. Cell Culture

CRL-2449 cells were suspended in 10 mL of prewarmed CM_{CRL} and seeded at 37°C and 5% CO_2 in 75 mm^2 culture flasks (Fisher). The culture media was replaced every 2-3 days depending on cell growth and the cell density of CRL-2449 was maintained between 2 x 10^5 and 1x 10^6 cells/mL. When the cell density approached 1x 10^6 cells/mL any weakly attached cells were recovered by scraping, centrifuged at 1000 RPM for 5 minutes, and the media replaced. RAW 264.7 cells were suspended in 10 mL of prewarmed CM_{RAW} and seeded at 37°C and 5% CO_2 in 75 mm^2 culture flasks. The culture media was removed every 2-3 days and replaced depending on cell growth. Cells were not allowed to become completely confluent in order to preserve proper cell morphology.

8.2.3. Protein Surface Adsorption and Stability Validation

The binding of rTp0483 and FN to plain and COO^- PSMs was characterized by BCA assay while stability of the protein coatings was determined by zeta potential analysis. 500 µL of 30 µg rTp0483/mL in DPBS was prepared and either 5 µL of 2.5% (w/v) 200 nm plain or COO^- PSMs were added. The samples were incubated on a rotating test tube rack at room temperature for 1 hour then the PSMs were recovered by centrifugation at 15,000 RPM for 30 minutes at 4°C. The supernatant was removed and saved for BCA analysis. The rTp0483-coated PSMs were resuspended in 1 mL of 2 mg BSA/mL in DPBS by sonication in 1 second pulses for 30 seconds and incubated on a rotating test tube rack at room temperature for 30 minutes in order to block any areas still not covered by rTp0483 against nonspecific

adsorption, then the PSMs were recovered by centrifugation at 15,000 RPM for 30 minutes at 4°C. The samples were resuspended in 1 mL of DPBS by sonication in 1 second pulses for 30 seconds and incubated on a rotating test tube rack for 15 minutes to wash away any remaining BSA in the sample tubes. The PSMs were recovered by centrifugation at 15,000 RPM for 30 minutes at 4°C and the samples resuspended in 1 mL of 50 μg FN/mL in DPBS by sonication in 1 second pulses for 30 seconds. 1 mL of 50 μg FN/mL in DPBS was also mixed with 5 μL of 2.5% (w/v) 200 nm plain or COO^- PSMs in separate vials. With identical BSA blocked, rTp0483 coated PSMs another 1 mL wash of DPBS was used to resuspend the PSMs in place of 50 μg FN/mL. The samples were incubated on a rotating test tube rack at room temperature for 1 hour then the PSMs were recovered by centrifugation at 15,000 RPM for 30 minutes at 4°C and the supernatant removed and saved for BCA analysis.

To test protein adsorption onto COO^- WPs 228 μL of 50 μg rTp0483/mL in DPBS or 200 μL of 100 μg FN/mL in DPBS was added to wells and incubated 1 hour at room temperature. Solutions were removed and saved for BCA analysis. Surfaces were gently washed with DPBS then 200 μL of 100 μg FN/mL in DPBS was added to rTp0483 coated wells and incubated 1 hour at room temperature. Solutions were removed and saved for BCA analysis.

A modified form of the BCA assay protocol outlined in Section 4.2.7 was used to measure protein concentration in solution. The samples and reagents were prepared as described; however, 25 μL of each sample and standard were combined with 200 μL of working reagent in a 96 well plate and incubated at 37°C for 1 hour. The change in sample absorbance was measured at 562 nm using a UV-Vis

spectrophotometer equipped with a Cary 50 MPR microplate reader. The amount of adsorbed protein was determined by subtracting the concentration of rTp0483 or FN in solution after incubation with PSMs from the initial concentration then multiplying by the sample volume to obtain the mass of adsorbed protein. The effect of left over BSA from the blocking step between rTp0483 and FN adsorption was accounted for by subtracting the BSA concentration left after washing with DPBS from the total protein concentration remaining after adsorption of FN to BSA blocked rTp0483.

Zeta potential analysis was conducted using a Zetasizer Nano-ZS (Malvern, UK) with disposable capillary cells (DTS1061) also from Malvern. Zeta potential is a measure of particle surface charge and is determined by measuring the response of particles in solution to an applied current. When a current is applied to charged particles in solution they move toward the electrode of opposite charge and by analyzing the direction and speed of the particles a measure of the polarity and strength of the surface charge can be made. Protein coatings were applied to plain and COO^- PSMs as described above and the PSMs were incubated at least an hour in 2 mg BSA/mL in DPBS to block any uncoated areas against nonspecific protein adsorption. Plain and COO^- PSMs blocked for an hour in 2 mg BSA/mL in DPBS as well as plain and COO^- PSMs in DPBS were also analyzed. After preparation, 100 µL of each sample group, coated and uncoated was combined with 1 mL of CM_{CRL} and analyzed immediately with the instrument. The zeta potential of each sample group was assayed in triplicate at an initial time point and again after 10, 20, and 30

minutes. At each time point the zeta potential of the sample was determined 30 times and averaged.

8.2.4. Phagocytosis of Protein Coated Microspheres

CRL-2449 cells were cultured as described in Section 8.2.2 then seeded into 24 well plates at a concentration of 2 x 10^5 cells/mL of CM_{CRL}. Cells were incubated overnight at 37°C and 5% CO_2 prior to stimulation with microspheres. 1 mL of 60 µg rTp0483/mL in DPBS was prepared and 10 µL of 2.5% (w/v) 200 nm either plain or COO^- PSMs were added. Fluorescent PSMs (ex = 441nm, em = 486nm) were used for flow cytometry experiments and non-fluorescent PSMs were used for all other studies. The sample was incubated on a rotating test tube rack at room temperature for 1 hour then the PSMs were recovered by centrifugation at 15,000 RPM for 30 minutes at 4°C and the supernatant was removed. The PSMs were blocked against nonspecific adsorption in 1 mL of DPBS with 2 mg BSA/mL by sonication in 1 second pulses for 30 seconds. The sample was incubated on a rotating test tube rack at room temperature for 30 minutes then the PSMs were recovered by centrifugation at 15,000 RPM for 30 minutes at 4°C and the supernatant was removed. The PSMs were resuspended in 1 mL of DPBS by sonication in 1 second pulses for 30 seconds. 500 µL of the rTp0483 coated PSM solution was combined with 500 µL of 100 µg FN/mL in DPBS for a final concentration of 50 µg FN/mL while the other 500 µL of rTp0483 coated PSM solution was further diluted with 500 µL of DPBS. In separate vials, 1 mL of 50 µg/mL FN in DPBS was prepared and 5 µL of 2.5% (w/v) plain or COO^- PSMs were added. The samples were incubated on

a rotating test tube rack at room temperature for 1 hour then the PSMs were recovered by centrifugation at 15,000 RPM for 30 minutes at 4°C and the supernatant removed. The coated PSMs were resuspended in 1 mL of DPBS with 2 mg BSA/mL by sonication in 1 second pulses for 30 seconds. In separate vials 1 mL of DPBS or 1 mL of DPBS with 2 mg BSA/mL was prepared and 5 µL of 2.5% (w/v) plain or COO^- PSMs were added as controls. All samples were incubated on a rotating test tube rack at room temperature for 1 hour then sonicated in 1 second pulses for 30 seconds and seeded at 1.5 x 10^9 microspheres/well. After stimulation with microspheres the plates were incubated at 37°C and 5% CO_2 for 1, 4, 16, or 24 hours. The cell samples were transferred to microcentrifuge tubes (Fisher) and the CM_{CRL} removed by centrifugation at 1000 RPM for 5 minutes at 4°C. The samples were washed twice for 10 minutes with 1 mL DPBS and the cells recovered each time by centrifugation at 1000 RPM for 5 minutes at 4°C. The cells were fixed by incubating 15 minutes in 500 µL of 1% paraformaldahyde. The paraformaldahyde was removed by centrifugation at 1000 RPM for 5 minutes at 4°C and the samples were resuspended in 1 mL of DPBS. The samples were stored at 4°C until ready for analysis. Just before analysis all samples were filtered through 35 µm, 12x75 mm round bottom cell strainers (BD Sciences) to break up any cell clumps. Samples were analyzed using the LSRII flow cytometer unit. CRL-2449 cells not stimulated with fluorescent PSMs were used as a negative control to calibrate the instrument. The forward light scattering (FSC), side light scattering (SSC), and fluorescence intensity were recorded for 15,000 events in each cell sample and used to generate dot plots comparing FSC and SSC in addition to a histogram showing the

fluorescence of all measured events. The CRL-2449 population was located on each dot plot and only the fluorescence of intact cells analyzed. The extent of PSM phagocytosis by CRL-2449 cells was determined by calculating the average fluorescence of the cell population.

8.2.5. Macrophage Viability and Adsorption

CRL-2449 cells were cultured as described in Section 8.2.2 then seeded into 24 well plates at a concentration of 2 x 10^5 cells/mL of CM_{CRL}. Cells were incubated overnight at 37°C and 5% CO_2 prior to stimulation with microspheres. Protein coatings were applied to plain and COO^- PSMs as detailed in Section 8.2.4 and seeded into wells containing CRL-2449 cells at a concentration of 1.5 x 10^9 microspheres/well. Alternately cells were stimulated directly by proteins in DPBS. rTp0483, BSA, and LPS were prepared at concentrations of 26, 52, and 260 pmol/well. Results in Chapter 6 indicated that each FN molecule binds a pair of rTp0483 molecules so a 1:2 molar ratio of FN compared to rTp0483 was employed for the studies in solution (13, 26, and 130 pmol/well). rTp0483 and FN (26 pmol rTp0483/well + 13 pmol FN/well, 52 pmol rTp0483/well + 26 pmol FN/well, and 260 pmol rTp0483/well + 130 pmol FN/well) were also preincubated together for 1 hour prior to addition to cells in order to investigate any effects of the rTp0483/FN complex in solution. LPS was included because it is used as a positive control for macrophage activation in later studies. After stimulation with PSMs or proteins in solution the plates were incubated at 37°C and 5% CO_2 for 24 hours. The cell samples were transferred to microcentrifuge tubes and the CM_{CRL} removed by

centrifugation at 1000 RPM for 5 minutes at 4°C. The samples were washed for 10 minutes with 1 mL DPBS and the cells recovered by centrifugation at 1000 RPM for 5 minutes at 4°C.

RAW 264.7 cells were cultured as described in Section 8.2.2. To coat COO^- WPs 700 µL of 50 µg rTp0483/mL in DPBS was added to wells and 500 µL of 100 µg FN/mL in DPBS was added to an equal number of wells and incubated 1 hour at room temperature. Surfaces were gently washed with DPBS, and 500 µL of 100 µg FN/mL in DPBS added to half of the rTp0483 coated wells while 500 µL of DPBS was added to the other half along with the FN coated wells then all were incubated 1 hour at room temperature. The surface with 100 µg FN/mL were washed gently with DPBS and the DPBS was removed from the other wells, after which 500 µL of 2 mg BSA/mL in DPBS was added to all wells and incubated at room temperature for 1 hour. Additional surfaces were blocked for 1 hour with 500 µL of 2 mg BSA/mL in DPBS or 500 µL DPBS as controls. RAW 264.7 cells were seeded onto protein coated surfaces or directly into COO^- WPs at a concentration of 4×10^5 cells/mL in CM_{RAW}. Cells seeded onto protein-coated surfaces were incubated overnight at 37°C and 5% CO_2 then the cell viability determined. Cells seeded onto uncoated WPs were incubated overnight at 37°C and 5% CO_2 then stimulated with the protein solutions outlined above and incubated at 37°C and 5% CO_2 for 24 hours before determining cell viability. In either case, CM_{RAW} was removed from the samples and they were gently washed with 1 mL of DPBS prior to analysis.

LIVE/DEAD® assay solution (Invitrogen) was prepared by combining 1.7 µL ethidium homodimer/mL assay solution and 1 µL calcein-AM/mL assay solution in

DPBS and 500 µL was added to cell samples and incubated at room temperature for 45 minutes. Ethidium homodimer is a red dye that targets DNA but does not penetrate the cell membrane of healthy cells. When cells die the outer membrane is disrupted allowing the dye to traverse the damaged membrane and dye cellular DNA red indicating nonviable cells. Calcein-AM is a green dye that is readily taken into living cells where it reacts to intercellular esterase activity only present in viable cells. Imaging was completed using the Nikon Eclipse LV100 microscope. Living cells were imaged using a FITC filter set (Ex: 450, Em: 500-550) while dead cells were imaged using a Texas Red filter set (Ex: 530-560, Em: 590-650). Cells were counted using NIS Elements BR 3.0 software (Nikon) and cell viability calculated by dividing the number of viable cells by the total number of cells. The cell density of adsorbed, viable RAW 264.7 cells was also determined.

8.2.6. Macrophage TNF-α Generation

CRL-2449 cells were cultured as described in Section 8.2.2 then seeded into 24 COO^- WPs at a concentration of 2×10^5 cells/mL of CM_{CRL}. Cells were incubated overnight at 37°C and 5% CO_2 prior to stimulation with PSMs. Protein coatings were applied to plain and COO^- PSMs as detailed in Section 8.2.4 and seeded into wells containing CRL-2449 cells at a concentration of 1.5×10^9 PSMs/well. Alternately cells were stimulated directly by proteins in DPBS at the concentrations described in Section 8.2.5. After stimulation with PSMs or proteins in solution the plates were incubated at 37°C and 5% CO_2 for 24 hours. The cell samples were transferred to microcentrifuge tubes and the CM_{CRL} collected by centrifugation at

15,000 RPM for 30 minutes at 4°C. The CM_{CRL} samples were stored at 4°C until ready for analysis.

RAW 264.7 cells were cultured as described in Section 8.2.2 then seeded onto protein coated surfaces prepared as detailed in Section 8.2.5 or directly into COO^- WPs at a concentration of 4×10^5 cells/mL in CM_{RAW}. Cells seeded onto protein coated surfaces were incubated overnight at 37°C and 5% CO_2 then the CM_{RAW} was collected and centrifuged 5 minutes at 1000 RPM to remove any remaining cells. Cells seeded onto uncoated COO^- WPs were incubated overnight at 37°C and 5% CO_2 then stimulated with the protein solutions described in Section 8.2.5 and incubated at 37°C and 5% CO_2 for 24 hours before collecting the CM_{RAW}. In either case, CM_{RAW} was stored at 4°C until ready for analysis.

The concentration of TNF-α generated by CRL-2449 and RAW 264.7 cells was determined using mouse TNF-α enzyme-linked immunosorbent analysis (ELISA) as per manufacturer instructions. ELISA is a sensitive and highly specific method based on antibody-antigen interactions used to investigate the concentration of proteins or cytokines in a sample solution. The process is illustrated in Figure 8.1. 96 well plates were purchased precoated with a TNF-α antibody that specifically bound TNF-α in media samples with a high affinity. Next, a biotin labeled TNF-α antibody was added, which bound to immobilized TNF-α forming a sandwich. Then, a streptavidin-horseradish peroxidase (HRP) complex was added, which bound to the biotin label on the TNF-α antibody completing the protein-antibody complex. Biotin and streptavidin are widely used because the two molecules form one of the strongest noncovalent bonds in nature.

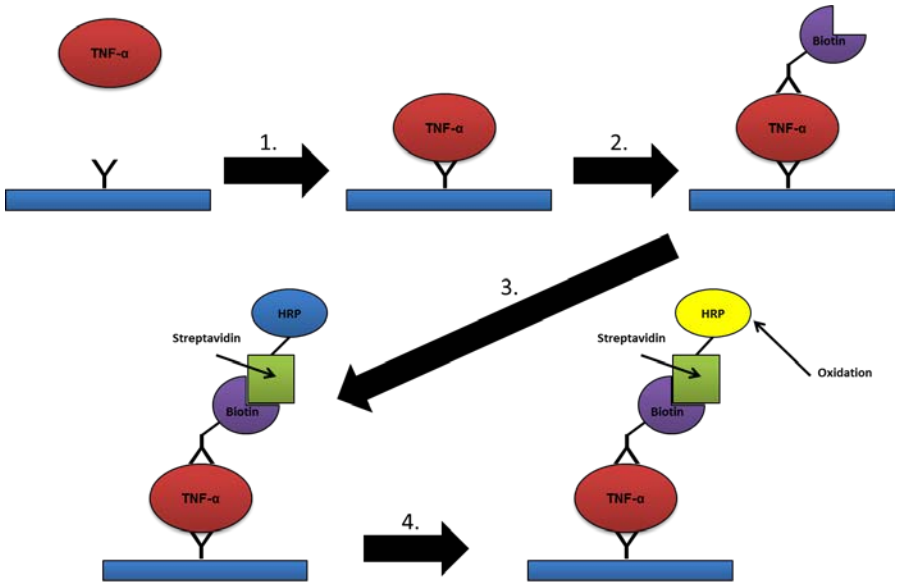

Figure 8.1: Overview of ELISA. WPs are purchased precoated with a TNF-α specific antibody. (1) TNF-α binds to the antibody on the surface, (2) a second biotin labeled TNF-α antibody binds to immobilized TNF-α, (3) streptavidin-HRP complex binds tightly to biotin label, (4) TMB substrate oxidizes HRP to produce a blue color then when the reaction is stopped with 0.16 M sulfuric acid the color changes to bright yellow. TNF-α concentration is determined by subtracting the absorbance measured at 550 nm from the absorbance at 450 nm.

The concentration of TNF-α was determined by subtracting the absorbance at 550 nm from that at 450 nm using the UV-Vis spectrophotometer equipped with a Cary 50 MPR microplate reader after oxidizing the HRP with TMB substrate and stopping the reaction with 0.16 M sulfuric acid. The concentration of TNF-α generated by adsorbed RAW 264.7 cells was normalized to the cell density determined in Section 8.2.5.

8.2.7. Macrophage Nitric Oxide Activity

CRL-2449 cells were cultured as described in Section 8.2.2 then seeded into 24 well plates at a concentration of 2 x 10^5 cells/mL of CM_{CRL}. Cells were incubated

overnight at 37°C and 5% CO_2 prior to stimulation with PSMs. Protein coatings were applied to plain and COO^- PSMs as detailed in Section 8.2.4 and seeded into wells containing CRL-2449 cells at a concentration of 1.5 x 10^9 PSMs/well. Alternately, cells were stimulated directly by proteins in DPBS at the concentrations described in Section 8.2.5. After stimulation with PSMs or proteins in solution the plates were incubated at 37°C and 5% CO_2 for 24 hours. The cell samples were transferred to microcentrifuge tubes and the CM_{CRL} collected by centrifugation at 15,000 RPM for 30 minutes at 4°C. The CM_{CRL} samples were stored at 4°C until ready for analysis.

RAW 264.7 cells were cultured as described in Section 8.2.2 then seeded onto protein coated surfaces prepared as detailed in Section 8.2.5 or directly into COO^- WPs at a concentration of 4 x 10^5 cells/mL in CM_{RAW}. Cells seeded onto protein coated surfaces were incubated overnight at 37°C and 5% CO_2 then the CM_{RAW} was collected and centrifuged 5 minutes at 1000 RPM to remove any remaining cells. Cells seeded onto uncoated COO^- WPs were incubated overnight at 37°C and 5% CO_2 then stimulated with the protein solutions described in Section 8.2.5 and incubated at 37°C and 5% CO_2 for 24 hours before collecting the CM_{RAW}. In either case, CM_{RAW} was stored at 4°C until ready for analysis.

Nitric oxide (NO) activity was investigated by measuring the stable end products nitrite (NO_2^-) and nitrate (NO_3^-) using a colorimetric Greiss assay as per manufacturer instructions, which is illustrated in Figure 8.2. Since the relative amounts of the two end products vary widely from cell to cell, NO_3^- was converted to NO_2^- using nitrate reductase enzyme and the combined concentration of both

used to measure NO activity. After conversion, NO_2^- was reacted with sulfanilamide in an acidic medium to form an intermediate compound, which in turn reacted with N-(1-naphthyl) ethylenediamine to form an azo product. The absorbance was measured at 540 nm using the UV-Vis spectrophotometer equipped with a Cary 50 MPR microplate reader. The concentration of NO_2^- generated by adsorbed RAW 264.7 cells was normalized to the cell density determined in Section 8.2.5.

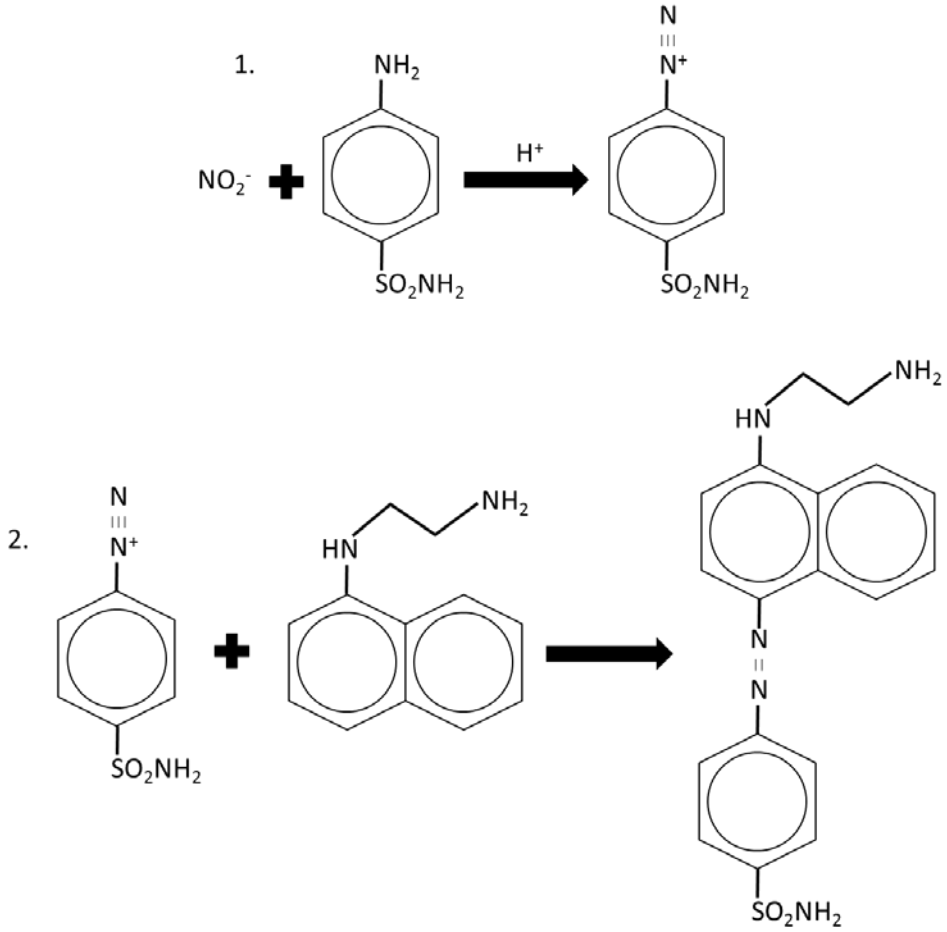

Figure 8.2: Illustration of the Greiss reaction for the detection of NO_2^-. (1) NO_2^- reacts with sulfanilamide in an acidic medium to form an intermediate compound then (2) this compound reacts with N-(1-naphthyl) ethylenediamine to form an azo product that can be measured photometrically at 540 nm.

8.2.8. Statistical Analysis

Statistical analysis was performed using the Microsoft Office Excel Data Analysis tool, StatPlus. Multiple pair-wise comparisons were made using one-way analysis of variance (ANOVA) with a maximum p-value of 0.05. All data are reported as a mean ± standard error. All studies are at minimum n=3 with specific sample group sizes noted in the text.

8.3. Results

8.3.1. Protein Surface Adsorption and Stability Validation

Adsorption of rTp0483 and or FN was investigated on 200 nm diameter plain and COO^- PSMs and on COO^- WPs using BCA assay. The mass of adsorbed proteins was divided by the total sample surface area to obtain a surface mass density of protein ($\mu g/cm^2$). Adsorption to PSMs is shown in Figure 8.3 and adsorption in COO^- WPs is shown in Figure 8.4. The surface mass densities of rTp0483 and FN adsorbed alone on plain and COO^- PSMs were statistically indistinguishable from adsorption on COO^- WPs; however, the FN binding of rTp0483 was significantly higher when rTp0483 was adsorbed to COO^- WPs ($3.47 \pm 0.54\ \mu g/cm^2$) compared to COO^- PSMs ($0.28 \pm .02\ \mu g/cm^2$) and plain PSMs ($0.27 \pm 0.04\ \mu g/cm^2$) ($p<0.05$).

The zeta potential of unmodified and protein coated plain and COO^- PSMs was analyzed to investigate potential reorganization of adsorbed proteins when the PSMs are added to CM_{CRL} as well as differences in surface charge that might influence phagocytosis. Protein adsorption is a rapid process so zeta potential was

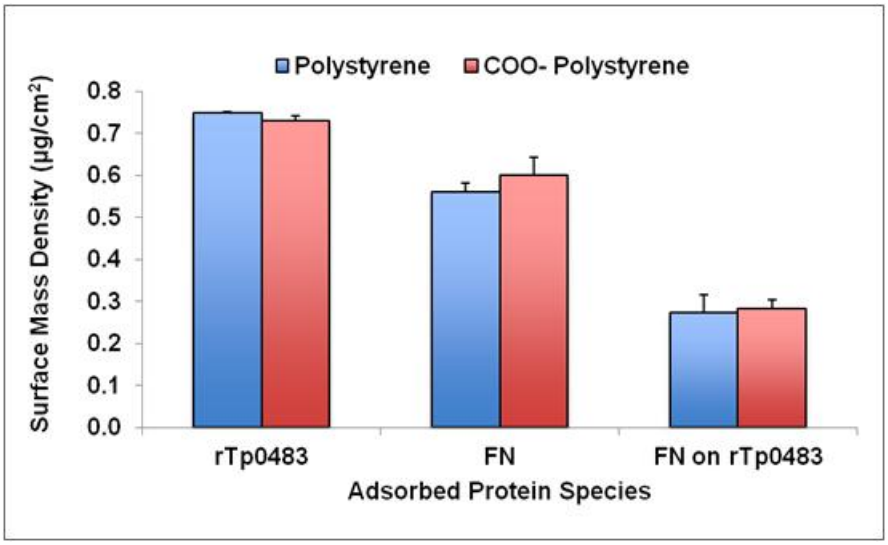

Figure 8.3: rTp0483 and FN adsorption to plain and COO^- PSMs. Surface mass density of rTp0483 or FN on each type of PSM was indistinguishable from the other. Surface density of FN on rTp0483 coated PSMs was less than for FN adsorbed directly onto PSMs ($p<0.05$). All data are n=3 and error bars represent standard error

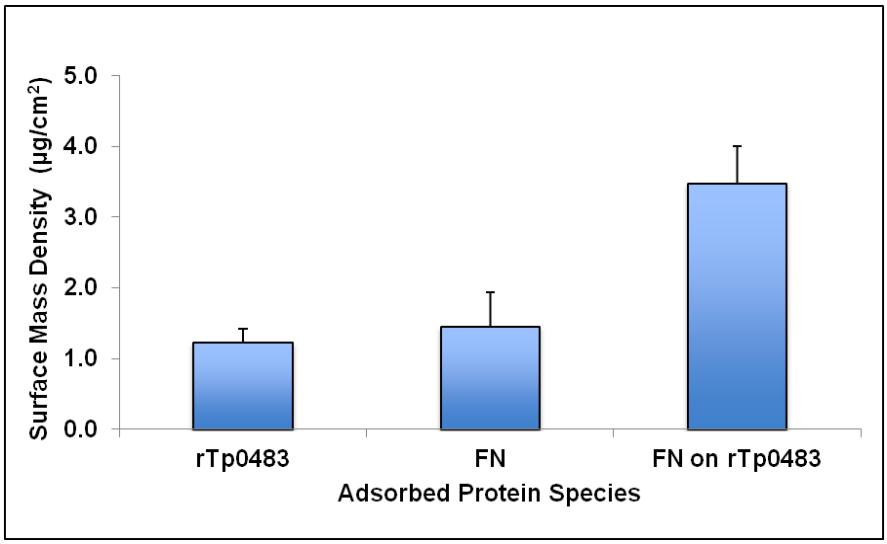

Figure 8.4: rTp0483 and FN adsorption to COO^- WPs. Surface mass density of FN on rTp0483 is significantly higher than FN adsorbed directly to WPs ($p<0.05$). All data are n=3 and error bars represent standard error.

measured as the PSMs were added to CM_{CRL} and every 10 minutes after up to 30 minutes. Note that the surface charge of all samples was negative but is shown as an absolute value for data presentation. Zeta potential values for plain PSM groups are shown in Figure 8.5 while values for COO^- PSM groups are shown in Figure 8.6. The zeta potentials of all protein coated plain and COO^- PSMs were stable over a 30 minute period. This indicates that the proteins adsorbed to the PSMs are stable in CM_{CRL}. Uncoated plain and COO^- PSMs initially had a lower zeta potential than the coated groups; however, after 10 minutes the values increased and stabilized at a zeta potential close to that other the coated groups. This indicates that the majority of the uncoated PSMs were covered with proteins from the serum in the CM_{CRL} within 10 minutes after exposure. The zeta potential of plain PSM groups were statistically indistinguishable after 30 minutes in CM_{CRL} while the zeta potential of FN coated COO^- PSMs was lower than all other groups with the exception of rTp0483+FN coated PSMs ($p<0.05$).

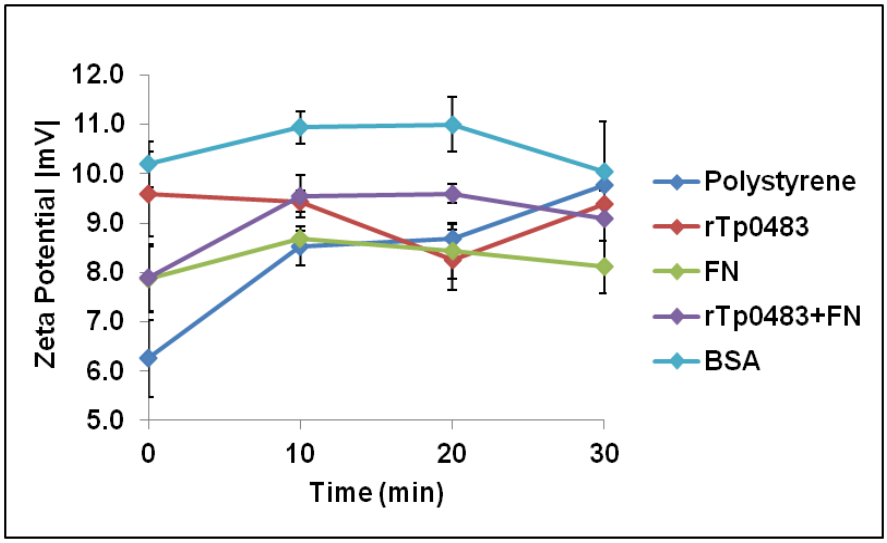

Figure 8.5: Zeta potential analysis of protein coated plain PSMs. Zeta potential of protein coated plain PSMs did not change after 30 min incubation in CM_{CRL} and the zeta potential of uncoated PSMs leveled off after 10 minutes. After 30 min all groups indistinguishable. All data are n=3 and error bars represent standard error.

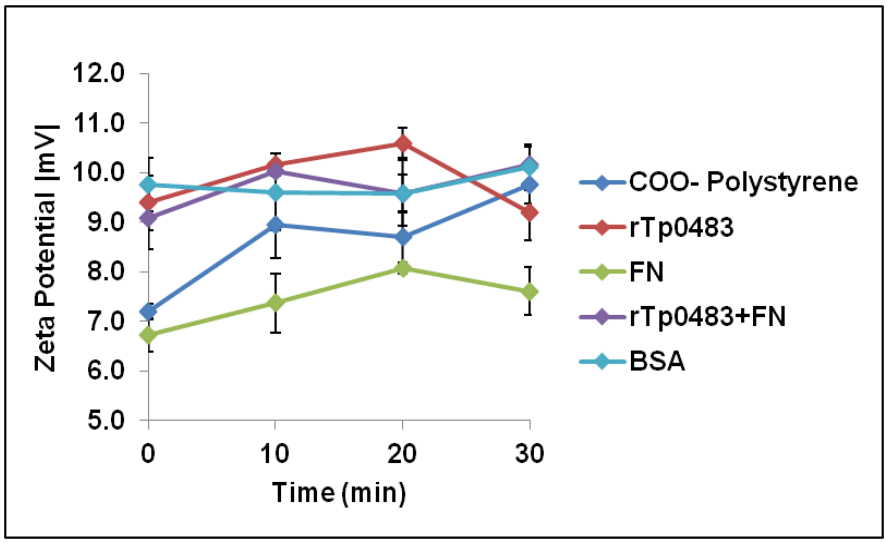

Figure 8.6: Zeta potential analysis of protein coated COO^- PSMs. Zeta potential of protein coated PSMs did not change after 30 minute incubation in CM_{CRL} and the zeta potential of uncoated PSMs leveled off after 10 minutes. After 30 min zeta potential of FN significantly less negative than the other groups ($p<0.05$). All data are n=3 and error bars represent standard error.

8.3.2. Phagocytosis of Protein Coated Microspheres

Uptake of protein coated plain and COO^- PSMs was analyzed to investigate the targeting of CRL-2449 macrophages against adsorbed rTp0483 and determine how the binding of FN to adsorbed rTp0483 affects this response. Figure 8.7 shows the phagocytosis of unmodified and protein coated plain PSMs over a 24 hour period and Figure 8.8 shows the response of unmodified and protein coated COO^- PSMs over the same time period. After 24 hours, the average cell fluorescence for plain PSMs was highest for rTp0483 (634 ± 14) and FN coated (608 ± 18) PSMs, which were indistinguishable. The average cell fluorescence of rTp0483+FN coated (521 ± 16) PSMs was significantly lower ($p<0.05$) than rTp0483 or FN alone and the average cell fluorescence of BSA coated (460 ± 6) and unmodified (413 ± 5) PSMs was lower than rTp0483, FN, or rTp0483+FN ($p<0.05$) but indistinguishable from each other. For COO^- PSMs the average cell fluorescence was highest for BSA coated (810 ± 10) PSMs followed by unmodified (630 ± 8) PSMs, and rTp0483 coated (542 ± 3) PSMs ($p<0.05$). The average cell fluorescence of FN coated (423 ± 11) and rTp0483+FN coated (432 ± 8) PSMs was lower than the other groups ($p<0.05$) and indistinguishable from each other.

The phagocytosis of rTp0483 and rTp0483+FN coated plain PSMs was the same after an hour; however, over time rTp0483 coated PSMs were taken up more readily than rTp0483+FN coated PSMs. On the other hand, the phagocytosis of rTp0483+FN coated COO^- PSMs was lower than for rTp0483 coated PSMs at all measured time points. Phagocytosis of both rTp0483 and rTp0483+FN coated plain PSMs was largely constant between 1 and 24 hours while phagocytosis of rTp043

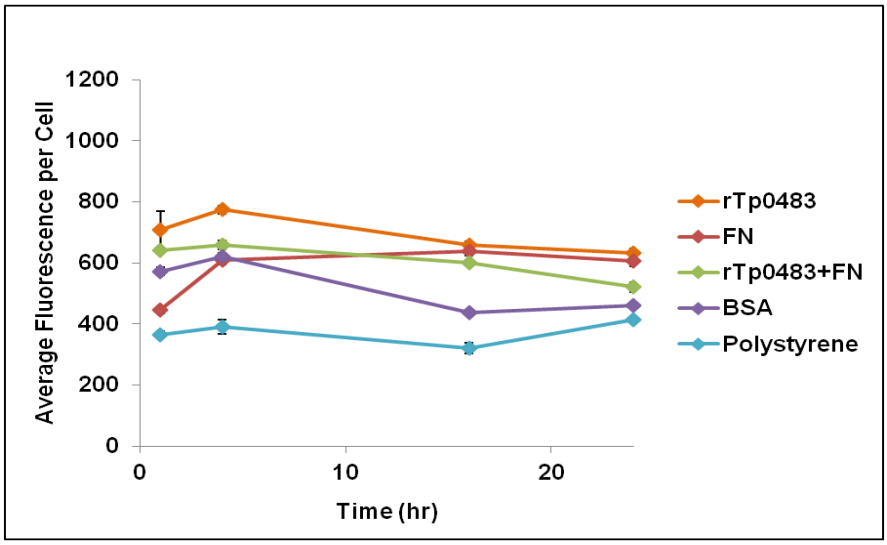

Figure 8.7: Phagocytosis of unmodified and protein coated plain PSMs over a 24 hour period. At t = 1 hour all groups reached a constant fluorescence values except for FN, which continued to increase until t = 4 hours. After 24 hours rTp0483+FN uptake significantly less than rTp0483 or FN ($p<0.05$) and BSA and unmodified PSM uptake significantly less than rTp0483+FN, rTp0483, or FN ($p<0.05$). All data are n=3 and error bars represent standard error.

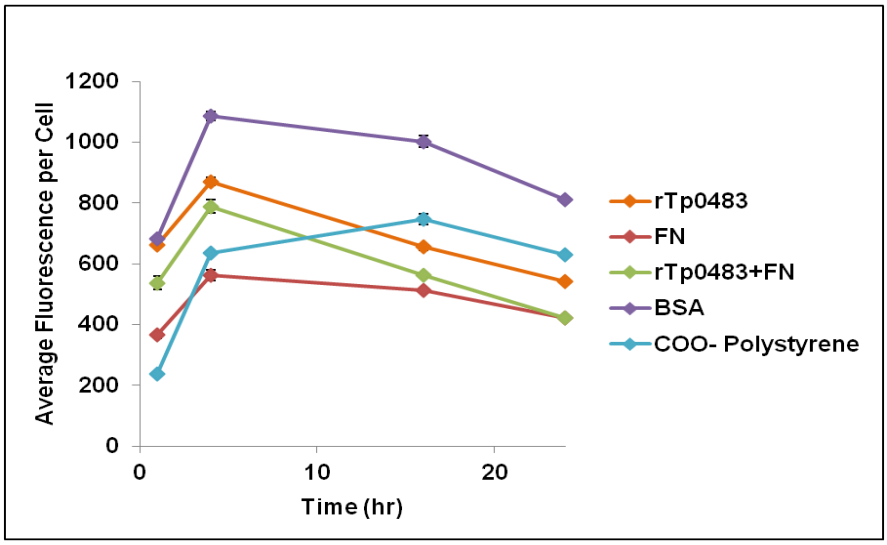

Figure 8.8: Phagocytosis of unmodified and protein-coated COO^- PSMs over a 24 hour period. All groups except unmodified PSMs peaked at t = 4 hours and either stayed constant or decreased. Unmodified PSMs spiked at t = 16 hours and decreased afterwards. After 24 hours all groups were significantly different except for FN and rTp0483+FN ($p<0.05$). All data are n=3 and error bars represent standard error.

and rTp0483+FN coated COO^- PSMs was initially lower than for coated plain PSMs, spiked above coated plain PSMs around 4 hours, and then fell below coated plain PSMs soon after. Phagocytosis of BSA coated and unmodified plain PSMs was low compared to the other sample groups; however, phagocytosis of BSA coated and unmodified COO^- PSMs was actually high compared to the other groups. For plain PSMs the addition of FN to adsorbed rTp0483 increased the initial rate of phagocytosis but reduced the overall amount after 24 hours compared to FN alone. Likewise, for COO^- PSMs, the addition of FN to adsorbed rTp0483 increased the initial rate of phagocytosis; however, unlike FN coated plain PSMs did not decrease the overall amount after 24 hours compared to FN alone.

8.3.3. Macrophage Viability and Adsorption

Potential cytotoxic effects of adsorbed proteins on CRL-2449 and RAW 264.7 macrophages were analyzed using a LIVE/DEAD assay. Any effects on RAW 264.7 macrophage adhesion were also investigated. The viability of macrophages was calculated by dividing the number of living cells by the total number of cells (living and dead) and expressing this value as a percentage. Figure 8.9 shows the viability of CRL-2449 macrophages exposed to free proteins in solution at a range of concentrations and immobilized on COO^- and plain PSMs compared to a macrophage activator (LPS), unmodified microspheres, and unstimulated cells. Figure 8.10 shows the viability of RAW 264.7 exposed to free proteins in solution at a range of concentrations and immobilized on COO^- WPs compared to LPS and unstimulated

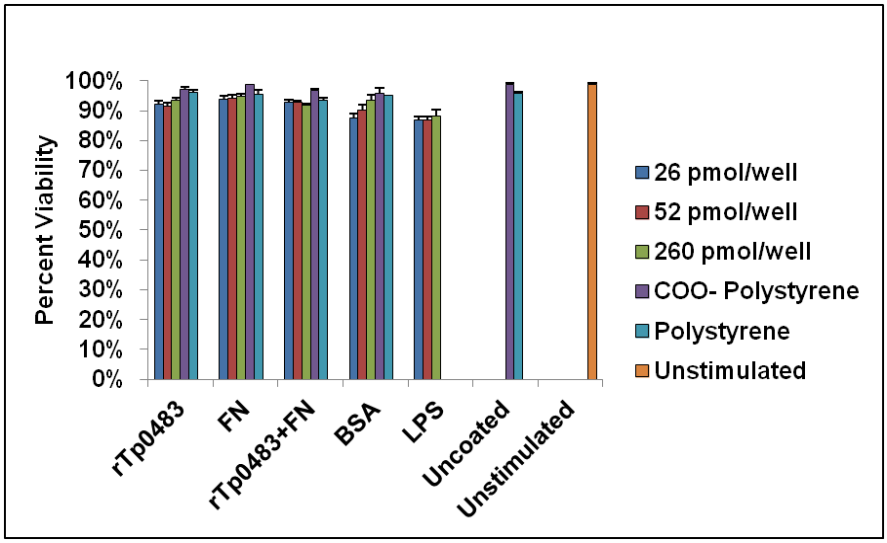

Figure 8.9: Viability of CRL-2449 cells exposed to free proteins in solution and proteins adsorbed to plain and COO^- PSMs compared with the viability of cells exposed to LPS, unmodified PSMs, and unstimulated cells. No significant effects were observed. All data are n=3 and error bars represent standard error.

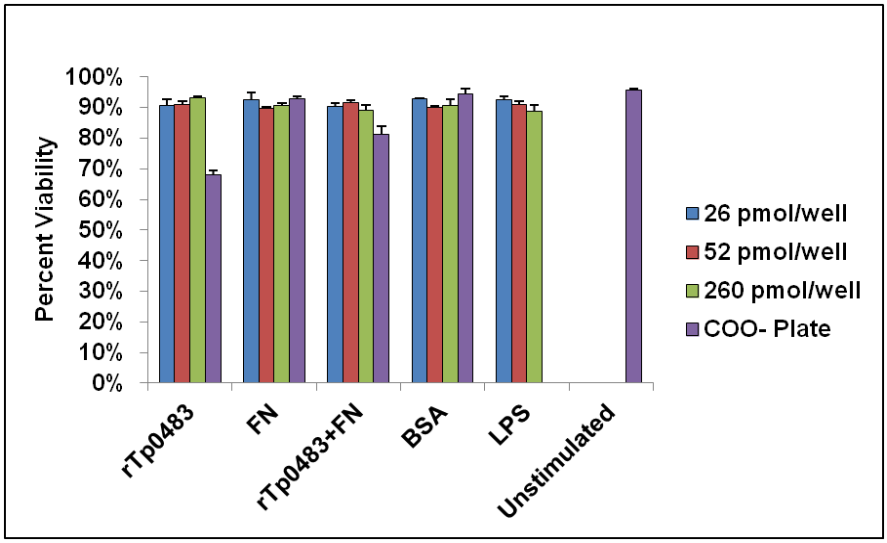

Figure 8.10: Viability of RAW 264.7 cells exposed to free proteins in solution and proteins adsorbed to COO^- WP surfaces compared with the viability of cells exposed to LPS and unstimulated cells. Adsorbed rTp0483 reduced RAW 264.7 viability significantly ($p<0.05$). All data are n=3 and error bars represent standard error.

cells. When the viability of RAW 264.7 cells was determined the number of adherent cells was also recorded as shown in Figure 8.11.

None of the protein groups were found to be cytotoxic to CRL-2449 cells in solution or when adsorbed to either type of PSM. When RAW 264.7 cells were incubated on rTp0483 coated surfaces a significant drop in viability was observed indicating a measureable cytotoxic effect on the adherent RAW 264.7 line. There were significant differences in the number of RAW 264.7 cells adsorbed to protein coated surfaces. The number of viable RAW 264.7 cells that adhered to rTp0483 and rTp0483+FN coated surfaces was indistinguishable from the number of cells adhered to unmodified COO^- WP surfaces. The number of viable RAW 264.7 cells that adhered to FN and BSA coated surface was significantly higher than the number adhered to unmodified COO^- WP surfaces ($p<0.05$) but indistinguishable from one another. The addition of FN to adsorbed rTp0483 led to significantly less cell binding than when FN was adsorbed directly to COO^- WP surfaces ($p<0.05$).

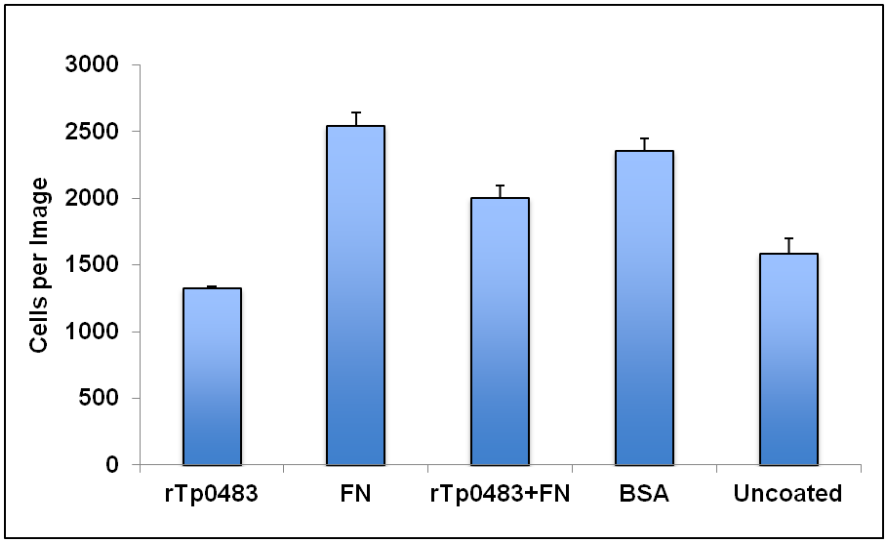

Figure 8.11: Number of viable adherent RAW 264.7 cells on unmodified and protein coated COO^- WP surfaces. Number of viable cells on rTp0483 and rTp0483+FN coated surfaces are indistinguishable compared to cells on unmodified surfaces. A coating of FN or BSA led to increased cell adhesion ($p<0.05$). Adsorption of rTp0483 prior to addition of FN led to less RAW 264.7 binding than FN alone ($p<0.05$). All data are n=3 and error bars represent standard error

8.3.4. Macrophage TNF-α Generation

TNF-α generation was measured to determine macrophage response to stimulation with rTp0483 and how the addition of FN affects this response. Plain and COO^- PSMs were coated with rTp0483, FN, rTp0483+FN, or BSA and added to CRL-2449 macrophages in solution. The response was compared to cells stimulated with uncoated PSMs, PSMs coated with rTp0483, FN, rTp0483+FN, BSA, or LPS proteins in solution, and cells not exposed to any sort of PSM. Figure 8.12 and Figure 8.13 show the results of this study. As expected, both types of FN coated, BSA coated, and uncoated PSMs produced no more TNF-α than unstimulated CRL-2449 cells. Both types of rTp0483 coated PSMs produced a significant amount of TNF-α compared to unstimulated cells (COO^- PSMs were 68.6 ± 2.5 pg/mL and plain PSMs

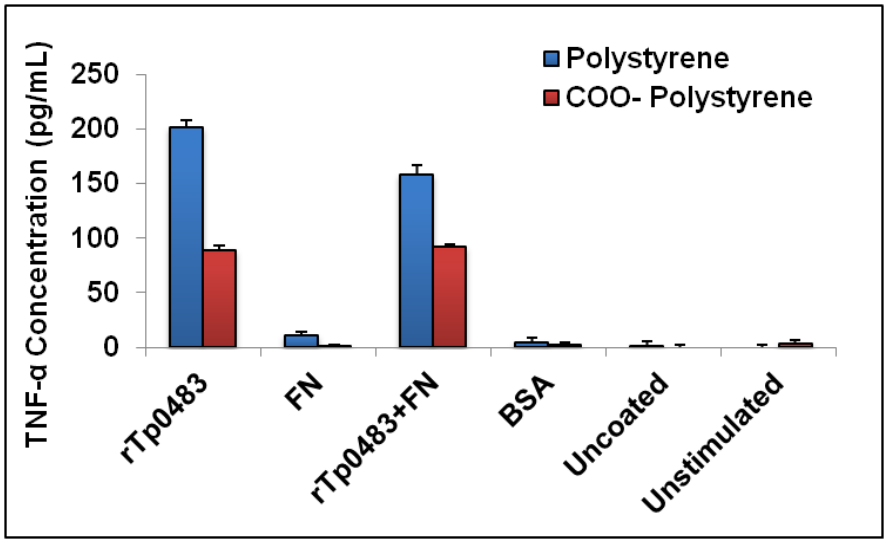

Figure: 8.12. CRL-2449 macrophage TNF-α generation in response to stimulation with protein coated and uncoated plain and COO^- PSMs compared to unstimulated cells. rTp0483 and rTp0438+FN coatings on both types of PSM resulted in significant TNF-α generation compared to unstimulated cells ($p<0.05$) while the response of COO^- PSMs were lower than plain PSMs ($p<0.05$). Addition of FN to rTp0483 lowered TNF-α for plain PSMs ($p<0.05$) but not COO^- PSMs. All data are n=6 and error bars represent standard error.

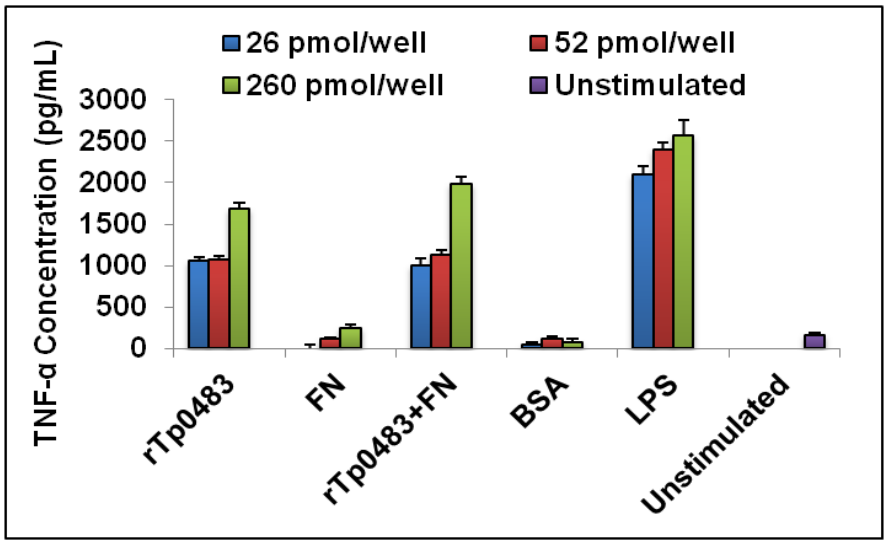

Figure 8.13: CRL-2449 macrophage TNF-α generation in response to stimulation of cells with proteins in solution. Stimulation with rTp0483, rTp0483+FN, or LPS resulted in significantly more TNF-α than unstimulated cells ($p<0.05$). There was no difference in TNF-α generation for rTp0483 and rTp0483+FN. All data are n=6 and error bars represent standard error.

were 198.2 ± 5.6 pg/mL, $p<0.05$). The addition of FN to adsorbed rTp0483 resulted in a decrease in TNF-α for plain PSMs (154.7 ± 8.4 pg/mL, $p<0.05$) but did not result in a change for COO^- PSMs (71.7 ± 2.7 pg/mL). For both coatings the response toward plain PSMs was larger than for COO^- PSMs ($p<0.05$). As with coated PSMs, the response of CRL-2449 cells to FN and BSA in solution were indistinguishable compared to unstimulated cells. TNF-α production was significantly greater than for unstimulated cells when rTp0483, rTp0483+FN, or LPS was added ($p<0.05$).

COO^- WPs were coated with rTp0483, FN, rTp0483+FN, or BSA then RAW 264.7 macrophages were cultured on the top of the protein layers and compared to cells cultured on uncoated wells. The results were normalized to the number of cells adsorbed to each surface, which were shown in Figure 8.11. Alternately, cells were cultured on uncoated wells then stimulated with rTp0483, FN, rTp0483+FN, BSA, or LPS in solution and the response compared to unstimulated cells. The results are shown in Figure 8.14 and Figure 8.15. TNF-α production of RAW 264.7 cells cultured on FN and BSA coated surfaces were indistinguishable from cells cultured on unmodified surfaces while cells cultured on rTp0483 produced significantly more TNF-α (1246.8 ± 141.4 pg/mL, $p<0.05$). Cells cultured on rTp0483+FN coated surfaces also produced significantly more TNF-α than cells cultured on unmodified surfaces; however, it was lower than rTp0483 alone (669.4 ± 23.8 pg/mL, $p<0.05$). FN and BSA in solution did not produce significantly more TNF-α than unstimulated cells; however, cells stimulated with rTp0483,

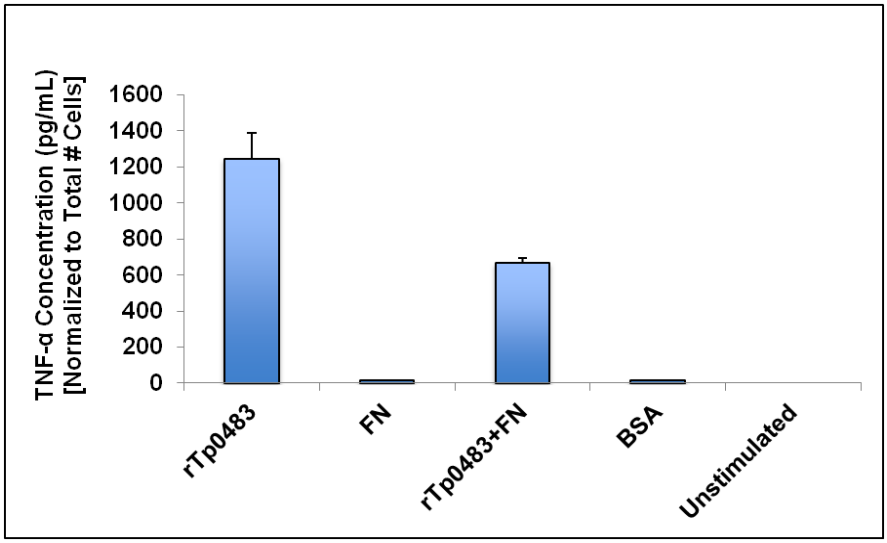

Figure 8.14: RAW 264.7 macrophage TNF-α generation in response to stimulation with protein coated COO^- WP surfaces compared to cells cultured on unmodified surfaces. rTp0483 and rTp0438+FN coatings resulted in significant TNF-α generation compared to cells on unmodified surfaces ($p<0.05$). Addition of FN to rTp0483 lowered TNF-α generation ($p<0.05$). All data are n=6 and error bars represent standard error.

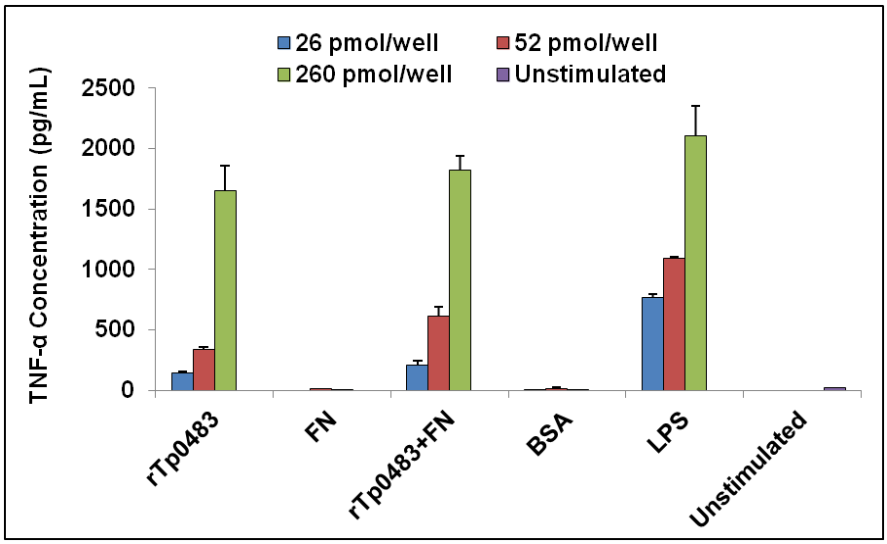

Figure 8.15: RAW 264.7 macrophage TNF-α generation in response to stimulation of cells with proteins in solution. Stimulation with rTp0483, rTp0483+FN, or LPS resulted in significantly more TNF-α than unstimulated cells ($p<0.05$). There was no difference in TNF-α generation for rTp0483 and rTp0483+FN. All data are n=6 and error bars represent standard error.

rTp0483+FN, and LPS in solution produced significantly more TNF-α than unstimulated cells ($p<0.05$). There was no statistical difference between cells stimulated with rTp0483 and cells stimulated with rTp0483+FN.

8.3.5. Macrophage Nitric Oxide Activity

NO activity was measured along with TNF-α generation to determine the activity of macrophage stimulated with rTp0483 and to determine the effect of FN binding. NO activity was determined by measuring the concentration of the end product NO_2^{-}. Plain and COO^- PSMs were coated with rTp0483, FN, rTp0483+FN, or BSA and added to CRL-2449 macrophages in solution. The response was compared to cells stimulated with uncoated PSMs, PSMs coated with rTp0483, FN, rTp0483+FN, BSA, or LPS proteins in solution, and cells not exposed to any sort of PSMs. Figure 8.16 and Figure 8.17 show the results of this study. The NO_2^- generation of CRL-2449 cells stimulated with uncoated PSMs of both types as well as all protein coated PSMs was equal to or less than unstimulated cells. The NO_2^- generation of cells stimulated with any of the proteins free in solution was also equal to or less than unstimulated cells.

COO^- WPs were coated with rTp0483, FN, rTp0483+FN, or BSA then RAW 264.7 macrophages were cultured on the top of the protein layers and compared to cells cultured on uncoated wells. The results were normalized to the number of cells adsorbed to each surface, which were shown in Figure 8.11. Alternately, cells were cultured on uncoated wells then stimulated with rTp0483, FN, rTp0483+FN, BSA, or LPS in solution and the response compared to unstimulated cells. The

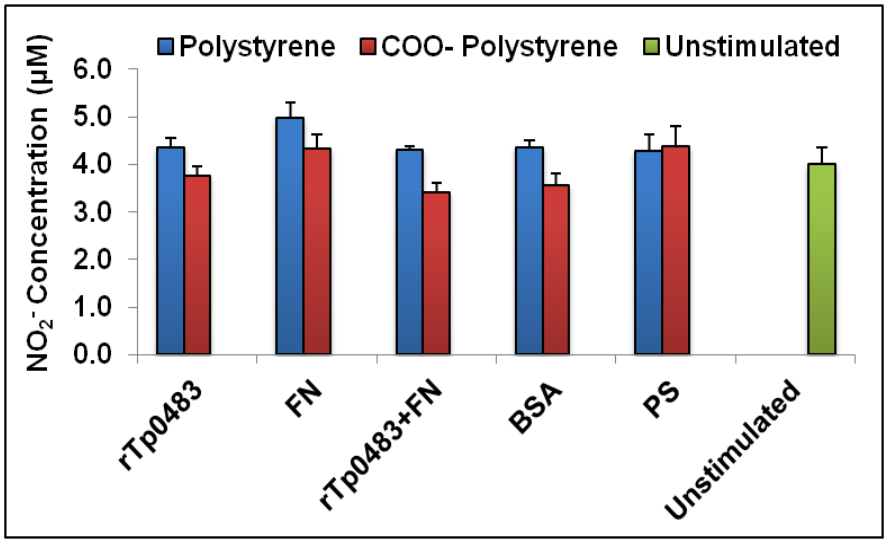

Figure 8.16: CRL-2449 macrophage NO_2^- generation in response to stimulation with protein coated and uncoated plain and COO^- PSMs compared to unstimulated cells. The amount of NO_2^- produced by cells exposed to uncoated and protein coated PSMs of both types was equal to or less than unstimulated cells. All data are n=6 and error bars represent standard error.

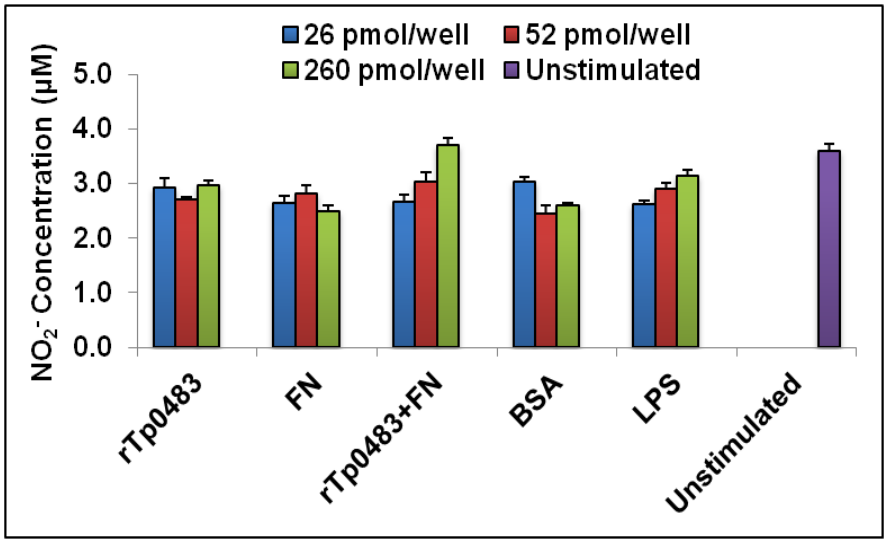

Figure 8.17: CRL-2449 macrophage NO_2^- generation in response to stimulation of cells with proteins in solution. The amount of NO_2^- produced by cells exposed proteins in solution was equal to or less than unstimulated cells. All data are n=6 and error bars represent standard error.

results are shown in Figure 8.18 and Figure 8.19. Cells cultured on FN or BSA coated wells led to less NO_2^- production than cells cultured on unmodified surfaces (0.68 ± 0.05 μM, 1.07 ± 0.10 μM, and 2.90 ± 0.11 respectively, $p<0.05$). Cells cultured on rTp0483+FN produced a similar amount of NO_2^- as cells cultured on unmodified surfaces (3.21 ± 0.11 μM) and cells cultured on rTp0483 produced a significantly higher amount (5.79 ± 0.13 μM, $p<0.05$).

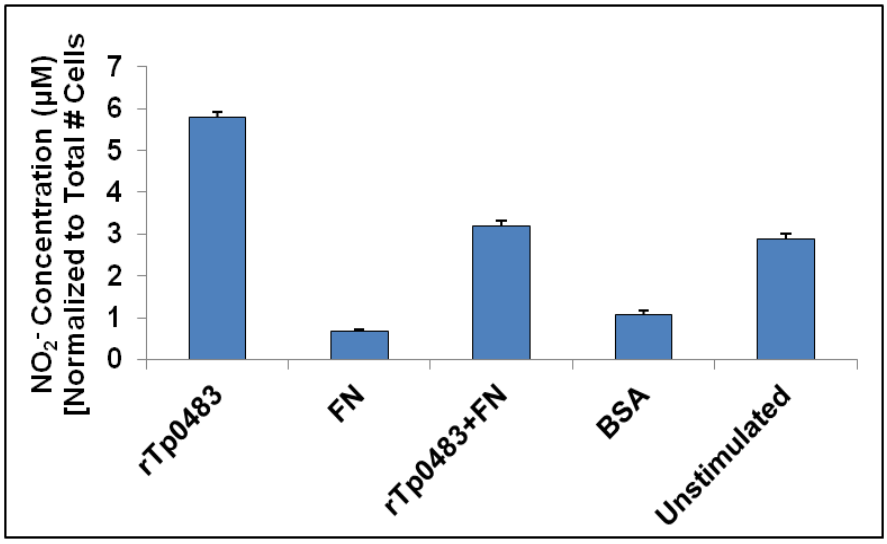

Figure 8.18: RAW 264.7 macrophage NO_2^- generation in response to stimulation with protein coated and uncoated COO^- WPs compared to unstimulated cells. Cells cultured on FN and BSA produced less than those on unmodified surfaces ($p<0.05$) while cells cultured on rTp0483 produced more than those on rTp0483+FN or on unmodified surfaces ($p<0.05$). All data are n=6 and error bars represent standard error.

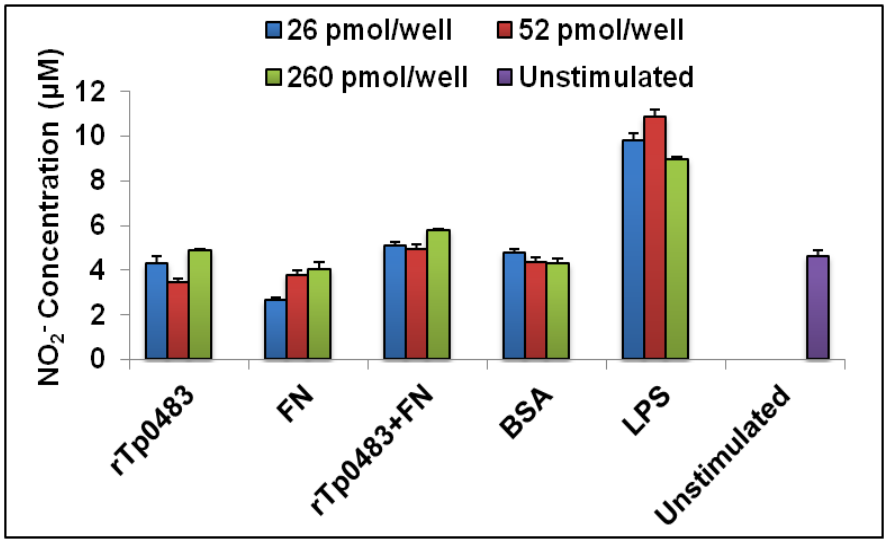

Figure 8.19: RAW 264.7 macrophage NO_2^- generation in response to stimulation of cells with proteins in solution. The amount of NO_2^- produced by cells exposed to LPS at all concentrations and 260 pmol rTp0483/well + 130 pmol FN/well was higher than controls ($p<0.05$). All data are n=6 and error bars represent standard error.

8.4. Discussion

The relative biocompatibility of rTp0483 coated surfaces and the influence of FN binding by adsorbed rTp0483 on biocompatibility were analyzed in a number of ways. Data presented in Chapter 6 indicated that rTp0483 adsorbed onto negatively charged SAMs led to the most efficient FN binding. For these studies a similar COO^- surface chemistry was chosen to mimic negatively charged COO^- SAMs. For microsphere studies plain PSMs without COO^- groups were also analyzed in order to determine the effect of surface charge on surfaces with curvature. PSMs were used along with a non-adherent macrophage line, CRL-2449, to investigate the impact of adsorbed and free rTp0483 with and without FN on cell response toward small particles in solution. COO^- WPs were used with an adherent macrophage line, RAW

264.7, to investigate the impact of adsorbed and free rTp0483 with and without FN on the cell response to large surfaces too big for the cells to engulf.

First, adsorption of rTp0483 and FN onto both types of PSMs and COO^- WP surfaces were measured. rTp0483 and FN binding were similar on all surfaces; however, significantly more FN bound to rTp0483 adsorbed onto the flat COO^- WP surfaces. While the plain PSMs lack COO^- groups they have sulfate groups (SO_4^{2-}) integrated throughout, which are a byproduct of the synthesis process. These groups have a high negative charge that likely accounts for the significant FN binding observed for plain PSMs. The significantly lower FN binding of both types of PSMs compared to flat surfaces may result from the curvature of the PSM surface. Past studies have demonstrated that the curvature of the substrate onto which proteins are adsorbed has a profound effect on the conformation and activity of the protein.[128, 129] The effect is dependent on the protein in question as shown in Roach *et al.* where albumin denatured as particle size increased (curvature decreased) while Fg denatured as particle size decreased (curvature increased).[129] Based on adsorption data, large flat, negatively charged surfaces facilitate an arrangement of rTp0483 that promotes high FN binding affinity. As curvature increases the conformation of adsorbed rTp0483 is impacted leading to decreased FN binding affinity. In addition to adsorption studies, the zeta potential of both types of coated and uncoated PSMs was analyzed. Zeta potential is a quantification of particle surface charge, which has been demonstrated to affect the phagocytosis of microspheres in past studies.[120, 130] All coated surfaces bore a negative charge that remained constant over the course of the study. This suggests that the initial

protein coats are stable. Uncoated plain and COO^- PSMs both began slightly less negative than the other groups and rapidly came to equilibrium due to the adsorption of serum proteins in the cell culture media. Only FN adsorbed on COO^- PSMs was significantly different from the other groups ($p<0.05$). Phagocytosis has been shown to decrease for particles with a weakly negative surface charge so this may help explain the low uptake of FN coated COO^- PSMs. In all other cases, the surface charge of the coated and uncoated PSMs likely did not account for differences in uptake. It is more likely that differences are a result of receptor-mediated interactions between the macrophages and coated PSM surfaces.

Phagocytosis is the process by which macrophages engulf foreign agents for elimination and removal from the body. Fluorescent plain and COO^- PSMs were coated with rTp0483, FN, rTp0483+FN or BSA and their phagocytosis by CRL-2449 macrophages compared to uncoated PSMs of both types using flow cytometry analysis. The phagocytosis of coated and uncoated plain PSMs increased to a maximum value and remained constant for the study period. FN coated PSMs reached a maximum value more slowly than the other groups. On the other hand, the phagocytosis of coated and uncoated COO^- PSMs increased more slowly than plain PSMs. Values for rTp0483, FN, and rTp0483+FN coated COO^- PSMs peaked and subsequently fell back to levels lower than the corresponding plain PSM groups while the responses of uncoated and BSA coated PSMs were higher for COO^- PSMs than for plain PSMs ($p<0.05$). Uncoated COO^- PSMs reached a maximum value more slowly than the other groups. As the surface charges of uncoated and protein coated PSMs of both types were indistinguishable ($p<0.05$), except for FN coated COO^-

PSMs, it is probable that the binding configuration of the selected proteins on coated PSMs and the binding configuration and species of serum proteins from media onto uncoated PSMs accounted for these differences. The surfaces of macrophages are covered with a range of receptors that are able to bind a variety of ligands. Binding is dependent on the recognition of targets, which varies based on the adsorbed protein configuration. Differences in target recognition likely led to variation in phagocytosis resulting in the observed trends. For both plain and COO^- PSMs uptake of rTp0483+FN was less than for rTp0483 alone and in the case of plain PSMs less than FN alone. This suggests that pre-adsorption of rTp0483 may be interfering with FN mediated macrophage interactions and that the addition of FN to rTp0483 could potentially inhibit rTp0483 specific interactions. Some of the possible explanations are discussed below.

Certain pathogenic microorganisms as well as synthetic materials may exhibit cytotoxic effects in the body leading to cell death. Viability assays were conducted in order to investigate the potential cytoxicity of uncoated and rTp0483, FN, rTp0483+FN, and BSA coated plain and COO^- PSMs using CRL-2449 macrophages. A similar study was conducted with protein coated and uncoated COO^- WPs using RAW 264.7 macrophages. Cytoxicity of the selected proteins was also compared to a positive control, LPS, in solution for both cell lines. None of the proteins in solution or adsorbed on either type of PSM were found to be cytotoxic to CRL-2449 cells while only RAW 264.7 cells adsorbed onto rTp0483 exhibited reduced viability. The total amount of rTp0483 adsorbed prior to addition of RAW 264.7 cells was equal to the highest concentration of free protein in solution added

to cells adsorbed to unmodified surfaces; however, since RAW 264.7 cells grow on surfaces, cells cultured on a layer of rTp0483 would be exposed to a higher local concentration compared to rTp0483 distributed throughout the culture media. This elevated rTp0483 concentration accounts for the moderate decrease in cell viability. The number of viable RAW 264.7 cells adsorbed to each of the surface coatings was also recorded and compared to cells cultured on unmodified surfaces. FN and BSA coatings resulted in increased cell adhesion compared to cells cultured on unmodified surfaces while rTp0483 coatings led to decreased cell adhesion. rTp0483+FN coatings bound more cells than rTp0483 but less than FN. The addition of FN to adsorbed rTp0483 had a measureable effect on RAW 264.7 binding ($p<0.05$). Adsorption of FN to a surface has been shown to increase macrophage adhesion and phagocytosis through specific receptors such as $\alpha_V\beta_3$ and $\alpha_5\beta_1$ along with more general scavenger receptors.[131, 132] Adsorption of rTp0483 prior to the addition of FN resulted in a reduction of RAW 264.7 adhesion and plain PSM uptake suggesting an inhibition of FN receptor targets. rTp0483 may bind to macrophages through a combination of toll-like receptor 2 (TLR-2) and cluster of differentiation 14 (CD14), which has been shown to play a role in the activation of inflammatory and antimicrobial responses in phagocytic cells for other *T. pallidum* proteins (TpN47 and Tp0751).[55] More general scavenger receptors likely also play a role in the adhesion of macrophages to rTp0483, FN, and rTp0483+FN.[133, 134] By binding FN some rTp0483 target ligands may be rendered inaccessible resulting in a smaller immunogenic reaction while FN specific targets are inhibited leading to decreased binding. Scavenger receptors help account for the remaining cell binding.

Macrophages react in a number of ways in response to a perceived threat including production of the inflammatory cytokines TNF-α, interleukin-10 (IL-10), IL-6, and IL-1β along with prostagladin E2 (PGE-2) and NO, which is quickly converted to the end products NO_2^- and NO_3^-.[55, 122, 125, 126] Two important representative molecules, TNF- α and NO_2^-, were chosen to investigate the immunogenic response of CRL-2449 and RAW 264.7 macrophages to adsorbed and free rTp0483, FN, rTp0483+FN and BSA compared to uncoated plain and COO^- PSMs and uncoated COO^- WP surfaces. TNF-α is an inflammatory cytokine that mainly serves to recruit additional macrophage and immune cells while NO acts as an antibacterial agent. Activation of the nuclear factor kappa-B (NF-κB) pathway of macrophages resulting from interactions with TLR-2 and CD14 receptors, which may play a role in rTp0483 binding, has been shown to control the production of inflammatory cytokines like TNF-α.[55, 122, 125, 126] NO synthesis is regulated by an enzyme, inducible NO synthase (iNOS), that is activated in response to stimulation with interferon-γ (IFN-γ), TNF-α, or endotoxins like LPS.[122, 124-126] Both CRL-2449 and RAW 264.7 macrophages produced significant amounts of TNF-α in response to rTp0483 and rTp0483+FN in solution ($p<0.05$). Moreover, there was no significant reduction in the TNF-α concentration when FN was added to rTp0483. This indicates that surface adsorption of rTp0483 is important to any immunosuppressive effect. Surface adsorbed rTp0483 is only accessible from a single direction, which is subsequently blocked by binding FN. On the other hand, rTp0483 in solution is accessible from 360° so when FN binds it occupies only a fraction of the area leaving a large portion of the protein open to macrophage

targeting. NO_2^- production in CRL-2449 macrophages was equal to or less than unstimulated controls for all proteins in solution and adsorbed on both types of microspheres. This corresponds to a study by Fleming *et al.* that found that even when stimulated with the endotoxin LPS CRL-2449 macrophages did not produce significantly more NO_2^- than unstimulated cells.[135] In solution, other than the positive control, LPS, only cells stimulated with 260 pmol rTp0483 + 130 pmol FN produced significantly more NO_2^- than unstimulated controls ($p<0.05$). The effect was small and may be a result of increased binding of rTp0483 via opsonization by bound FN while in solution.

When adsorbed onto plain and COO^- PSMs rTp0483 and rTp0483+FN produced a significant amount of TNF-α ($p<0.05$). The addition of FN to adsorbed rTp0483 reduced TNF-α production for CRL-2449 cells stimulated with plain PSMs ($p<0.05$) but not for those stimulated with COO^- PSMs. TNF-α generated by cells stimulated with rTp0483 and rTp0483+FN coated COO^- PSMs was lower than for coated plain PSMs ($p<0.05$). This is likely due to the phagocytosis profiles of rTp0483 and rTp0483+FN coated plain and COO^- PSMs seen in Figure 8.7 and Figure 8.8. The uptake of coated COO^- PSMs proceeded more slowly than for plain PSMs and while it peaked at a higher value it rapidly fell to levels below plain PSMs. TNF-α is known to reduce the growth rate of macrophages, which may account for the difference in uptake. Adsorption to COO^- PSMs produced protein configurations that led to slower phagocytosis compared to proteins adsorbed on plain PSMs. Consequently, TNF-α production in response to coated COO^- PSMs was lower leading to faster cell proliferation. Conversely, cells stimulated with coated plain PSMs

proliferated at a slower rate due to elevated TNF-α. The uptake of microspheres is a linear process while cell proliferation proceeds at an exponential rate. As a result, cells stimulated with rTp0483 and rTp0483+FN coated COO^- PSMs proliferated more rapidly relative to microsphere uptake leading to a short term spike in response followed by a steady decline. Conversely, cells stimulated with rTp0483 and rTp0483+FN coated plain PSMs grew more slowly allowing each cell to uptake more microspheres. TNF-α production was lower for rTp0483 and rTp0483+FN coated COO^- PSMs; however, the charge distribution of SO_4^{2-} in plain PSMs provided a more effective substrate for reduction of TNF-α generation in response to adsorbed rTp0483 via FN binding. Both rTp0483 and rTp0483+FN adsorbed on COO^- WP surfaces resulted in significant TNF-α and NO_2^- production ($p<0.05$). rTp0483 adsorbed on COO^- WP surfaces displayed a higher FN binding ability than either type of PSM and reduced TNF-α and NO_2^- ($p<0.05$) generation in RAW 264.7 cells. This reinforces the importance of surface chemistry and curvature and supports the hypothesis that binding of FN to adsorbed rTp0483 decreases the antigenicity of rTp0483. A possible explanation is that adsorption of FN to adsorbed rTp0483 prevents a portion of interactions through the TLR-2 and CD14 receptors on macrophages. TNF-α generation, and ultimately NO_2^-, is controlled by the NF-κB pathway, which is in turn activated by binding through these two receptors. By inhibiting those interactions the associated immune responses are suppressed. Differences in NO_2^- production for RAW 264.7 when rTp0483 and rTp0483+FN were adsorbed as opposed to free in solution may point toward a concentration dependent response. In solution the highest concentration of rTp0483+FN

produced a small but significant ($p<0.05$) response compared to unstimulated controls while rTp0483 alone did not. When RAW 264.7 cells were cultured on protein coated surfaces rTp0483 alone was significantly higher than unstimulated controls ($p<0.05$) while rTp04843+FN was indistinguishable. This indicates that in solution addition of FN may slightly increase interactions with RAW 264.7 cells; however, when RAW 264.7 cells are forced into contact with protein coated surfaces the addition of FN to adsorbed rTp0483 appears to attenuate NO_2^- generation.

8.5. Conclusions

rTp0483 and FN were successfully adsorbed to plain and COO^- PSMs and COO^- WP surfaces. Based on zeta potential analysis the assembled protein surface coatings were determined to be stable in culture media. Phagocytosis of PSMs by CRL-2449 cells was dependent on the species of adsorbed proteins as well as the surface chemistry of the PSMs. Above a threshold rTp0483 adsorbed prior to RAW 264.7 seeding was determined to be cytotoxic and RAW 264.7 binding was dependent on adsorbed protein species. rTp0483 in solution resulted in generation of TNF-α in CRL-2449 and RAW 264.7 cells and the addition of FN had no effect suggesting that immunosuppression via FN capture was a surface adsorption related property. Adsorption of rTp0483 on COO^- PSMs generally led to less TNF-α generation than on plain PSMs as a result of slower uptake and increased cell proliferation rate; however, for adsorption onto 200 nm PSMs plain polystyrene surfaces provided a more effective substrate for reduction of TNF-α generation via FN binding to adsorbed rTp0483. The addition of FN to adsorbed rTp0483 on COO^-

WP surfaces was effective in reducing TNF-α generation in RAW 264.7 cells. NO_2^- production in CRL-2449 cells was confirmed to be unresponsive to stimulation. Above a certain concentration the addition of FN to rTp0483 in solution may slightly increase RAW 264.7 NO_2^- production, but when adsorbed to a surface prior to cell seeding the addition of FN to rTp0483 led to a decrease in production.

Chapter 9: CONCLUSIONS

The first primary objective of this work was to investigate the application of surface adsorbed rTp0483 with human serum FN in the preparation of a biocompatible coating. In order to accomplish this primary objective a number of specific objectives were developed. The conclusions drawn from these specific objectives are summarized below.

The adsorption of rTp0483 onto functionalized SAMs was analyzed along with FN binding onto rTp0483 coated SAMs. It was determined that while rTp0483 binds to a number of surface chemistries, $-COO^-$ SAM surfaces produce the highest potential surface concentration. It was also found that rTp0483 on $-COO^-$ SAM surfaces serves as the most preferred substrate for FN adsorption. These results indicate that a hydrophilic, negatively charged chemistry is the best choice for physical adsorption of FN to rTp0483 coated surfaces.

The adsorption of rTp0483 was further characterized by examining the ratio of dissipation energy to frequency change in adsorbed protein monolayers. SAM surface chemistry was found to affect this ratio. Higher dissipation energy corresponds to a loosely packed, labile protein layer. Hydrophilic, negatively charged $-COO^-$ SAMs were found to have moderate dissipation energy to frequency change ratio compared to other surfaces indicating that a specific rTp0483 configuration is required for FN binding, which is fulfilled by the $-COO^-$ surface chemistry.

The binding and desorption kinetics of rTp0483 adsorption onto SAMs and the adsorption of FN onto rTp0483 coated SAMs was investigated. rTp0483 adsorption was best represented by a 1:1 Langmuir adsorption model with mass transfer limitations while FN adsorption to rTp0483 was best modeled as a bivalent analyte event. It was also observed that the concentration of adsorbed rTp0483 plays a role in the subsequent adsorption of FN by influencing the relative rates of the two binding events.

The surface distribution of rTp0483 was analyzed using AFM to visualize the topography of adsorbed protein monolayers. Aggregation of rTp0483 into protein islands was observed along with a relationship between aggregate area and surface chemistry. $-COO^-$ SAMs displayed the smallest, most evenly distributed aggregate areas, which may help account for the excellent binding characteristics.

Blocking studies using peptides and antibodies were conducted to elucidate the regions on rTp0483 and FN responsible for binding. rTp0483 antibody studies indicated the involvement of both selected sequences in FN binding while a corresponding peptide study suggested the involvement of only one of the two. An accompanying study focused on the binding regions of FN found that the cell-binding and collagen/gelatin-binding regions were involved in rTp0483 binding.

The adsorption of Fg, HSA, and FXII was compared on rTp0483, FN, and rTp0483+FN coated $-COO^-$ SAMs as a measurement of hemocompatibility. Adsorption of rTp0483 prior to FN led to a decrease in Fg and HSA binding compared to FN alone while the addition of FN to adsorbed rTp0483 led to decreased binding of Fg, HSA, and FXII compared to rTp0483 alone. Decreased Fg

binding may correlate to a reduction in the rate of fibrin network formation, which indicates an increase in hemocompatibility. Decrease in HSA binding further shows that adsorption of rTp0483 prior to FN alters the adhesive properties of FN.

Hemocompatibility was further evaluated by analyzing the activation of the intrinsic clotting pathway on -COO^- SAMs coated with rTp0483, FN, and rTp0483+FN. Adsorption of rTp0483 prior to the addition of FN did not alter the response at the surface compared to FN alone while rTp0483 alone produced a smaller surface response than rTp0483+FN despite binding more FXII than either of the other surface coatings. Activation of adsorbed FXII is facilitated by a negative surface charge, thus the positive net charge of rTp0483 likely led to a reduction in the rate of activation. The response of rTp0483+FN and FN was similar because the net charge of FN was comparable in each case.

In addition to protein adsorption and intrinsic clotting pathway activation, the activation of platelets in contact with rTp0483, FN, and rTp0483+FN coated -COO^- SAMs was analyzed to quantify surface hemocompatibility. Adsorption of rTp0483 prior to the addition of FN resulted in a drastic reduction of platelet activation compared to FN alone. By reducing this response the hemocompatibility of the coated surface will increase substantially.

Biocompatibility was examined by observing the impact of rTp0483, FN, and rTp0483+FN coatings on phagocytosis of COO^- and plain PSMs. The addition of FN to adsorbed rTp0483 resulted in decreased phagocytosis for both types of PSMs compared to rTp0483 alone and for plain PSMs the adsorption of rTp0483 prior to the addition of FN led to decreased phagocytosis compared to FN alone. The surface

chemistry of the PSMs also affected phagocytosis. COO^- PSMs were initially taken up more slowly than plain PSMs and while the average fluorescence for macrophages with plain PSMs was largely constant over 24 hours, the average fluorescence for macrophages with COO^- PSMs increased more slowly, peaked above macrophages with plain PSMs, then feel back to lower values.

The impact of rTp0483, FN, and rTp0483+FN coating on macrophage surface adhesion was also investigated. FN coated surfaces bound more macrophages than rTp0483 coated surfaces and when rTp0483 was adsorbed prior to the addition of FN the number of cells decreased compared to FN. This result indicated that when FN binds to adsorbed rTp0483 it undergoes a change that reduces its ability to bind macrophage cells. Suppression of macrophage adhesion may lead to an increase in biocompatibility.

Potential cytotoxic effects of rTp0483, FN, and rTp0483+FN free in solution and adsorbed to surfaces were examined as an indicator of biocompatibility. No cytotoxic effects were observed for proteins in solution or adsorbed to PSMs; however, moderate cytotoxicity was observed when rTp0483 was adsorbed alone to COO^- WP surfaces prior to macrophage seeding. This is believed to be due to high local rTp0483 concentrations in direct contact with adsorbed macrophages.

In addition to phagocytosis and cytotoxicity, generation of TNF-α and NO_2^- by macrophages exposed to rTp0483, FN, and rTp0483+FN free in solution and adsorbed to surface were examined as indicators of biocompatibility. Addition of FN to rTp0483 on plain PSMs resulted in a decrease in TNF-α production compared to rTp0483 alone while on COO^- PSMs it had no effect. In contrast, the addition of

FN to rTp0483 on COO^- WP surfaces led to a reduction in TNF-α production compared to rTp0483 alone. Surface curvature of PSMs compared to flat WPs likely accounts for this difference. Macrophages exposed to rTp0483+FN or rTp0483 in solution produced significant TNF-α and were indistinguishable from one another indicating that any reduction in TNF-α production as a consequence of FN binding by rTp0483 is a surface mediated event. NO_2^- production by CRL-2449 cells exposed to proteins free in solution and protein coated PSMs was equal to or less than unstimulated controls while NO_2^- production by adherent macrophages was greater than unstimulated controls for positive LPS controls, adsorbed rTp0483, and for the highest concentration of rTp0483+FN in solution. For CRL-2449 cells this outcome indicates that the activation response does not include elevated nitric oxide activity. RAW 264.7 cells responded appropriately to stimulation with LPS, producing an elevated level of NO_2^-; however, while cells adsorbed to rTp0483 and rTp0483+FN coated surfaces produced significant TNF-α only cells adsorbed to rTp0483 coated surfaces produced significantly more NO_2^- than unstimulated controls. When exposed to free protein in solution only the highest concentration of rTp0483+FN elicited a response higher than unstimulated controls. This may indicate that in solution binding of FN by rTp0483 increases macrophage response in contrast to when adsorbed.

APPENDIX A: CELL AND PROTEIN PATTERNING VIA MOLECULARLY IMPRINTED BIOFOULING RESISTANT POLYMERS

A.1. Introduction

Biomaterial biocompatibility depends greatly on the reaction of natural immune and wound healing processes on and around an implanted device. These responses are largely predicated on cell and protein interactions with the surface of the device, thus by directing the host response it is possible to attenuate the immune response and facilitate natural wound healing around the implant area. A material synthesis technique known as molecular imprinting was employed with a goal of synthesizing a polymer coating capable of binding predetermined proteins or short oligopeptides for the purpose of generating organized cell arrays and potentially controlling host material interactions. Preliminary studies were conducted at Tokyo University in association with Dr. Kazuhiko Ishihara to generate a BSA specific substrate during the summer of 2009. A copolymer integrating fouling resistant MPC was used in the formation of the polymer coating to eliminate nonspecific protein interactions. Silica microspheres were functionalized with a copolymer of 3-(methacryloxy) propyl trimethoxysilane (MPTS), MPC, and p-nitrophenyloxycarbonylethylene glycol methacrylate (MEONP) called PMSiN. A similar copolymer was formed from MPC, MEONP, and butyl methacrylate (BMA) called PMBN. MPTS can form strong chemical bonds with silica microspheres that were used as physical support for the imprinting template, MPC prevents nonspecific protein interactions, and MEONP where the reactive p-nitrophenol (pNP) terminal group reacts with amino functionalities in the selected protein to

form a stable bond.[136] Once the protein is bound the remaining pNP groups are consumed by hydrolysis. The protein coated silica microspheres served as a template in the formation of molecularly imprinted surfaces. BSA was immobilized on the silica microspheres and the template added to a layer of photoreactive 2-methacryloyloxyethyl phosphorylcholine-co-2-methacryloyloxyethyloxycarbonyl 4-phenylazido (PMPAz). After the PMPaz coating was cross-linked via UV initiated polymerization the protein templates were removed and the adsorption of BSA compared to non-templated PMPaz, PMPaz templated with microspheres without BSA, and hydrophobic BMA using QCM and BSA ELISA.

A.2. Experimental Procedures

A.2.1. Biomolecules and Reagents

MPC, MEONP, and PMPaz were synthesized as previously detailed.[137-139] BMA was purchased from Kanto Chemical (Tokyo, Japan) and MPTS was purchased from Shin-Etsu Chemical (Tokyo, Japan). All other materials were obtained from Kanto Chemical unless stated otherwise. Silica microspheres (15 μm diameter) were purchased from Fuji Silysia Chemical (Tokyo, Japan). The structures of selected monomer units are shown in Figure A.1.

A.2.2. PMBN and PMSiN Polymer Synthesis

PMBN was synthesized by combining MPC, BMA, and MEONP in a molar ratio of 20/60/20. A total molar concentration of 1.0 M was employed with monomer

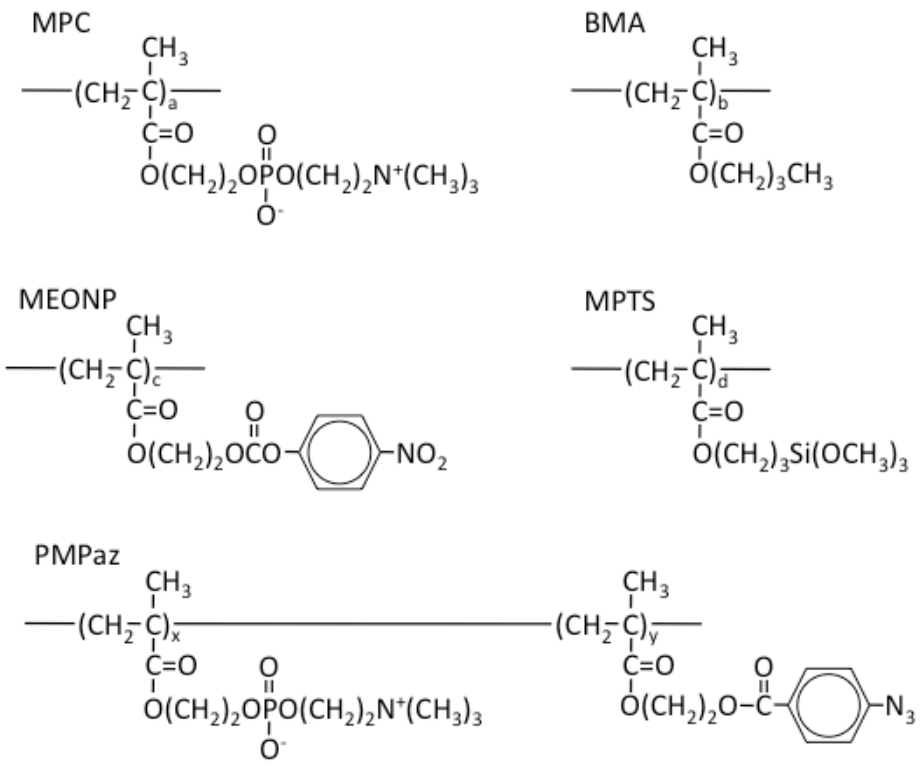

Figure A.1: Monomer unit structures. Subscripts indicate the molecular ratios of various monomers for copolymer formulations. MPC resists nonspecific protein adsorption, BMA is a hydrophobic unit included in the formulation of PMBN to make the copolymer non water soluble, MEONP is able to react with proteins to form a chemical bond, MPTS is able to form a chemical bond with silica surfaces, and MPMaz is a photoreactive form of MPC.

concentrations of 0.2 M MPC, 0.6 M BMA, and 0.2 M MEONP and the reaction was initiated with 10 mM AIBN. The monomers were dissolved in 50 mL of ethanol along with AIBN initiator and the solution degassed 10 minutes with argon (Ar). After degassing, the samples were moved to a -20° C freezer for 5 minutes then sealed in a glass tube. The sealed tube was immersed in a 60°C hot oil bath for 3 hours to initiate the polymerization reaction. The sealed tube was moved to the -20°C freezer for 10 minutes. At the same time, a 1000 mL of 80:20 ether to chloroform was prepared. After 10 minutes in the freezer the tube was unsealed

and the polymer solution was slowly added to the solvent solution under a fume hood. After 10 minutes the solvent solution was decanted off and replaced with fresh solvent. The sample solution was stirred for 1 hour then the precipitate was recovered. The polymer was dried under vacuum for 2 days. Polymerization was verified using a nuclear magnetic resonance (NMR) instrument manufactured by JEOL (Tokyo, Japan). The structure of PMBN is shown in Figure A.2.

PMSiN was synthesized by combining MPC, MPTS, and MEONP in a molar ratio of 70/10/20. A total molar concentration of 0.3 M was employed with monomer concentration of 0.21 M MPC, 0.03 M MPTS, and 0.06 M MEONP while the reaction was initiated with 5 mM AIBN. The monomers were dissolved in 25 mL of ethanol with AIBN. The polymerization protocol was identical to PMBN. After the polymer had been precipitated it washed in ethanol overnight before it was vacuum dried. Polymerization was verified using NMR. The structure of PMSiN is shown in Figure A.2. PMSiN was chosen for molecular imprinting studies because it can form a strong chemical bond with the silica microspheres chosen as the protein template substrate.

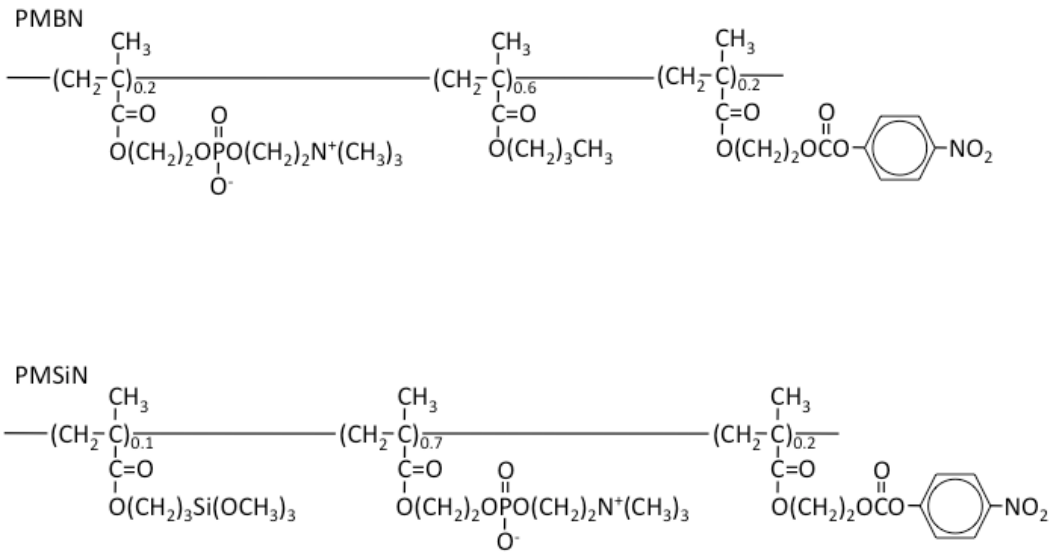

Figure A.2: Synthesized copolymer structures. Subscripts indicate the molecular ratios of monomer units. PMBN is physically adsorbed to a surface and is capable of chemically bonding proteins. PMSiN chemically bonds with silica surfaces as well as proteins.

A.2.3. Silica Microsphere PMSiN Coating

Silica microspheres were cleaned for 20 minutes under oxygen plasma in a PR500 Plasma Cleaner from Yamato Scientific (Tokyo, Japan). At the same time 0.5 % (w/v) PMSiN was dissolved in ethanol. After being cleaned, 250 mg of silica microspheres were added to 25 mL of PMSiN solution and incubated for 1 hour on a rotating test tube rack. The microspheres were recovered by centrifugation at 1000 RPM for 1 minute. The polymer solution was decanted off and the microspheres were dried at room temperature for 2 hours. The microspheres were incubated at 70°C for 3 hours to crosslink the PMSiN polymer. The coated microspheres were washed with ethanol for 1 hour and centrifuged at 1000 RPM for 1 minute. The ethanol was removed and the coated microspheres were dried at room

temperature. Phosphate buffered saline (PBS) (0.1 M potassium dihydrogenphosphate (Sigma) and 0.1 M NaOH in diH_2O, pH 7.8) and 0.5 M NaOH were prepared. The surface concentration of PMSiN was estimated by measuring the concentration of pNP liberated from MEONP groups when coated microspheres were exposed to NaOH. A similar liberation of pNP would be observed when a protein (BSA) became chemically bound to adsorbed PMSiN. A solution containing 1 mg/mL pNP was prepared in NaOH and diluted to 10, 5, 2, 1, and 0.1 μg/mL pNP. The absorbance spectrum was measured from 250-600 nm and a peak corresponding to pNP recorded at 400 nm. Using this information a pNP calibration curve was generated for the coated microspheres. 10 mg of coated microspheres were mixed with 0.5 M NaOH, centrifuged at 1000 RPM for 1 minute and the concentration of pNP liberated measured.

A.2.4. BSA Template Imprinting

Circular or rectangular glass slides were washed with ethanol then cleaned by exposing them to oxygen plasma for 20 minutes. Chrome was sputter coated onto the slides for 10 seconds followed by gold for 30 seconds. Coated rectangular slides were cut into squares. Alternately, gold QCM substrates were purchased from Biolin. The gold coated slides and QCM substrates were cleaned by exposing them to oxygen plasma for 20 minutes. A thin layer of BMA was spin coated onto sputter coated slides and QCM substrates to facilitate PMPaz adhesion. 50 μL of BMA was added to the substrate surfaces and spun in a spin coater for 10 seconds at low speed followed by 5 seconds at high speed. 50 μL of PMB30 (30:70 copolymer of

MPC:BMA) was also added to the backs of the sputter coated slides to prevent nonspecific BSA adsorption. 10 mg of PMSiN coated microspheres were either incubated 24 hours in 1 mg/mL BSA in PBS (pH 7.8) or in PBS alone. The binding of BSA was confirmed by analyzing the concentration of pNP liberated from the surface of the PMSiN coated microspheres by measuring the absorbance at 400 nm. Coated microspheres were washed with 1 mL of PBS and recovered by centrifugation at 1000 RPM for 1 minute. The coated microspheres were washed two more times and after the supernatant had been removed they were resuspended in 1.6 µg SDS/mL and 2.5 mg PMPaz/mL in diH_2O. 100 µL of PMPaz solution alone was added to a portion of surfaces while 100 µL of PMPaz solution with SDS and BSA coated templates (BSA imprinted PMPaz - BI-PMPaz) and PMPaz solution with just PMSiN coated microspheres (microsphere imprinted PMPaz - MI-PMPaz) were added to an equal number of surfaces. Lastly, an equal number were left as BMA. The liquid was evaporated at 37°C and polymerization initiated using UV radiation for 1 minute at 800 power in a CL-1000 UV crosslinker from Funakoshi (Tokyo, Japan). Polymer coverage and template removal were verified on the square gold coated slides using an AXIS-His165 XPS instrument from Kratos/Shimadzu (Kyoto, Japan).

A.2.5. QCM Analysis of BSA Adsorption

A Q-Sense D-300 QCM from Biolin was employed for all QCM measurements. Flow was manually controlled using a knob on the instrument to open and close the flow path. The temperature inside the sample chamber was held at 37°C and

experimental data recorded using a Q-Sense software package on an attached computer. Frequency change in the 7th overtone was measured in hertz (Hz) for the 5 Mhz substrates as a function of time. PBS was used to dilute BSA to 1 mg BSA/mL and also used to equilibrate the QCM substrates.

QCM substrates were prepared as indicated with PMPaz, MI-PMPaz, BI-PMPaz, or BMA coatings. A coated substrate was loaded and PBS flowed over it until the QCM signal was stable. The sample loop was filled with 1 mg BSA/mL and then flowed over the substrate until 5 drops left the exit line. Flow was stopped and the BSA incubated with the coated substrate for 30 minutes. The lines were flushed well with PBS then the flow was stopped and the QCM signal allowed to stabilize. The response was calculated by subtracting the frequency after BSA adsorption from the initial frequency before exposure to BSA.

A.2.6. ELISA Analysis of BSA Adsorption

PMPaz, MI-PMPaz, BI-PMPaz, and BMA coatings were applied to circular gold coated glass slides as previously detailed. Surfaces were rinsed with PBS and half were incubated 3 hours at 37°C in 0.1% (w/v) BSA in PBS while the other half were incubated in PBS with no BSA. All groups were prepared in triplicate. The liquid was removed from the samples and they were washed 4x with 1 mL portions of PBS. The PBS was removed and the samples were incubated 15 minutes at 37°C in 500 µL of a 1:5 dilution of blocking solution (NOF (Tokyo, Japan)) in PBS to prevent nonspecific antibody binding. 1:1000 dilutions of primary (Bethyl Laboratories (Montgomery, TX)) and secondary (R&D Systems) BSA antibodies were prepared in

stabilizing solution (NOF (Tokyo, Japan)) and 500 µL of primary antibody solution was added to each sample and incubated 1 hour at 37°C. The primary antibody solution was removed and the samples were washed 4x with 1 mL portions of PBS. 500 µL of secondary antibody solution was added to each sample and incubated 1 hour at 37°C. The samples were again washed 4x with 1 mL portions of PBS. 500 µL of HRP-substrate (SUMILION (Tokyo, Japan)) was added to each sample and incubated 20 minutes at RT then 500 µL of stop solution (SUMILION) was added to halt the reaction. BSA adsorption was determined by measuring sample absorbance at 450 nm using a Wallac 1420 ARVOsr microplate reader from Perkin Elmer (Waltham, MA)

A.2.7. Statistical Analysis

Statistical analysis was performed using the Microsoft Office Excel Data Analysis tool, StatPlus. Multiple pair-wise comparisons were made using one-way analysis of variance (ANOVA) with a maximum p-value of 0.05. All data are reported as a mean $\pm$ standard error. All studies are at minimum n=3 with specific sample group sizes noted in the text.

A.3. Results

A.3.1. PMBN and PMSiN Polymer Synthesis

PMBN and PMSiN were successfully synthesized. This was verified using NMR analysis. Figure A.3 illustrates the unique protons that were used to identify

each monomer unit. Figure A.4 shows the NMR spectra for PMBN. The two peaks observed at 7.5 and 8.3 ppm are MEONP, the peak at 3.0 ppm is MPC, and the two peaks at 1.4 and 1.6 ppm are BMA. The peaks at 5.5 and 6.0 ppm are unreacted MPC monomer. The ratio of components was determined by dividing the value of each set of peaks by the number of proteins represented. A molar ratio of 20/60/20 of MPC, BMA, and MEONP was combined to form PMBN and actual composition of the resulting polymer was determined to be 25/68/7. Figure A.5 shows the NMR spectra for PMSiN. The two peaks at 7.5 and 8.3 ppm are MEONP, the peak at 3.0 ppm is MPC, and the peak at 0.6 ppm is MPTS. Once again the two peaks at 5.5 and 6.0 ppm are unreacted MPC monomer. A molar ratio of 70/10/20 for MPC, MPTS, and MEONP was combined to form PMSiN and the actual composition of the resulting polymer was determined to be 90/3/7.

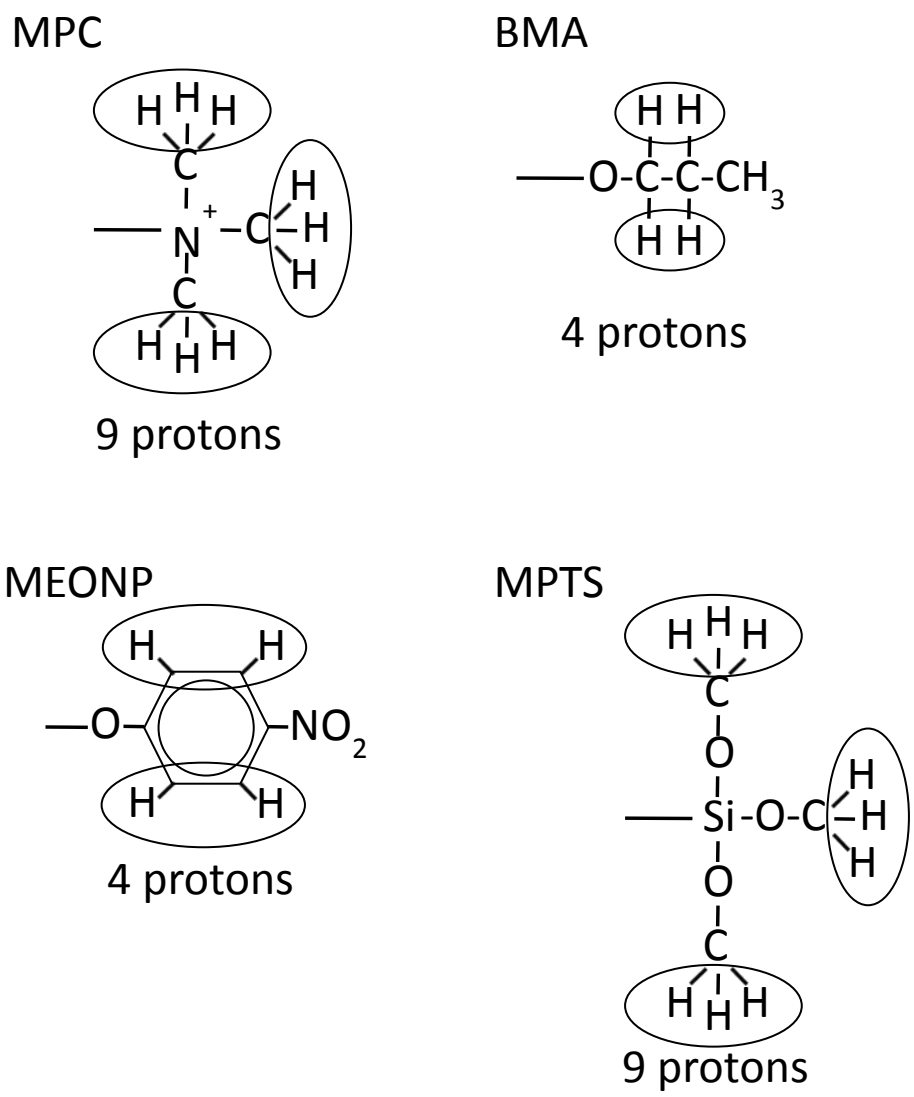

Figure A.3: Illustration of unique proton configurations used to identify each monomer. For MPC and MPTS all protons analyzed are the same (single peak) while for BMA and MEONP there are two types (double peak).

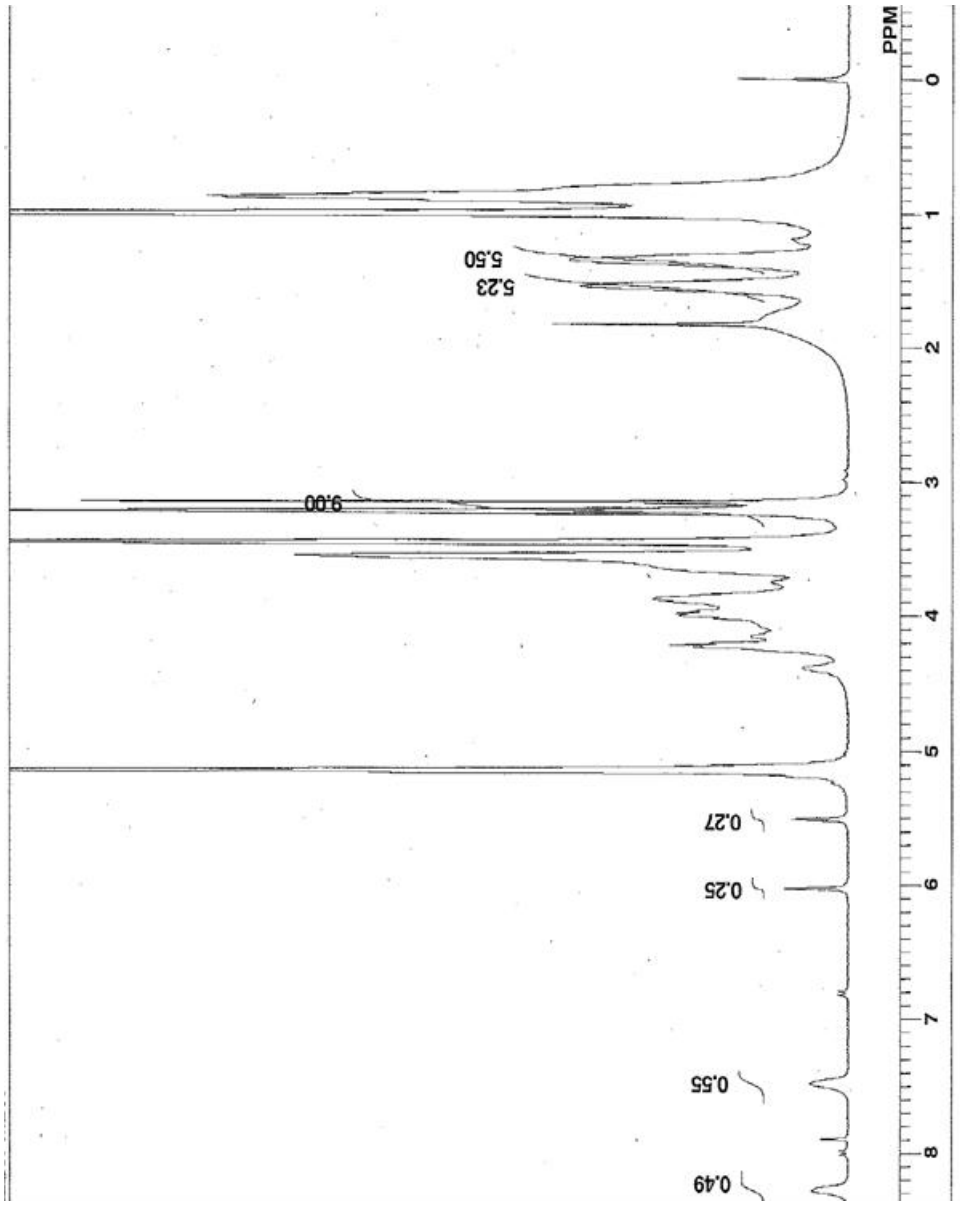

Figure A.4: NMR spectra for PMBN polymer. Peaks at 7.5 and 8.3 ppm are MEONP, peaks at 5.5 and 6.0 ppm are MPC monomer, peak at 3.0 ppm is MPC, and peaks at 1.4 and 1.6 ppm are BMA.

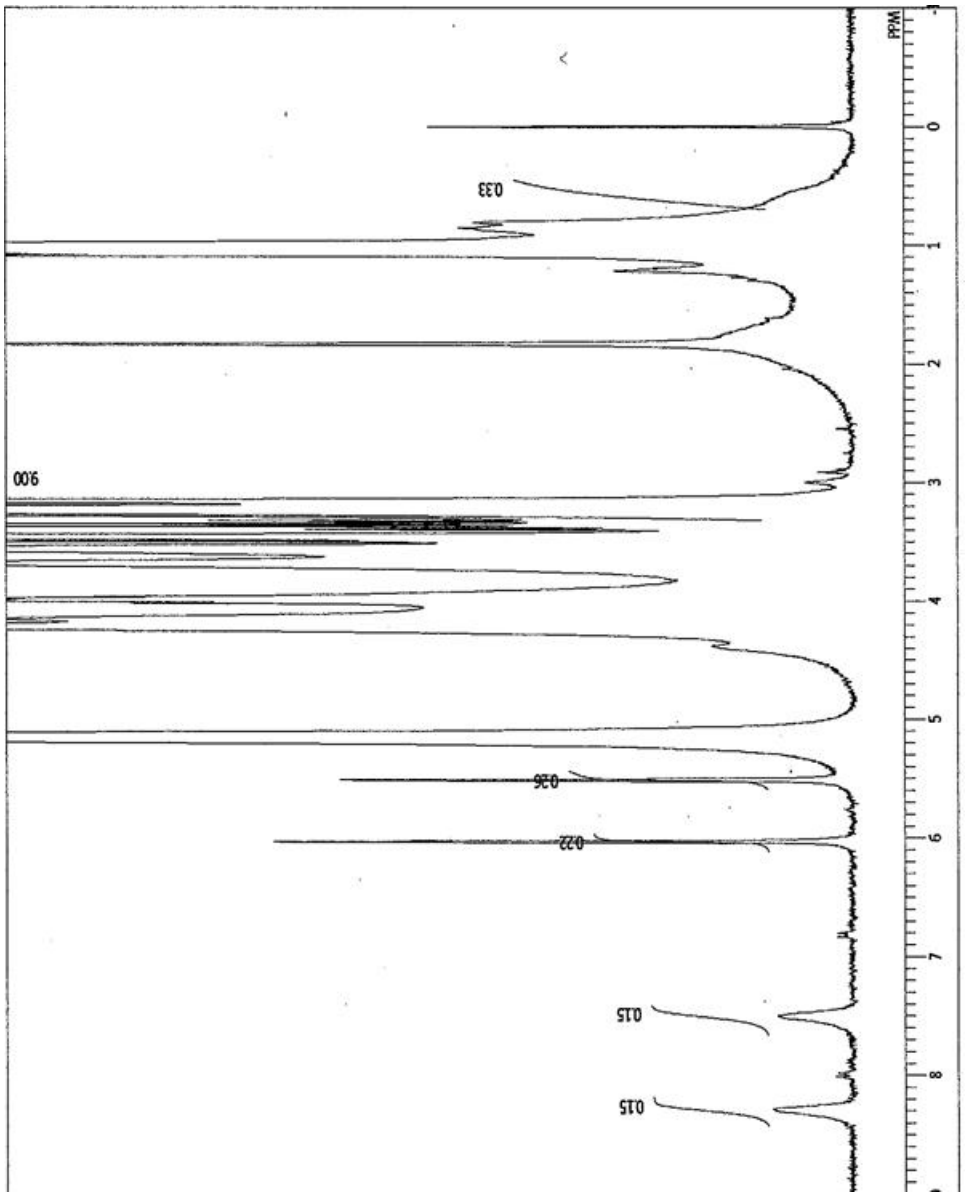

Figure A.5: NMR spectra for PMSiN Polymer. The peaks at 7.5 and 8.3 ppm are MEONP, peaks at 5.5 and 6.0 ppm are MPC monomer, the peak at 3.0 ppm is MPC, and the peak at 0.6 ppm is MPTS.

A.3.2. Silica Microsphere PMSiN Coating

Silica microspheres were successfully coated with PMSiN polymer. MEONP in the adsorbed PMSiN polymer was hydrolyzed in 0.5 M NaOH and the release of pNP measured at 400 nm. A calibration curve (shown in Figure A.6) was constructed using known pNP concentrations and the amount liberated from coated microspheres was calculated. The liberated pNP was found to be 0.19 µg pNP/mg silica microspheres. This provides sufficient surface concentration of MEONP to facilitate saturation by BSA.

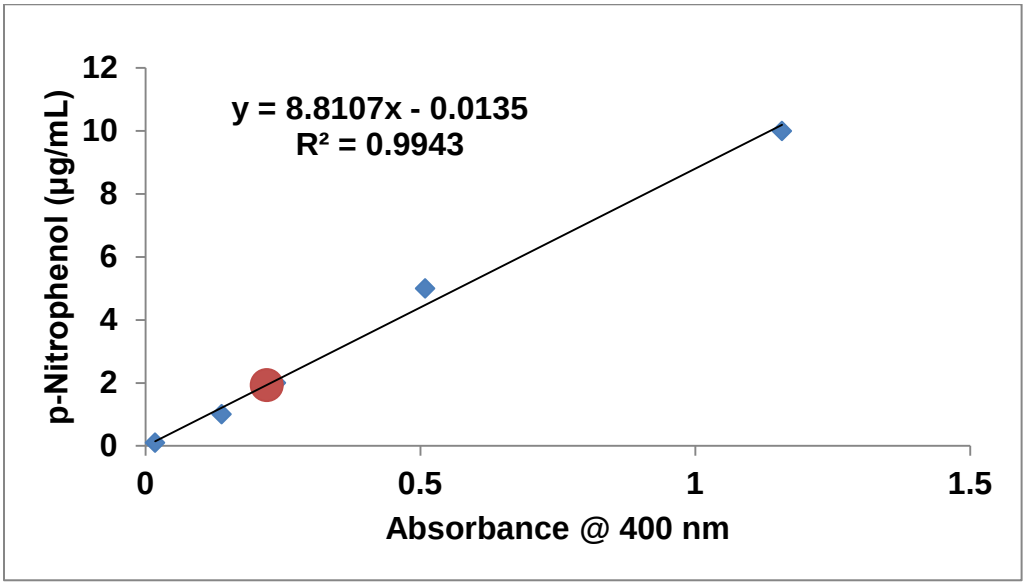

Figure A.6: pNP calibration curve for determination of PMSiN surface concentration. Absorbance measured at 400 nm is proportional to the concentration of pNP in solution. Linear regression of pNP standards allows for the determination of surface concentration of coated silica microspheres. (●)- PMSiN coated silica microspheres and (◆)- pNP controls.

A.3.3. BSA Template Imprinting

Measurement of pNP liberation in PBS at pH 7.8 indicated that all MEONP subunits were hydrolyzed after 24 hours. Samples in PBS with no BSA released 0.164 ± 0.029 μg pNP/mg microspheres while samples in PBS with 1 mg BSA/mL release only 0.156 ± 0.002 μg pNP/mg microspheres. This indicates that no unreacted groups remain to react with other amine containing materials during testing.

XPS was used to investigate the surface composition of BI-PMPaz and MI-PMPaz compared to unmodified gold surfaces. The results are shown in Table A.1. The gold surface had small traces of hydrocarbons likely from the atmosphere as the samples were loaded. High levels of carbon and oxygen indicate successful polymer coating for both BI-PMPaz and MI-PMPaz. Absence of nitrogen indicates the successful removal of BSA from BI-PMPaz.

Table A.1: XPS Data for BI-PMPaz, MI-PMPaz, and an unmodified gold surface.

Sample	Carbon	Phosphate	Gold	Nitrogen	Oxygen	Sulfur
Gold Control	2%	0%	97%	0%	1%	0%
BI-PMPaz	30%	1%	52%	1%	17%	0%
MI-PMPaz	65%	1%	4%	1%	29%	0%

A.3.4. QCM Analysis of BSA Adsorption

QCM analysis of BSA adsorption was used to determine whether BI-PMPaz was able to successfully facilitate BSA specific protein adsorption while MI-PMPaz

retains the anti-fouling properties of PMPaz alone. Figure A.7 shows the results of the QCM study. The BSA binding of PMPaz and MI-PMPaz was indistinguishable with responses of 34.5 ± 3.9 Hz and 30.6 ± 10.1 Hz respectively. The BSA binding of BI-PMPaz was significantly higher than PMPaz or MI-PMPaz (70.0 ± 10.2 Hz, $p<0.05$) and the binding of BMA was higher than any of the other three groups (126.5 ± 6.0 Hz, $p<0.05$). This indicates that PMPaz was able to significantly reduce protein binding compared to BMA and that by integrating a protein specific imprint BSA binding can be increased for PMPaz.

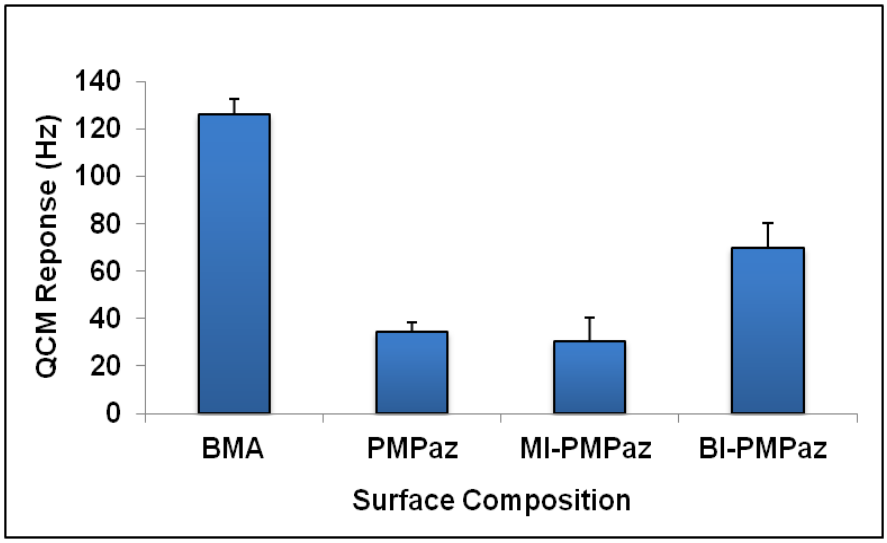

Figure A.7: QCM analysis of BSA binding to selected polymer coatings. The 7th overtone of 5 MHz quartz crystals was analyzed. BSA binding on MI-PMPaz was indistinguishable compared to PMPaz; however, BI-PMPaz bound significantly more protein ($p<0.05$). BMA bound more than the other three groups ($p<0.05$).

A.3.5. ELISA Analysis of BSA Adsorption

To verify the findings of the QCM study a BSA ELISA was carried out. The results are shown in Figure A.8. The absorbance of BMA and BI-PMPaz coated

surfaces incubated with 1 mg BSA/mL were significantly higher than the absorbance of surfaces incubated in PBS (0.036 ± 0.013 and 0.021 ± 0.005 respectively, $p<0.05$). PMPaz and MI-PMPaz coated surfaces incubated with 1 mg BSA/mL were indistinguishable from surfaces incubated in PBS (0.005 ± 0.003 and 0.015 ± 0.016 respectively).

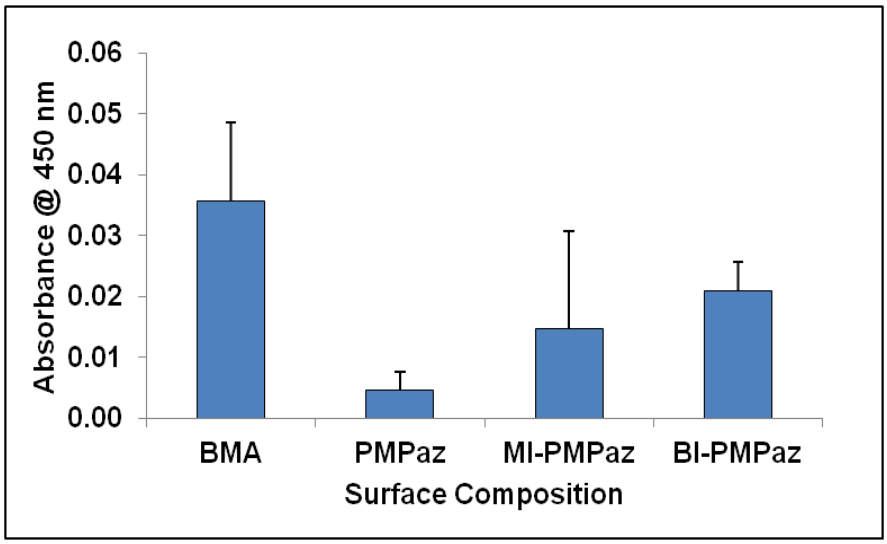

Figure A.8: ELISA analysis of BSA binding to selected polymer coatings. Absorbance at 450 nm for surfaces incubated in PBS was subtracted from the absorbance of surfaces incubated in 1 mg BSA/mL. BSA binding on PMPaz and MI-PMPaz was insignificant; however, BMA and BI-PMPaz bound a significant amount of protein ($p<0.05$).

A.4. Conclusions

Surface biocompatibility is dependent on the adsorption of cells and proteins. By controlling which components bind it may one day be possible to guide the host response to implanted biomaterials. The goal of this project was to prepare a non-fouling MPC polymer coating capable of selectively binding a target protein. A

protein stamp was manufactured by chemically coupling MPC based polymer chains to silica microspheres and then chemically bonding a model protein (BSA) to the surface of the silica microspheres. The stamp was combined with a surfactant (SDS) to assist in template removal and the bulk polymer substrate (PMPaz) to form the molecularly imprinted polymer coating (BI-PMPaz). NMR analysis established successful production of PMBN and PMSiN while XPS and UV absorbance measurement of pNP demonstrated functionalization of silica microspheres. Improved BSA binding for BI-PMPaz coatings compared to PMPaz alone was observed in QCM and ELISA studies. Similarly, MI-PMPaz coatings did not impact BSA binding indicating that the addition of the BSA template was critical in increasing protein binding.

REFERENCES

(1) Lafond, R. E. and Lukehard, S. A. (2006) Biological basis for syphilis. *Clinical Microbiology Review 19*, 29-49.

(2) Lukehart, S. A. (2008) Syphilis. McGraw Hill

(3) Radolf, J. D., Hazlett, R. O., and Lukehard, S. A. (2006) Pathogenesis of syphilis. Caister Academic Press

(4) Langer, R. and Peppas, N. A. (2003) Advances in biomaterials, drug delivery, and bionanotechnology. *AIChE Journal 49*, 2990-3006.

(5) Rosellini, E., Barbani, N., Giusti, P., and Ciardelli, G. (2010) Novel bioactive scaffolds with fibronectin recognition nanosites based on molecular imprinting technology. *Journal of Applied Polymer Science 118*, 3236-3244.

(6) Vozzi, G., Morelli, I., Vozzi, F., Andreoni, C., Salsedo, E., Morachioli, A., Giusti, P., and Ciardelli, G. (2010) SOFT-MI: A novel microfabrication technique integrating soft-lithography and molecular imprinting for tissue engineering applications. *Biotechnology and Bioengineering 106*, 804-817.

(7) Feng, W., Zhu, S., Ishihara, K., and Brash, J. L. (2005) Adsorption of fibrinogen and lysozyme on silicon grafted with poly(2-methacryloyloxyethyl phosphorylcholine) via surface-initiated atom transfer radical polymerization. *Langmuir 21*, 5980-5987.

(8) Konno, T., Hasuda, H., Ishihara, K., and Ito, Y. (2005) Photo-immobilization of a phospholipid polymer for surface modification. *Biomaterials 26*, 1381-1388.

(9) Sibarani, J., Takai, M., and Ishihara, K. (2007) Surface modification on microfluidic devices with 2-methacryloyloxyethyl phosphorylcholine polymers forrReducing unfavorble protein adsorption. *Colloids and Surfaces B: Biointerfaces 54*, 88-93.

(10) Carter, C. B. and Norton, M. G. (2007) Ceramic Materials: Science and Engineering. 635, Springer Science + Business Media, LLC

(11) Huebsch, N. and Mooney, D. J. (2009) Inspiration and application in the evolution of biomaterials. *Nature 462*, 426-432.

(12) Suh, H. (1998) Recent advances in biomaterials. *Yonsei Medical Journal 39*, 87-96.

(13) Geetha, M., Singh, A. K., Asokamani, R., and Gogia, A. K. (2009) Ti based biomaterials, the ultimate choice for orthopaedic implants - A review. *Progress in Materials Science 54*, 397-425.

(14) Saenz, A., Rivera-Munoz, E., Brostow, W., and Castano, V. M. (1999) Ceramic biomaterials: An introductory overview. *Journal of Materials Education 21*, 297-306.

(15) Nakase, T., Jujii, M., Myoui, A., Tamai, N., Hayaishi, Y., Ueda, T., Hamada, M., Kawai, H., and Yoshikawa, H. (2009) Use of hydroxyapatite ceramics for treatment of nonunited osseous defect after open fracture of lower limbs. *Archives of Orthopaedic and Trauma Surgery 129*, 1539-1547.

(16) Ripamonti, U. (1996) Osteoinduction in porous hydroxyapatite implanted in heterotopic sites of different animal models. *Biomaterials 17*, 31-35.

(17) Griffith, L. G. (1999) Polymeric biomaterials. *Acta Materialia 48*, 263-277.

(18) Seal, B. L., Otero, T. C., and Panitch, A. (2001) Polymeric biomaterials for tissue and organ regeneration. *Materials Science and Engineering R 34*, 147-230.

(19) Alberts, B., Johnson, A., and Lewis, J. (2002) Molecular Biology of the Cell. 4th Edition. Garland Science

(20) Coburn, J. C. and Pandit, A. (2007) Development of naturally-derived biomaterials and optimization of their biomechanical properties. *Topics in Tissue Engineering 3*, 1-32.

(21) Helmus, M. N., Gibbons, D. F., and Cebon, D. (2008) Biocompatibility: Meeting a key functional requirement of next-generation medical devices. *Toxicologic Pathology 36*, 70-80.

(22) Ratner, B. D. (2004) Biomaterials Science: An Introduction to Materials in Medicine Elsevier Acedemic Press

(23) Benhabbour, S. R., Sheardown, H., and Adronov, A. (2008) Protein resistance of PEG-functionalized dendronized surfaces: effect of PEG molecular weight and dendron generation. *Macromolecules 41*, 4817-4823.

(24) Ngadi, N., Abrahamson, J., Fee, C., and Morison, K. (2009) Are PEG molecules a universal protein repellent. *World Acedemy of Science, Engineering and Technology 49*, 144-148.

(25) Luk, Y.-Y., Kato, M., and Mrksich, M. (2000) Self-assembled monolayers of alkanethiolates presenting mannitol groups are inert to protein adsorption and cell attachment. *Langmuir 16*, 9604-9608.

(26) Fernandez, I. C. S., Domingues, J. F. D. S., van Kooten, T. G., Metzger, S., Grainger, D. W., Busscher, H. J., and van der Mei, H. C. (2011) Macrophage response to staphlococcal biofilms on crosslinked poly(ethylene) glycol polymer coatings and common biomaterials *in vitro*. *European Cells and Materials 21*, 73-79.

(27) Hubbell, J. A. (1999) Bioactive biomaterials. *Current Opinion in Biotechnology 10*, 123-129.

(28) Tabata, Y. (2003) Tissue regeneration based on growth factor release. *Tissue Engineering 9*, S-5 - S-15.

(29) Karp, G. (2008) Cell and Molecular Biology: Concepts and Experiments. John Wiley & Sons

(30) Remes, A. and Williams, D. F. (1991) Immune response in biocompatibility. *Biomaterials 13*, 731-743.

(31) Ehrnthaller, C., Ignatius, A., Gebhard, F., and Huber-Lang, M. (2011) New insights of an old defense system: structure, function, and clinical relevance of the complement system. *Molecular Medicine 17*, 317-329.

(32) Amara, U., Flierl, M. A., Rittirsch, D., Klos, A., Chen, H., Acker, B., Bruckner, U. B., Nilsson, B., Gebhard, F., Lambris, J. D., and Huber-Lang, M. (2010)

Molecular intercommunication between the complement and coagulation systems. *The Journal of Immunology 185*, 5628-5636.

(33) Janvier, G., Baquey, C., Roth, C., Benillan, N., Belisle, S., and Hardy, J.-F. (1996) Extracorporeal circulation, hemocompatibility, and biomaterials. *The Annals of Thoracic Surgery 62*, 1926-1934.

(34) Lestelius, M., Liedberg, B., and Tengvall, P. (1997) *In vitro* plasma protein adsorption on w-functionalized alkanethiolate self-assembled monolayers. *Langmuir 13*, 5900-5908.

(35) Amarnath, L. P., Srinivas, A., and Ramamurthi, A. (2006) *In vitro* hemocompatibility testing of UV-modified hyaluronan hydrogels. *Biomaterials 27*, 1416-1424.

(36) Benesch, J., Svedhem, S., Svensson, S. C. T., Valiokas, R., Liedberg, B., and Tengvall, P. (2001) Protein adsorption to oligo(ethylene glycol) self-assembled monolayers: Experiments with fibrinogen, heparinized plasma, and serum. *Journal of Biomaterials Science, Polymer Edition 12*, 581-597.

(37) Chang, Y., Shu, S. H., Shih, Y. J., Chu, C. W., Ruaan, R. C., and Chen, W. Y. (2009) Hemocompatible mixed-charge copolymer brushes of pseudozwitterionic surfaces resistant to nonspecific plasma protein fouling. *Langmuir 26*, 3522-3530.

(38) Chatterjee, K., Guo, Z., Vogler, E. A., and Siedlecki, C. A. (2008) Contributions of contact activation pathways of coagulation factor XII in plasma. *Journal of Biomedical Materials Research Part A* 27-34.

(39) Fischer, M., Sperling, C., and Werner, C. (2010) Synergistic effect of hydrophobic and anionic surface groups triggers blood coagulation *in vitro*. *Journal of Materials Science: Materials in Medicine 21*, 931-937.

(40) Lin, W. C., Liu, T. Y., and Yang, M. C. (2004) Hemocompatibility of polyacrylonitrile dialysis membrane immobilied with chitosan and heparin conjugate. *Biomaterials 25*, 1947-1957.

(41) Norris, L. A. (2003) Blood coagulation. *Best Practice & Research Clinical Obstetrics & Gynaecology 17*, 369-383.

(42) Rodrigues, S. N., Goncalves, I. C., Martins, M. C. L., Barbosa, M. A., and Ratner, B. D. (2006) Fibrinogen adsorption, platelet adhesion and activation on mixed hydroxyl-/methyl-terminated self-assembled monolayers. *Biomaterials 27*, 5357-5367.

(43) Sperling, C., Fischer, M., Maitz, M. F., and Werner, C. (2009) Blood coagulation on biomaterials requires the combination of distinct activation processes. *Biomaterials 30*, 4447-4456.

(44) Weber, N., Wendel, H. P., and Ziemer, G. (2001) Hemocompatibility of heparin-coated surfaces and the role of selective plasma protein adsorption. *Biomaterials 23*, 429-439.

(45) Werner, C., Maitz, M. F., and Sperling, C. (2007) Current strategies towards hemocompatible coatings. *Journal of Materials Chemistry. 17*, 1-10.

(46) Adams, R. L. and Bird, R. J. (2009) Review article: coagulation cascade and therapeutics update: relevance to nephrology. Part 1: overview of coagulation, thrombophilias and history of anticoagulants. *Nephrology 14*, 462-470.

(47) Balakrishnan, B. and Jayakrishnan, A. (2005) Chemical modification of poly (vinyl choride) using poly (ethylene glycol) to improve blood compatibility. *Trends in Biomaterials & Artificial Organs 18*, 230-236.

(48) Chen, K. Y. and Kuo, J. F. (2002) Surface characterization and platelet adhesion studies of aliphatic polyurethanes grafted by fluorocarbon oligomers: effect of fluorocarbon chain length and caqrboxylic acid group. *Journal of Materials Science: Materials in Medicine 13*, 37-45.

(49) Anderson, K. V. (2000) Toll signalling pathways in the innate immune response. *Current Opinion in Immunology 12*, 13-19.

(50) Desrosiers, D. C., Anard, A., Luthra, A., Dunham-Ems, S. M., LeDoyt, M., Cummings, M. A. D., Eshghi, A., Cameron, C. E., Cruz, A. R., Salazar, J. C., Caimano, M. J., and Radolf, J. D. (2011) Tp0326, a Treponema pallidum β-barrel assembly machinery A (BamA) orthologue and rare outer membrane protein. *Molecular Microbiology 80*, 1496-1515.

(51) Brinkman, M. B., McGill, M. A., J., P., Rogers, A., Matejkova, P., Smajs, D., Weinstock, G. M., Norris, S. J., and Palzkill, T. (2008) A novel Treponema pallidum antigen, Tp0136, is an outer membrane protein that binds human fibronectin. *Infection and Immunity 76*, 1848-1857.

(52) Cameron, C. E. (2003) Identification of a *Treponema pallidum* Laminin-Binding Protein. *Infection and Immunity 71*, 2525-2533.

(53) Cameron, C. E., Brown, E. L., Kuroiwa, J. M. Y., Schnapp, L. M., and Brouwer, N. L. (2004) *Treponema pallidum* fibronectin-binding proteins. *Journal of Bacteriology 186*, 7019-7022.

(54) Cox, D. L., Luthra, A., Dunham-Ems, S., Desrosiers, D. C., Salazar, J. C., Caimano, M. J., and Radolf, J. D. (2010) Surface immunolabeling and consensus computational framework to identify candidate rare outer membrane proteins of *Treponema pallidum*. *Infection and Immunity 78*, 5178-5194.

(55) Liu, S. Q., Wang, S. P., Wu, Y. M., Zhao, F. J., Zeng, T. B., J., Z. Y., Zhang, Q. G., and Gao, D. M. (2010) Production of proinflammatory cytokines in the human THP-1monocyte cell line following induction by Tp0751, a recombinant protein of *Treponema pallidum*. *Science China, Life Sciences 53*, 229-233.

(56) Radolf, J. D. (1994) Role of outer membrane architecture in immune evasion by *Treponema pallidum* and *Borrelia burgdorferi*. *Trends in Microbiology 2*, 307-311.

(57) Salazar, J. C., Hazlett, K. R. O., and Radolf, J. D. (2002) The immune response to infection with *Treponema pallidum*, the stealth pathogen. *Microbes and Infection 4*, 1133-1140.

(58) Tomson, F. L., Conley, P. G., Norgard, M. V., and Hagman, K. E. (2007) Assessment of cell-surface exposure and vaccinogenic potentials of *Treponema pallidum* candidate outer membrane proteins. *Microbes and Infection 9*, 1267-1275.

(59) Radolf, J. D., Norgard, M. V., and Schulz, W. W. (1989) Outer membrane ultrastructure explains the limited antigenicity of virulent Treponema pallidum. *Proceedings of the National Academy of Sciences (USA) 86*, 2051-2055.

(60) Walker, E. M., Zampighi, G. A., Blanco, D. R., Miller, J. N., and Lovett, M. A. (1989) Demonstration of rare protein in the outer membrane of Treponema pallidum subsp. pallidum by freeze-fracture analysis. *Journal of Bacteriology 171*, 5005-5011.

(61) Cameron, C. E., *T. pallidum outer membrane and outer membrane proteins.*, in *Pathogenic Treponema: Molecular and Cellular Biology*. 2006, Caister Academic: Norfolk, UK.

(62) Centurion-Lara, A., Castro, C., Barrett, L., Cameron, C. E., Mostowfi, M., Van Voorhis, W. C., and Lukehart, S. A. (1999) Treponema pallidum major sheath protein homologue Tpr K is a target of opsonic antibody and the protective immune response. *Journal of Experimental Medicine 189*, 647-656.

(63) Pankov, R. and Yamada, K. M. (2002) Fibronectin at a glance. *Journal of Cell Science 115*, 3861-3863.

(64) Lee, J. H., Choi, H. J., Jung, J., Lee, M. G., Lee, J. B., and Lee, K. H. (2003) Receptors for *Treponema pallidum* attachment to the surface and matrix proteins of cultured human dermal microvascular endothelial cells. *Yonsei Medical Journal 44*, 371-378.

(65) Ouaissi, M. A. (1988) Role of the RGD sequence in parasite adhesion to host cells. *Parasitology Today 4*, 169-173.

(66) Thomas, D. D., Baseman, J. B., and Alderete, J. F. (1985) Fibronectin mediates Treponema pallidum cytadherence through recognition of fibronectin cell-binding domain. *Journal of Experimental Medicine 161*, 514-525.

(67) Thomas, D. D., Baseman, J. B., and Alderete, J. F. (1985) Fibronectin tetrapeptide is target for syphilis spirochete cytoadherence. *Journal of Experimental Medicine 162*, 1715-1719.

(68) Kimizuka, F., Ohdate, Y., Kawase, Y., Shimojo, T., Taguchi, Y., Hashino, H., Goto, S., Hashi, H., Kato, I., Titani, K., and Sekiguchi, K. (1989) Isolation and characterization of two monoclonal antibodies that recognize remote epitopes on the cell-binding domain of human fibronectin. *Experimental Cell Research 185*, 229-236.

(69) Zhang, Y., Chai, C., Jiang, X. S., Teoh, S. H., and Leong, K. W. (2007) Fibronectin immobilized by covalent conjugation or physical adsorption shows different bioactivity on animated-PET. *Materials Science and Engineering 27*, 213-219.

(70) Atkin, K. E., Brentnall, A. S., Harris, G., Bingham, R. J., Erat, M. C., Millard, C. J., Schwarz-Linek, U., Staunton, D., Vakonakis, I., Campbell, I. D., and Potts, J. R. (2010) The streptococcal binding site in the gelatin-binding domain of fibronectin is consistent with a non-linear arrangement of modules. *The Journal of Biological Chemistry 285*, 36977-36983.

(71) van der Flier, M., Chhun, N., Wizemann, T. M., Min, J., McCarthy, J. B., and Tuomanen, E. I. (1995) Adherence of *Streptococcus pneumoniae* to immobilized fibronectin. *Infection and Immunity 63*, 4317-4322.

(72) Fitzgerald, T. J. and Repesh, L. A. (1985) Interaction of fibronectin with *Treponema pallidum*. *Genitourinary Medicine 61*, 147-155.

(73) Peterson, K. M., Baseman, J. B., and Alderete, J. F. (1983) *Treponema pallidum* receptor binding proteins interact with fibronectin. *Journal of Experimental Medicine 157*, 1958-1970.

(74) Lukehart, S. A., Shaffer, J. M., and Baker-Zander, S. A. (1992) A subpopulation of *Treponema pallidum* is resistant to phagocytosis: possible mechanism of persistence. *The Journal of Infectious Diseases 166*, 1449-1453.

(75) Ghasemi, A., Namaki, S., and Mirshafiey, A. (2009) *Streptococcus pyogenes*. *Journal of Chinese Clinical Medicine 4*, 9-18.

(76) Seelig, R., Pott, G., Seelig, H. P., Liehr, H., Metzger, P., and Waldherr, R. (1984) Virus-binding activity of fibronectin: masking of hepatitis A virus. *Journal of Virological Methods 8*, 335-347.

(77) Dixon, M. C. (2008) Quartz crystal microbalance with dissipation monitoring: Enabling real-time characterization of biological materials and their interactions. *Journal of Biomolecular Techniques 19*, 151-158.

(78) Hemmersam, A. G., Rechendorff, K., Foss, M., Sutherland, D. S., and Besenbacher, F. (2008) Fibronectin adsorption on gold, Ti-, and Ta-oxide

investigated by QCM-D and RSA modelling. *Journal of Colloid and Interface Science 320*, 110-116.

(79) Xu, J., Liu, K.-W., Matthews, K. S., and Biswal, S. L. (2011) Monitoring DNA binding to Escherichia coli lactose repressor using quartz crystal cicrobalance with dissipation *Langmuir 27*, 4900-4905.

(80) Liu, Z., Choi, H., Gatenholm, P., and Esker, A. R. (2011) Quartz crystal microbalance with dissipation monitoring and surface plasmon resonance studies of carboxymethyl cellulose adsorption onto regenerated cellulose surfaces. *Langmuir 27*, 8718-8728.

(81) Hansson, K. M., Tengvall, P., Lundstrom, I., Ranby, M., and Lindahl, T. L. (2002) Surface plasmon resonance and free oscillation rheometry in combination: a useful approach for studies on haemostasis and interactions between whole blood and artificial surfaces *Biosensors and Bioelectronics 17*, 747-759.

(82) Hlady, V. and Jogikalmath, G. (2007) Albumin binding and insertion into PS-b-PEO monolayers at air–water interface. *Colloids and Surfaces B: Biointerfaces 54*, 179-187.

(83) Zhou, Y., Liedberg, B., Gorochovceva, N., Makuska, R., Dedinaite, A., and Claesson, P. M. (2007) Chitosan-N-poly(ethylene oxide) brush polymers for reduced nonspecific protein adsorption. *Journal of Colloid and Interface Science 305*, 62-71.

(84) Stenberg, E., Persson, B. R., H., and Urbaniczky, C. (1991) Quantitative determination of surface concentration of protein with surface plasmon resonance by using radiolabeled proteins. *Colloids and Interface Science 143*, 513-526.

(85) Engel, A. and Muller, D. J. (2000) Observing single biomolecules at work with the atomic force microscope. *Nature Structural Biology 7*, 715-718.

(86) Gan, Y., Wanless, E. J., and Franks, G. V. (2007) Lattice-resolution imaging of the sapphire (0001) surface in air by AFM. *Surface Science 601*, 1064-1071.

(87) Suehira, N., Tomiyoshi, Y., Sugiyama, K., Watanabe, S., and Fujii, T. (2000) Development of low temperature ultrahigh vacuum noncontact atomic force microscope with PZT cantilever. *Applied Surface Science 157*, 343-348.

(88) Ge, G., Han, D., Lin, D., Chu, W., Sun, Y., Jiang, L., Ma, W., and Wang, C. (2007) MAC mode atomic force microscopy studies of living samples, ranging from cells to fresh tissue. *Ultramicroscopy 107*, 299-307.

(89) Wang, A., McAllister, J. P. I., Finlayson, P., Li, J., Brabant, K., Tang, H., Black, C., Cao, T., Liang, X., Salley, S. O., Auner, G. W., and Ng, K. Y. S. (2007) Short- and long- term neural biocompatibility of heparin coated sapphire implants. *Materials Science and Engineering 27*, 237-243.

(90) Bippes, C. A. and Muller, D. J. (2011) High-resolution atomic force microscopy and spectroscopy of native membrane proteins. *Reports on Progress in Physics 74*, 1-34.

(91) Autissier, P., Soulas, C., Burdo, T. H., and Williams, K. C. (2010) Immunophenotyping of lymphocyte, monocyte and dendritic cell subsets in normal rhesus macaques by 12-color flow cytometry: Clarification on DC heterogeneity. *Journal of Immunological Methods 360*, 119-128.

(92) Dyer, K. D., Garcia-Crespo, K. E., Killoran, K. E., and Rosenberg, H. F. (2011) Antigen profiles for the quantitative assessment of eosinophils in mouse tissues by flow cytometry. *Journal of Immunological Methods 369*, 91-97.

(93) Kim, G. G., Donnenberg, V. S., Donnenberg, A. D., Gooding, W., and Whiteside, T. L. (2007) A novel multiparametric flow cytometry-based cytotoxicity assay simultaneously immunophenotypes effector cells: Comparisons to a 4 h 51Cr-release assay. *Journal of Immunological Methods 325*, 51-66.

(94) Silin, V., Weetall, H., and Vanderah, D. J. (1997) SPR studies of the nonspecific adsorption kinetics of human IgG and BSA on gold surfaces modified by self-assembled monolayers (SAMs). *Journal of Colloid and Interface Science 185*, 94-103.

(95) (1997) BIAevaluation 3.0 Software Handbook. Uppsala, Sweden: Biacore AB

(96) Cameron, C. E., Lukehart, S. A., Castro, C., Molini, B., Godornes, C., and Van Voorhis, W. C. (2000) Opsonic potential, protective capacity, and sequence conservation of the Treponema pallidum subspecies pallidum Tp92. *The Journal of Infectious Disease 181*, 1401-1413.

(97) Zhang, H. H., Blanco, D. R., Exner, M. M., Shang, E. S., Champion, C. I., Phillips, M. L., Miller, J. N., and Lovett, M. A. (1999) Renaturation of recombinant *Treponema pallidum* rare outer membrane protein 1 into a trimeric, hydrophobic, and porin-active conformation. *Journal of Bacteriology 181*, 7168-7175.

(98) Chung, Y. C., Chiu, Y. H., W., W. Y., and T., T. Y. (2005) Self-assembled biomimetic monolayers using phospholipid-containing disulfides. *Biomaterials 26*, 2313-2324.

(99) Keselowsky, B. G., Collard, D. M., and Garcia, A. J. (2003) Surface chemistry modulates fibronectin conformation and directs integrin binding and specificity to control cell adhesion. *Journal of Biomedical Materials Research Part A 66A*, 247-259.

(100) Lin, J. C. and Chuang, W. H. (2000) Synthesis, surface characterization, and platelet reactivity evaluation for the self-assembled monolayer of alkanethiol with sulfonic acid functionality. *Journal of Biomedical Materials Research 51*, 413-423.

(101) Michael, K. E., Vernekar, V. N., Keslowsky, B. G., Meredith, J. C., Latour, R. A., and Garcia, A. J. (2003) Adsorption-induced conformational changes in fibronectin due to interactions with well-defined surface chemistries. *Langmuir 19*, 8033-8040.

(102) Nuzzo, R. G., Dubois, L. H., and Allara, D. L. (1990) Fundamental studies of microscopic wetting on organic surfaces. 1. Formation and structural characerization of self-consistent series of polyfunctional organic monolayers. *Journal of the American Chemical Society 112*, 558-569.

(103) Sperling, C., Schweiss, R. B., Streller, U., and Werner, C. (2005) *In vitro* hemocompatibility of self-assembled monolayers displaying various functional groups. *Biomaterials 26*, 6547-6557.

(104) Tanahashi, M. and Matsuda, T. (1997) Surface functional group dependence on apatite formation on self-assembled monolayers in a simulated body fluid. *Journal of Biomedical Materials Research 34*, 305-315.

(105) Dickerson, M. T., Abney, M. B., Cameron, C. E., Knecht, M., Bachas, L. G., and Anderson, K. W. (2011) Fibronectin binding to the *Treponema pallidum* adhesin protein fragment rTp0483 on functionalized self-assembled monolayers. *Bioconjugate Chemistry In Press*,

(106) Harpaz, Y., Gerstein, M., and Chothia, C. (1994) Volume changes on protein folding. *Structure 15*, 641-649.

(107) Laszlo, J. A. and Evans, K. O. (2007) Influence of self-assembled monolayer surface chemistry on *Candida antarctica* lipase B adsorption and specific activity. *Journal of Molecular Cataysis B: Enzymatic 48*, 84-89.

(108) Berrocal, M. J., Johnson, R. D., Badr, I. H. A., Liu, M., Gao, D., and Bachas, L. G. (2002) Improving the blood compatibility of ion-selective electrodes by employing poly(MPC-co-BMA), a copolymer containing phosphorylcholine, as a membrane coating. *Analytical Chemistry 74*, 3644-3648.

(109) Makogonenko, E., Tsurupa, G., Ingham, K., and Medved, L. (2002) Interaction of fibrin(ogen) with fibronectin: further characterization and localization of the fibronectin-binding site. *Biochemistry 41*, 7907-7913.

(110) Cho, J. and Mosher, D. F. (2006) Enhancement of thrombogenesis by plasma fibronectin cross-linked to fibrin and assembled in platelet thrombi. *Blood 107*, 3555-3563.

(111) Reheman, A., Yang, H., Zhu, G., Jin, W., He, F., Spring, C. M., Bai, X., Gross, P. L., Freedman, J., and Ni, H. (2009) Plasma fibronectin depletion enhances platelet aggregation and thrombus formation in mice lacking fibrinogen and von Willebrand factor. *Blood 113*, 1809-1817.

(112) Haverstick, D. M., Cowan, J. F., Yamada, K. M., and Santoro, S. M. (1985) Inhibition of platelet adhesion to fibronectin, fibrinogen, and von Willebrand factor substrates by a synthetic tetrapeptide derived from the cell-binding domain of fibronectin. *Blood 66*, 946-952.

(113) Anderson, J. M. (1994) Inflammation and the foreign body response. Problems. *General Surgery 11*, 147-160.

(114) Horbett, T. A. (1993) Principles underlying the role of adsorbed plasma protein in blood interaction with foreign materials. *Cardiovascular Pathology 2*, 137S-148S.

(115) Anderson, J. M. and Miller, K. M. (1984) Biomaterial biocompatibility and the macrophage. *Biomaterials*

(116) Salthouse, T. N. (1984) Some aspects of macrophage behavior at the implant interface. *Journal of Biomedical Materials Research 18*, 395-401.

(117) Nathan, C. F. (1987) Secretory products of macrophages. *The Journal of Clinical Investigation 79*, 319-326.

(118) Ziats, N. P., Miller, K. M., and Anderson, J. M. (1988) In vitro and in vivo interaction of cells with biomaterials. *Biomaterials 9*, 5-13.

(119) Behling, C. A. and Spector, M. (1986) Quantitative characterization of cells at the interface of long-term implants of selected polymers. *Journal of Biomedical Materials Research 20*, 653-666.

(120) Foged, C., Brodin, B., Frokjaer, S., and Sundblad, A. (2005) Particle size and surface charge affect particle uptake by human dendritic cells in an in vitro model. *International Journal of Pharmaceuticals 298*, 315-322.

(121) Page, J., Heitz, B. A., Joubert, J. R., Keogh, J. P., Sparer, T., Saavedra, S. S., and He, W. (2011) In vitro assessment of macrophage attachment and phenotype on polymerized phospholipid bilayers. *Journal of Biomedical Materials Research A 97A*, 212-217.

(122) Ci, X., Liang, X., Luo, G., Yu, Q., Li, H., Wang, D., Li, R., and Deng, X. (2010) Regulation of inflammatory mediators in lipopolysaccharide-stimulated RAW 264.7 cells by 2″-hydroxy-3″-en-anhydroicaritin involves down-regulation of NF-κB and MAPK expression. *International Immunopharmacology 10*, 995-1002.

(123) Kanno, S., Shouji, A., Tomizawa, A., Hiura, T., Osanai, Y., Ujibe, M., Obara, Y., Nakahata, N., and Ishikawa, M. (2006) Inhibitory effect of naringin on lipopolysaccharide (LPS)-induced endotoxin shock in mice and nitric oxide production in RAW 264.7 macrophages. *Life Sciences*

(124) MacMicking, J., Xie, Q., and Nathan, C. (1997) Nitric oxide and macrophage function. *Annual Review of Immunology 15*, 323-350.

(125) Scuro, L. S., Simioni, P. U., Grabriel, D. L., Saviani, E. E., Modolo, L. V., Tamashiro, W., and Salgado, I. (2004) Suppression of nitric oxide production in mouse macrophages by soybean flavonoids accumulated in response to nitroprusside and fungal elicitation. *BMC Biochemistry 5*, 1-8.

(126) Ahn, K. S., Noh, E. J., Cha, K.-H., Kim, Y. S., Lim, S. S., Shin, K. H., and Jung, S. H. (2006) Inhibitory effects of Irigenin from the rhizomes of Belamcanda chinensis on nitric oxide and prostaglandin E2 production in murine macrophage RAW 264.7 cells. *Life Sciences 78*, 2336-2342.

(127) Shen, M. and Horbett, T. A. (2001) The effects of surface chemistry and adsorbed proteins on monocyte/macrophage adhesion to chemically modified polystyrene surfaces. *Journal of Biomedical Materials Research 57*, 336-345.

(128) Lundqvist, M., Sethson, I., and Jonsson, B.-H. (2004) Protein adsorption onto silica nanoparticles: conformational changes depend on the particles' curvature and the protein stability. *Langmuir 20*, 10639-10647.

(129) Roach, P., Farrar, D., and Perry, C. C. (2006) Surface tailoring for controlled protein adsorption: effect of topography at the nanometer scale and chemistry. *Journal of the American Chemical Society 128*,

(130) Zahr, A. S., Davis, C. A., and Pishko, M. V. (2006) Macrophage uptake of core-shell nanoparticles surface modified with poly(ethylene glycol). *Langmuir 22*, 8178-8185.

(131) Blystone, S. D., Graham, I. L., Lindberg, F. P., and Brown, E. J. (1994) Integrin αVβ3 differentially regulates adhesive and phagocytic functions of the fibronectin receptor α5β1. *The Journal of Cell Biology 127*, 1129-1137.

(132) Aderem, A. and Underhill, D. M. (1999) Mechanisms of phagocytosis in macrophages. *Annual Review of Immunology 17*, 593-623.

(133) Beppu, M., Hora, M., Watanabe, T., Kawaguchi, H., Mishima, E., Makino, M., and Kikugawa, K. (2001) Substrate-bound fibronectin enhances scavenger receptor activity of macrophages by calcium signaling. *Archives of Biochemistry and Biophysics 390*, 243-252.

(134) Medzhitov, R. and Janeway, C. A. J. (1997) Innate immunity: impact on the adaptive immune response. *Current Opinion in Immunology 9*, 4-9.

(135) Fleming, S. D. and Campbell, P. A. (1996) Macrophages have cell surface IL-10 that regulates macrophage bactericidal activity. *Journal of Immunology 56*, 1143-1150.

(136) Torchilin, V. P., Levchenko, T. S., Lukyanov, A. N., Khaw, B. A., Klibanov, A. L., Rammohan, R., Samokhin, G. P., and Whiteman, K. R. (2001) p-Nitrophenylcarbonyl-PEG-PE-liposomes: fast and simple attachment of specific ligands, including monoclonal antibodies, to distal ends of PEG chains via p-nitrophenylcarbonyl groups. *Biochimica et Biophysica Acta 1511*, 397-411.

(137) Ishihara, K., Ueda, T., and Nakabayashi, N. (1990) Preparation of phospholipid polymers and their properties as polymer hydrogel membranes. *Polymer Journal 22*, 355-360.

(138) Konno, T., Watanabe, J., and Ishihara, K. (2004) Conjugation of enzymes on polymer nanoparticles covered with phosphorylcholine groups. *Biomacromolecules 5*, 342-347.

(139) Fukazawa, K. and Ishihara, K. (2009) Fabrication of a cell-adhesive protein imprinting surface with an artificial cell membrane structure for cell capturing. *Biosensors and Bioelectronics 25*, 609-614.

VITA

Matthew Thomas Dickerson was born on December 24, 1981 in Danville, KY. He earned his Bachelor of Science in Chemical Engineering from the University of Kentucky in May of 2006. As an undergraduate, Matthew worked with Dr. Paul Bummer in the Department of Pharmaceutical Sciences on the development of phospholipid, mixed micelle based systems for delivery of low solubility anti-cancer agents. Matthew began his pursuit of a Doctorate of Philosophy in Chemical Engineering at the University of Kentucky in August of 2006. From June to September of 2009 Matthew worked in the lab of Kazuhiko Ishihara at the Tokyo University in Tokyo, Japan synthesizing and characterizing molecularly imprinted MPC polymer surfaces capable of selectively binding target molecules. During his Ph.D. candidacy, Matthew obtained an NSF Integrative Graduate Education and Research Traineeship (IGERT) Fellowship and an NSF East Asia & Pacific Summer Institutes for U.S. Graduate Students (EAPSI) Fellowship.

Publications

Matthew T. Dickerson, Morgan B. Abney, Caroline E. Cameron, Leonidas G. Bachas, Marc R. Knecht, and Kimberly W. Anderson. Fibronectin binding to the *Treponema pallidum* adhesin protein fragment Tp0483 on functionalized self-assembled monolayers. *Bioconjugate Chemistry (2011) in press*

Matthew T. Dickerson, Morgan B. Abney, Caroline E. Cameron, Leonidas G. Bachas, and Kimberly W. Anderson. Hemocompatibility analysis of fibronectin binding, recombinant *T. pallidum* protein fragment RTp0483 on carboxylate terminated self-assembled monolayers. *In preparation*

Matthew T. Dickerson, Caroline E. Cameron, Marc R. Knecht, and Kimberly W. Anderson. The role of *T. pallidum* fibronectin binding protein fragment Tp0483 in cytokine production and nitrite production for mouse macrophages and the impact of fibronectin binding. *In preparation*

Presentations

Matthew Dickerson, Morgan Abney, Leonidas Bachas, and Kimberly Anderson. Hemocompatibility Enhancement by Incorporation of *T. pallidum* Antigenic Disguise Protein Tp0483. 2008 Biomedical Engineering Society Annual Meeting, St. Louis, MO, October 2008

Matthew Dickerson, Morgan Abney, Leonidas Bachas, and Kimberly Anderson. Hemocompatibility Enhancement through the Integration of the Antigenic Disguise Protein Tp0483 on a Material Surface. 2008 American Institute of Chemical Engineers Annual Meeting, Philadelphia, PA, November 2008

Matthew Dickerson, Keaton Osborne, Morgan Abney, Leonidas Bachas, and Kimberly Anderson. Biocompatibility Enhancement Through Surface Adsorbed Antigenic Disguise Protein Tp0483 and Fibronectin. Society of Biomaterials, Lexington, KY, September 2009 & Biomedical Engineering Society Annual Meeting, Pittsburgh, PA, October 2009

Matthew Dickerson, Keaton Osborne, Morgan Abney, Leonidas Bachas, and Kimberly Anderson. Binding Site Analysis and Plasma Protein Inhibition Study for the Recombinant Protein Tp0483 and Human Plasma Fibronectin using Surface Plasmon Resonance (SPR). 2009 American Institute of Chemical Engineers Annual Meeting, Nashville, TN, November 2009

Matthew Dickerson, Morgan Abney, Caroline Cameron, Leonidas Bachas, and Kimberly Anderson. Analysis of the Hemocompatibility Enhancing Effect of Surface Adsorbed Recombinant Protein Tp0483 in Conjunction with Human Serum Fibronectin. 2010 American Institute of Chemical Engineers Annual Meeting, Salt Lake City, UT, November 2010

Kimberly Anderson, Matthew Dickerson, and Marc Knecht. Using Antigenic Disguise to Inhibit Protein and Cellular Interactions with Surfaces. 2011 American Institute of Chemical Engineers Annual Meeting, Minneapolis, MN, October 2011.

Matthew Dickerson, Caroline Cameron, Marc Knecht, and Kimberly Anderson. Role of Fibronectin Binding Protein rTp0483 in the Pathogenesis and Antigenic Disguise of *Treponema Pallidum*. 2011 Society for Biomaterials Biomaterials Day, West Lafayette, IN, October 2011